ISSN 2782-2427

CONTROL SCIENCES

4/2023

[1]Russian Academy of Sciences.

CONTROL SCIENCES
Scientific Technical Journal

6 issues per year
ISSN 2782-2427
Open access

Published since 2021

Original Russian Edition
Problemy Upravleniya
Published since 2003

FOUNDER AND PUBLISHER
V.A. Trapeznikov
Institute of Control Sciences
of Russian Academy of Sciences

Editor-in-Chief
D.A. Novikov, RAS Academician

Deputy Editor-in-Chief
F.F. Pashchenko

Executive Editor-in-Chief
N.E. Maximova

Editor
L.V. Petrakova

Editorial address
65 Profsoyuznaya st., office 410,
Moscow 117997, Russia

☎/🖷 +7(495) 198-17-20, ext. 1410

✉ pu@ipu.ru

URL: http://controlsciences.org

Published: September 15, 2023

Registration certificate of
Эл № ФС 77-80482
of 17 February 2021
issued by the Federal Service
for Supervision of Communications,
Information Technology, and Mass
Media

CONTROL SCIENCES

4.2023

CONTENTS

DOI: http://doi.org/10.25728/cs.2023.4.1

PARAMETRIC OPTIMIZATION OF A NONLINEAR MODEL IN TUMOR CELL GROWTH IDENTIFICATION

V.N. Afanas'ev[1] and N.A. Frolova[2]

[1]HSE Tikhonov Moscow Institute of Electronics and Mathematics, Moscow, Russia,
[2]Lomonosov Moscow State University

[1]✉ afanval@mail.ru, [2]✉ matveeva.nataljja@physics.msu

Abstract. This paper presents an identification method for time-varying objects that involves mathematical models with parametric tuning. The deviation of object's transients and its mathematical model are estimated in terms of a quadratic performance criterion; the parametric tuning of the object model is a constrained optimization problem. The parametric optimization algorithm is developed using the vector projection property in a Krein space and the second Lyapunov method for a targeted change in the model parameters. The method is applied to estimate parameters in a tumor cell growth model. The nonlinear model describes the relationship between the populations of normal, immune, and tumor cells that can be measured in the presence of Gaussian white noise. Numerical simulation illustrates the design procedure and shows the effectiveness of this method.

Keywords: parametric optimization, identification, cost function, nonlinear differential equations, Lyapunov method, Wiener–Hopf equation.

INTRODUCTION

The theory of control of objects with incomplete information about the state, parameters, and interaction with the environment (the class of uncertain objects) has been developing for over 50 years. Numerous books, articles in peer-reviewed periodicals, and papers in the proceedings of various-level scientific and practical conferences have been devoted to this topic. Nevertheless, there is still a high interest of researchers and engineers in it; for example, see [1–11]. This fact is explained by the appearance of more complex uncertain objects of different physical nature and tougher requirements for the accuracy and reliability of the tasks performed by such objects (on the one hand) and by the development of computer means to implement complex algorithms, reduce, or eliminate the undesirable consequences of uncertainty (on the other hand). A separate branch of automatic control is the identification of uncertain objects, i.e., the design of their mathematical representations with parametric tuning.

For time-varying control systems, analytical design methods [12] do not yield implementable solutions of identification problems. Therefore, it is reasonable to design such systems based on additional loops. These loops are used to optimize the system in terms of a selected performance criterion during system operation and the accumulation and processing of necessary information [7–11]. The implemented solutions can be obtained by means of special algorithmic procedures. In this paper, we present an algorithmic design method [13] for a time-varying system with incomplete information about the parameters and the environment that contains a set of algorithms to optimize the system in terms of a given performance criterion [14–17]. This method is applied to the problem of tumor cell growth identification using a mathematical model with tunable parameters.

In the general case, the identification of dynamic objects consists in determining their structure and model parameters from observed data: input and output. Note that the stage of choosing the model structure is crucial [9, 10]. The appropriateness, applicability, and efficiency of the resulting estimate significant-

ly depend on the degree of reliability with which the mathematical model describes the real situation (object, measurements, and exogenous parametric disturbances). In most applications, there is no complete and accurate model, and its construction incurs great difficulties. Therefore, an estimate on the measured characteristics of the process has to be designed under incomplete knowledge of the model. The problem gets even more complicated when external impacts or (and) object's parameters vary in an uncontrolled way. Moreover, determining the state of a stochastic object described by nonlinear differential equations from measurements of its phase components under disturbances requires implementing the solutions of nonlinear differential equations. For example, a nonlinear filter cannot be designed with perfect precision; most importantly, estimating the approximation accuracy of a suboptimal nonlinear filter is either difficult or even impossible.

In such conditions, one alternative is to design a model with tunable parameters. The quality of the resulting solution of the identification problem is assessed using a loss function (an even residual function of the object's outputs) and its mathematical model. The method for minimizing a quadratic performance criterion used below to tune the object's model parameters corresponds to the widespread least squares procedure [7, 9, 14–17].

The state dependent coefficient (SDC) linearization method [9] is often used for practically convenient representation when the object's model is described by an ordinary nonlinear differential equation.

Different parametric identification problems formulated in spaces with an indefinite metric and different deterministic and stochastic criteria can be solved within a uniform geometric framework. These are the so-called Krein spaces [18, 19]. In identification problems, parametric optimization algorithms for a nonlinear model are developed using the projection of a linear transformation of the model output and the identification error. In this case, tunable model parameters are purposefully varied by means of appropriate operators (sensitivity functions). They are defined using the corresponding Lyapunov function.

The parametric optimization algorithm is applied below to study tumor growth. The mathematical model of this process is described by a system of ordinary differential equations [20, 21]. The mathematical model includes the growth of populations of normal, immune, and tumor cells separately as well as their interpopulation relations. This model has already served to construct various chemotherapy protocols with completely known model parameters [21, 22], to design an extended Kalman filter [23], and to determine the drug dose under an incomplete set of parameters [20].

This paper is organized as follows. Section 1 provides a general description of the solution of the identification problem and explains the algorithmic parameterization method. Conditions for the successful identification of a time-varying object by purposeful tuning of its model parameters are established. Section 2 illustrates mathematical modeling results for the identification problem of a time-varying system (tumor cell growth) based on a model with tunable parameters. The results can be applied to determine the drug dose for chemotherapy of a tumor patient.

1. IDENTIFICATION OF A TIME-VARYING SYSTEM

1.1. Problem Statement

Consider an observable uncertain object described by the nonlinear ordinary differential equation

$$\begin{gathered}\frac{d}{dt}x(t) = f\left(x(t), \eta(t), w(t)\right),\\ x(t_0) = x_0,\\ y = Cx(t) + n(t),\end{gathered} \tag{1.1}$$

with the following notations: $x \in R^n$ is the state vector; $y \in R^m$ is the vector of state measurements, $n \geq m$; $\eta \in R^k$ is the vector of unknown (time-varying) parameters; finally, $w \in R^h$ and $n \in R^m$ are noises with the characteristics

$$\begin{gathered}M\left[w(t)\right] = 0,\ M\left[n(t)\right] = 0,\\ M\left[w(t)w^{\mathrm{T}}(\tau)\right] = W_w\delta(t-\tau),\\ M\left[n(t)n^{\mathrm{T}}(\gamma)\right] = N_n\delta(t-\gamma),\\ M\left[n(t)w^{\mathrm{T}}(t)\right] = 0,\ M\left[x(t_0)w^{\mathrm{T}}(t)\right] = 0,\\ M\left[x(t_0)n^{\mathrm{T}}(t)\right] = 0,\end{gathered} \tag{1.2}$$

where W_w and N_n are the intensities of the corresponding noises. The rate of change of the unknown parameters of the object (1.1) is bounded:

$$\left|\frac{d\eta(t)}{dt}\right| \leq \Lambda,\ \Lambda = \text{const} > 0. \tag{1.3}$$

For the tunable model, we use the equation

$$\begin{gathered}\frac{d}{dt}\hat{x}(t) = f_m\left(y(t), \alpha(t)\right),\\ \hat{x}(t_0) = x_0,\end{gathered} \tag{1.4}$$

where $\hat{x}(t) \in R^n$ is the state estimate vector; $\alpha \in R^k$, $\alpha(t) \subset \mathrm{A}$, is the vector of tunable parameters in the model, introduced for the parametric identification of the original object.

Assumptions 1.1.

(A1) The function $f\left(x(t), \eta(t), w(t)\right)$: $\left[t_0, t_f\right) \times R^n \times R^k \times W_w \times R^n$ is continuous and satisfies the constraints $\left\|f\left(x(t), \eta(t), w(t)\right)\right\| \le \left(1+\|x\|\right)R_f$ for all $\left(t,\ x,\ \eta,\ w\right) \in \left[t_0, t_f\right) \times R^n \times R^k \times W_w$, where $R_f > 0.$

The function $f_m\left(y(t), \alpha(t)\right): \left[t_0, t_f\right) \times R^n \times R^k \times R^n$ is continuous and satisfies the constraints $\left\|f_m\left(y(t), \alpha(t)\right)\right\| \le \left(1+\|\hat{x}(t)\|\right)R_s$ for all $\left(t,\ y,\ a\right) \in \left[t_0, t_f\right) \times R^n \times R^k$, where $R_s > 0$.

(A2) The function $f\left(x(t), \eta(t), w(t)\right)$ satisfies the Lipschitz condition in the variable x: $\left\|f\left(x+z, \eta, w\right) - f\left(x, \eta, w\right)\right\| \le \mu\|z\|,\ \mu > 0,$ for all $\left(t,\ x,\ \eta,\ w\right) \in \left[t_0, t_f\right) \times R^n \times R^k \times W_w,\ z \in R^n.$

The function $f_m\left(y(t), \alpha(t)\right)$ satisfies the Lipschitz condition in the variable y: $\left\|f_m\left(y+\nu, \alpha\right) - f_m\left(y, \alpha\right)\right\| \le \varsigma\|v\|,\ \varsigma > 0,$ for all $\left(t,\ y,\ a\right) \in \left[t_0, t_f\right) \times R^n \times R^k,\ R_s > 0.$

(A3) The function $f\left(x(t), \eta(t), w(t)\right)$ is smooth and continuously differentiable over the set of variables η as many times as necessary.

The function $f_m\left(y(t), \alpha(t)\right)$ is smooth and continuously differentiable over the set of variables a as many times as necessary. ♦

We write the state mismatch between the object (1.1) and its model (1.4) as

$$\varepsilon(t) = \Phi x(t) - \Psi\hat{x}(t). \qquad (1.5)$$

Here, $\varepsilon(t) \in R^l$ is the state tracking error; $\Phi: R^n \to R^l$ and $\Psi: R^m \to R^l$ are the linear operators transforming the dimension of the state vector and the state estimate vector.

The identification problem for the object (1.1) is to minimize a criterion (cost function) of the form

$$\min_{a \subset A} J(\varepsilon) = M\left[F\left(\varepsilon(\eta, \alpha)\right)\right] \qquad (1.6)$$

by tuning the parameters of the model (1.4). In the expression (1.6), $F\left(\varepsilon(\eta, \alpha)\right)$ is a scalar nonnegative symmetric and (or) quadratic function.

Assumption 1.2. The tunable parameter domain A of the model (1.4) contains the parameters $\alpha \in R^k$ that solve the identification problem (1.6). ♦

1.2. Necessary Minimum Conditions for the Cost Function

In view of Assumptions 1.1, the local minimum conditions for the criterion (1.6) with respect to the variable parameters $\eta(t)$ of the object (1.1) and the tunable parameters $\alpha(t)$ of the model (1.4) have the form

$$\frac{\partial}{\partial\alpha} J(\varepsilon) = M\left[\frac{\partial F\left(\varepsilon(\eta, \alpha)\right)}{\partial\alpha}\right] = 0,$$

$$\frac{\partial^2}{\partial\alpha_i \partial\alpha_j} J(\varepsilon) = M\left[\frac{\partial^2 F\left(\varepsilon(\eta, \alpha^0)\right)}{\partial\alpha_i\ \partial\alpha_j}\right] > 0, \qquad (1.7)$$

$$i,\ j = 1, ..., k.$$

The vector in the first equation of (1.7) represents the gradients of the mean losses [6, 9]:

$$\frac{\partial F\left(\varepsilon(\eta, \alpha)\right)}{\partial\alpha} = \left(\frac{\partial F\left(\varepsilon(\eta, \alpha)\right)}{\partial\alpha_1}, ..., \frac{\partial F\left(\varepsilon(\eta, \alpha)\right)}{\partial\alpha_k}\right).$$

The matrices in the second equation of (1.7) are the Hessians describing the gradients of the mean losses. Using the necessary conditions for a local minimum, we write the parametric optimization algorithm [7, 9, 14]

$$\frac{d}{dt}\alpha(t) = -\Gamma M\left[\frac{\partial F(\varepsilon(\eta, \alpha))}{\partial\alpha}\right], \qquad (1.8)$$

$$\alpha(t_0) = \alpha_0,$$

where Γ is a positive definite gain matrix. This matrix affects the convergence of the algorithm and its ability to resist disturbances.

Theorem 1.1. *Under Assumptions 1.1 and 1.2 for the model* (1.2) *and the object* (1.1), *let the initial states of the model and object parameters be given and* $\alpha(t_0) \ne \eta(t_0)$. *Then the algorithm* (1.8) *asymptotically optimizes the criterion* (1.6) *if the rates of change of the parameters* $\alpha(t)$ *and* $\eta(t)$, $t \in \left[t_0, t_f\right)$, *are related by*

$$\left|\frac{d}{dt}\alpha(t)\right| > \left\{M\left|\left[\frac{\partial F\left(\varepsilon(\eta,\alpha)\right)}{\partial\eta}\right]^{\mathrm{T}}\left[\frac{\partial F\left(\varepsilon(\eta,\alpha)\right)}{\partial\alpha}\right]\right|\right\}^{-1}$$

$$\times\left|M\left[\frac{\partial F\left(\varepsilon(\eta,\alpha)\right)}{\partial\eta}\right]^{\mathrm{T}} M\left[\frac{\partial F\left(\varepsilon(\eta,\alpha)\right)}{\partial\eta}\right]\Lambda\right|.$$

P r o o f. We introduce the Lyapunov function

$$V_L\left(\varepsilon(\eta,\alpha)\right)=J\left(\varepsilon(\eta,\alpha)\right).$$

The criterion (1.6) does not explicitly depend on time. Hence, the total derivative of the Lyapunov function is given by

$$\frac{d}{dt}J\left(\varepsilon(\eta,\alpha)\right)=\frac{\partial J\left(\varepsilon(\cdot)\right)}{\partial\alpha}\frac{d}{dt}\alpha(t)+\frac{\partial J\left(\varepsilon(\cdot)\right)}{\partial\eta}\frac{d}{dt}\eta(t)$$
$$=-\left\{M\left[\frac{\partial F\left(\varepsilon(\eta,\alpha)\right)}{\partial\alpha}\right]\right\}\frac{d}{dt}\alpha(t)$$
$$+\left\{M\left[\frac{\partial F\left(\varepsilon(\eta,\alpha)\right)}{\partial\eta}\right]\right\}\frac{d}{dt}\eta(t)\le 0.$$

Considering the expression (1.8) and the constraint (1.3) on the rate of change of the object's parameters, it follows that

$$\left|M\left[\frac{\partial F\left(\varepsilon(\eta,\alpha)\right)}{\partial\alpha}\right]\frac{d}{dt}\alpha(t)\right|\ge\left|M\left[\frac{\partial F\left(\varepsilon(\eta,\alpha)\right)}{\partial\eta}\right]\Lambda\right|. \quad (1.9)$$

Multiplying (1.9) on the left by the vector $M\left[\partial F\left(\varepsilon(\eta,\alpha)\right)/\partial\eta\right]^{\mathrm{T}}$ and taking (1.3) into account, we obtain

$$\left|M\left[\frac{\partial F\left(\varepsilon(\eta,\alpha)\right)}{\partial\eta}\right]^{\mathrm{T}}\right|\left|M\left[\frac{\partial F\left(\varepsilon(\eta,\alpha)\right)}{\partial\alpha}\right]\frac{d}{dt}\alpha(t)\right|$$
$$\ge\left|M\left[\frac{\partial F\left(\varepsilon(\eta,\alpha)\right)}{\partial\eta}\right]^{\mathrm{T}}\right|\left|M\left[\frac{\partial F\left(\varepsilon(\eta,\alpha)\right)}{\partial\eta}\right]\Lambda\right|.$$

This nonstrict inequality finally yields the desired asymptotic optimization condition for the criterion (1.6). More precisely, it suffices to solve the parametric identification problem for the time-varying object (1.1) using the model (1.4) and the optimization algorithm (1.8):

$$\left|\frac{d}{dt}\alpha(t)\right|>\left\{M\left|\left[\frac{\partial F\left(\varepsilon(\eta,\alpha)\right)}{\partial\eta}\right]^{\mathrm{T}}\left[\frac{\partial F\left(\varepsilon(\eta,\alpha)\right)}{\partial\alpha}\right]\right|\right\}^{-1}\times$$
$$\times\left|M\left[\frac{\partial F\left(\varepsilon(\eta,\alpha)\right)}{\partial\eta}\right]^{\mathrm{T}}M\left[\frac{\partial F\left(\varepsilon(\eta,\alpha)\right)}{\partial\eta}\right]\Lambda\right|.\blacklozenge$$

1.3 Identification of a Time-Varying Object in a Krein Space

This subsection considers models (1.2) with the quadratic performance criterion

$$J(\varepsilon)=M\left\|\varepsilon(t)\right\|^2=M\left\|\Phi x(t)-\Psi\hat{x}(t)\right\|^2=J(x,\hat{x}). \quad (1.10)$$

As has been mentioned in subsection 1.1, different parametric identification problems formulated in spaces with an indefinite metric and different deterministic and stochastic criteria can be solved within a uniform geometric framework. Such spaces include the Krein space [18, 19] (*K*-space). The Krein space is an extension of the Hilbert space and has its basic properties. The main difference is that a Krein space can be decomposed into two orthogonal subspaces, $K=K_+\oplus K_-$, so that K_+ and K_- are Hilbert spaces and $\langle v,z\rangle=0$ for any $v\in K_+$ and $z\in K_-$. The projection $\langle v,z\rangle=0$ for both subspaces exists and is unique [18, 19]. We will write this projection property in terms of the identification problem under consideration. Let $\Im\{y(t)\}$, $\Im\in\Re$, be a linear operator. Then, in the case of the identification problem (1.6), the condition $\Im\{y(t)\}\perp\varepsilon(t)$ holds for both Krein subspaces. In other words, $\left\langle\Im\{y(t)\},\varepsilon(t)\right\rangle=0$, and the orthogonal projection can be written as

$$M\left[\left\{\Im\{y(t)\}\right\}^{\mathrm{T}}\left\{\Phi x(t)-\Psi\hat{x}(t)\right\}\right]=0. \quad (1.11)$$

In Krein spaces, this projection exists and is unique, i.e., it must hold for any operators $\Im\in\Re$. Obviously, the expression (1.11) is nothing else but the Wiener–Hopf equation [9, 23]:

$$\mathrm{tr}M\left[\left\{\Im\{y(t)\}\right\}\left\{\Phi x(t)-\Psi\hat{x}(t)\right\}^{\mathrm{T}}\right]=0,$$
$$\Im\in\Re,\ t\in\left[t_0,t_f\right), \quad (1.12)$$

which is a necessary and sufficient condition for the minimum of the criterion (1.10). Since condition (1.12) fails for $\alpha(t)\ne\eta(t)$, it can be applied to organize the parametric optimization algorithm for the object's model. Let $\Im\{y(t)\}=\left\{\partial\Psi\hat{x}(t)/\partial\alpha\right\}^{\mathrm{T}}$, where $\partial\Psi\hat{x}(t)/\partial\alpha$ is the sensitivity function of the process $\hat{x}(t)$ to the variation of the model parameters $\alpha(t)$. Then the parametric optimization algorithm for the model (1.4) has the form

$$\frac{d}{dt}\alpha(t)=-\Gamma M\left[\left\{\frac{\partial\Psi\hat{x}(t)}{\partial\alpha}\right\}^{\mathrm{T}}\left\{\Phi x(t)-\Psi\hat{x}(t)\right\}\right], \quad (1.13)$$
$$\alpha(t_0)=\alpha_0.$$

However, for the object (1.1) and its model (1.4) with parametric tuning, this condition cannot generally serve for parametric optimization. Consider an example illustrating this fact.

With a slight simplification, condition (1.11) reduces to

$$\left\langle \Im\{y(t)\}, \varepsilon(t)\right\rangle = \mathrm{tr}MC\left[x(t)x^{\mathrm{T}}(t)\right] - \mathrm{tr}MC\left[\hat{x}(t)\hat{x}^{\mathrm{T}}(t)\right]C^{\mathrm{T}} - \mathrm{tr}M\left[n(t)\hat{x}^{\mathrm{T}}(t)\right]C^{\mathrm{T}}. \quad (1.14)$$

Here,

$$x(t) = \varepsilon(t) + \hat{x}(t),\ \mathrm{tr}M\left[\varepsilon(t)\hat{x}^{\mathrm{T}}(t)\right] = 0$$

due to the problem statement and condition (1.12).

The second term in equation (1.14) is

$$\mathrm{tr}M\left[\hat{x}(t)n^{\mathrm{T}}(t)\right] = \mathrm{tr}M\left[\hat{x}(t_0)n^{\mathrm{T}}(t) + \int_{t_0}^{t} f(Cx(\tau) + n(\tau), \alpha(\tau))n^{\mathrm{T}}(t)d\tau\right]$$

$$= \mathrm{tr}\left[\int_{t_0}^{t} M\left[f(Cx(\tau) + n(\tau), \alpha(\tau))n^{\mathrm{T}}(t)\right]d\tau\right].$$

Therefore, for $\alpha(t) = \eta(t)$, the value of (1.14) depends on the (generally unknown) intensity N_n of the white noise $n(t)$ in the measurements $y(t)$. To eliminate this dependence, in view of $M\left[n(t)n^{\mathrm{T}}(\gamma)\right] = N_n\delta(t-\gamma)$, we introduce into (1.12) a linear operator such that

$$\Im^*\{y(t)\} = \Im\{y(t+\xi)\},\ \xi > \gamma\ .$$

According to the problem statement, $\mathrm{tr}M\left[n(t)n^{\mathrm{T}}(t+\xi)\right] = 0;$ as a result,

$$\mathrm{tr}M\left[\left\{\Im^*\{y(t)\}\right\}\left\{\Phi x(t) - \Psi\hat{x}(t)\right\}^{\mathrm{T}}\right] = 0\ .$$

This condition is necessary and sufficient for the minimum of the criterion $J^*(\varepsilon) = M\left[\varepsilon^{\mathrm{T}}(t)\varepsilon(t+\xi)\right]$.

Note that the criteria $J(\varepsilon)$ and $J^*(\varepsilon)$ achieve minimum for the same relationship of the parameters of the object (1.1) and its model (1.5), i.e., under the condition $\alpha(t) = \eta(t)$.

Based on these considerations, the parametric optimization algorithm of the model (1.5) for solving the identification problem takes the form

$$\frac{d}{dt}\alpha(t) = -\Gamma M\left[\left\{\frac{\partial\Psi\hat{x}((t+\xi)}{\partial\alpha}\right\}^{\mathrm{T}} \times\left\{\Phi x(t) - \Psi\hat{x}(t)\right\}\right],\ \xi > \gamma,\ \alpha(t_0) = \alpha_0. \quad (1.15)$$

2. RESULTS OF MATHEMATICAL MODELING

To demonstrate the effectiveness of this parametric optimization method, we consider the nonlinear tumor growth model [20, 21] as the object (1.1). The model consists of three components: the number of normal cells (*N*), the number of tumor cells (*T*), and the number of immune cells (*I*). The nonlinear system of equations has the form

$$\frac{d}{dt}N = r_2N(1-b_2N) - c_4NT + w_N,$$

$$\frac{d}{dt}T = r_1T(1-b_1T) - c_2IT - c_3TN + w_T, \quad (2.1)$$

$$\frac{d}{dt}I = s + \frac{\rho IT}{\alpha+T} - c_1IT - d_1I + w_I,$$

where $N(t)$, $T(t)$, and $I(t)$ denote the normalized population sizes of normal, tumor, and immune cells, respectively. (Immune cells include lymphocytes, etc.) The model parameters are described in Table 2.1.

The growth dynamics of normal cells and tumor cells with the density-dependent mechanism are influenced by the effects of overpopulation and resource limitation. The populations of normal cells and tumor cells are described using the logistic growth function; see the first terms of the equations for *N* and *T*. Its disadvantage is the a priori knowledge of the limiting population size (the parameters $1/b_1$ and $1/b_2$, each interpreted as the potential capacity of the population predetermined by the available amount of resources). Tumor cells and normal cells are assumed to propagate with constant specific rates r_1 and r_2, respectively. The tumor growth rate is restricted due to the destruction of malignant cells by killer lymphocytes (immune cells; see the term $c_2T(t)I(t)$). In addition, the lymphocyte dynamics equation contains the term $\rho T(t)I(t)/\left[\alpha+T(t)\right]$ describing their propagation, where ρ is the growth rate of lymphocytes under their maximum stimulation and the parameter α characterizes tumor antigenicity (immune response provocation). Within this model, tumor stimulates the proliferation (increased growth) of lymphocytes when the value T is small and suppresses it otherwise. The other two terms in the second equation correspond to the natural death of lymphocytes (the term $d_1I(t)$) and the constant afflux of lymphocytes from stem cells (the parameter *s* in the third equation) [23]. The death of

lymphocytes during interaction with tumor cells is not considered explicitly since one lymphocyte can kill several tumor cells.

The nonlinear system has several equilibria (N_E, T_E, I_E) depending on the parameters described above. They are determined by the intersections of planes satisfying the equations

$$\frac{dN}{dt}=0\Rightarrow\begin{cases}N_E=0,\\ N_E=\dfrac{r_2-c_4T_E}{r_2b_2},\end{cases}$$

$$\frac{dT}{dt}=0\Rightarrow\begin{cases}T_E=0,\\ T_E=\dfrac{r_1-c_2I_E-c_3N_E}{r_1b_1},\end{cases}\qquad(2.2)$$

$$\frac{dI}{dt}=0\Rightarrow I_E=\frac{s(\alpha+T_E)}{(\alpha+T_E)(d_1+c_1T_E)-\rho T_E}.$$

Depending on the parameter values, the model (2.1) can have one, two, or three equilibria. The stability of equilibria (2.2) also depends on the parameter values. To analyze stability, it is necessary to linearize the system in the neighborhood of a given equilibrium and examine the eigenvalues of the system matrix.

The tumor-free state (no tumor cells) is determined by the relations $N_E=1,\ T_E=0,$ and $I_E=s/d_1$; the lifeless state (abiosis, no normal cells) is determined by the ratios $N_E=0,\ T_E=0,$ and $I_E=s/d_1$, or by the relations

$$N_E=0,\qquad T_E=\frac{r_1-c_2I_E}{r_1b_1},$$

$$I_E=\frac{s(\alpha+T_E)}{(\alpha+T_E)(d_1+c_1T_E)-\rho T_E}.$$

Note that one lifeless equilibrium, $(0,\ 0,\ s/d_1)$, is always unstable and depends on the values of the corresponding parameters. The second lifeless equilibrium can be stable or unstable. Selecting the parameter values according to Table 2.1, we obtain the model (2.1) with 4 equilibria: 3 unstable (2 lifeless equilibria, 1 tumor-free equilibrium) and 1 stable equilibrium (coexistence).

We rewrite system (2.1) by shifting the tumor-free equilibrium to the origin of coordinates [23]:

$$x_1=N-1/b_2,\ x_2=T,\ x_3=I-s/d_1.$$

Table 2.1

Model parameters and their variation ranges

Parameter	Description	Value	Constraints
b_1	Tumor cell population capacity	1.0	$b_1^{-1}<b_2^{-1}$
b_2	Normal cell population capacity	1.0	-
c_1	The destruction rate of immune cells by tumor cells	1.0	$c_1>0$
c_2	The destruction rate of tumor cells by immune cells	0.5	$c_2>0$
c_3	The destruction rate of tumor cells by normal cells	1.0	$c_3>0$
c_4	The destruction rate of normal cells by tumor cells	1.0	$c_4>0$
d_1	The natural death rate of immune cells	0.2	-
r_1	The growth rate of tumor cells	1.5	$r_1>r_2,\ r_1<\dfrac{sc_2}{d_1}+c_3$
r_2	The growth rate of normal Cells	1.0	-
s	The afflux of lymphocytes from stem cells	0.33	$0<s<0.5$
α	Tumor antigenicity	0.3	$\alpha>0$
ρ	The growth rate of lymphocytes under maximum stimulation	0.01	$0<\rho<2$

In the new coordinates, system (2.1) takes the form

$$\frac{dx_1}{dt} = -r_2 x_1 (1 + b_2 x_1) - \frac{c_4}{b_2} x_2 - c_4 x_1 x_2 + w_1,$$

$$\frac{dx_2}{dt} = r_1 x_2 \left(1 - b_1 x_2\right) - \left(\frac{sc_2}{d_1} + \frac{c_3}{b_2}\right) x_2 - c_3 x_1 x_2$$

$$-c_2 x_2 x_3 + w_2,$$

$$\frac{dx_3}{dt} = -\frac{c_2 s}{d_1} x_2 - d_1 x_3 + \rho \frac{s}{d_1} \frac{x_2}{(\alpha + x_2)}$$

$$+\rho \frac{x_2 x_3}{\alpha + x_2} - c_2 x_2 x_3 + w_3,$$

$$y(t) = x(t) - \hat{x}(t) + n(t),$$

where $x = \left(x_1, x_2, x_3\right)^{\mathrm{T}}$ is the state vector of the system. The parameter values of this model were given in many publications; for example, see [23]. Table 2.2 shows the values of the unknown process parameters to be identified (they are set in bold).

Table 2.2

Parameter values for the object and its model

Parameter	Value for model	Value for object	Parameter	Value for model	Value for object
b_1	1.0	1.0	d_1	0.2	0.2
b_2	1.0	1.0	r_1	1.7	**1.5**
c_1	1.0	**1.1**	r_2	1.0	**1.3**
c_2	0.45	**0.58**	S	0.3	0.3
c_3	0.9	**1.0**	A	0.3	0.3
c_4	1.0	1.0	ρ	0.01	0.06

The system of equations for estimating the state vector (the tracking model for the object) has a similar form [24, 25]:

$$\frac{d\hat{N}(t)}{dt} = \tilde{r}_2 \hat{N}(t)\left[1 - \tilde{b}_2 \hat{N}(t)\right] - \tilde{c}_4 \hat{T}(t)\hat{N}(t),$$

$$\frac{d\hat{T}(t)}{dt} = \tilde{r}_1 \hat{T}(t)\left[1 - \tilde{b}_1 \hat{T}(t)\right] - \tilde{c}_2 \hat{T}(t)\hat{I}(t) - \tilde{c}_3 \hat{T}(t)\hat{N}(t),$$

$$\frac{d\hat{I}(t)}{dt} = \tilde{s} + \frac{\tilde{\rho}\hat{T}(t)\hat{I}(t)}{\tilde{\alpha} + \hat{T}(t)} - \tilde{d}_1 \hat{I}(t) - \tilde{c}_1 \hat{T}(t)\hat{I}(t),$$

where $\hat{N}(t)$, $\hat{T}(t)$, and $\hat{I}(t)$ are the estimated population sizes of normal, tumor, and immune cells, respectively. (Note that all or some parameter values may differ from (2.1).) With $\hat{x}_1 = \hat{N} - 1/\tilde{b}_2$, $\hat{x}_2 = \hat{T}$, and $\hat{x}_3 = \hat{I} - \tilde{s}/\tilde{d}_1$, the model is pre-transformed as follows:

$$\frac{d\hat{x}_1}{dt} = -\tilde{r}_2 \hat{x}_1 (1 + \tilde{b}_2 \hat{x}_1) - \frac{\tilde{c}_4}{\tilde{b}_2} \hat{x}_2 - \tilde{c}_4 \hat{x}_1 \hat{x}_2,$$

$$\frac{d\hat{x}_2}{dt} = \tilde{r}_1 \hat{x}_2 \left(1 - \tilde{b}_1 \hat{x}_2\right) - \left(\frac{\tilde{s}\tilde{c}_2}{\tilde{d}_1} + \frac{\tilde{c}_3}{\tilde{b}_2}\right) \hat{x}_2$$

$$-\tilde{c}_3 \hat{x}_1 \hat{x}_2 - \tilde{c}_2 \hat{x}_2 \hat{x}_3, \qquad (2.3)$$

$$\frac{d\hat{x}_3}{dt} = -\frac{\tilde{c}_2 \tilde{s}}{\tilde{d}_1} \hat{x}_2 - \tilde{d}_1 \hat{x}_3 + \tilde{\rho} \frac{\tilde{s}}{\tilde{d}_1} \frac{\hat{x}_2}{(\tilde{\alpha} + \hat{x}_2)}$$

$$+\tilde{\rho} \frac{\hat{x}_2 \hat{x}_3}{\tilde{\alpha} + \hat{x}_2} - \tilde{c}_1 \hat{x}_2 \hat{x}_3.$$

According to the SDC linearization method [9], equations (2.3) are represented in the vector form

$$\frac{d}{dt}\hat{x}(t) = A(\hat{x}(t), \alpha(t))\hat{x}(t) + k(t)\varepsilon(t + \xi),$$

$$\hat{x}(0) = M\left[\hat{x}(0)\right]$$

with the matrix

$$A\left(\hat{x}(t), \tilde{a}(t)\right)$$

$$= \begin{pmatrix} -\tilde{r}_2(1 + \tilde{b}_2 \hat{x}_1) & -\frac{\tilde{c}_4}{\tilde{b}_2} - \tilde{c}_4 \hat{x}_1 & 0 \\ -\tilde{c}_3 \hat{x}_2 & \tilde{r}_1\left(1 - \tilde{b}_1 \hat{x}_2\right) - \left(\frac{\tilde{s}\tilde{c}_2}{\tilde{d}_1} + \frac{\tilde{c}_3}{\tilde{b}_2}\right) & -\tilde{c}_2 \hat{x}_2 \\ 0 & -\frac{\tilde{c}_2 \tilde{s}}{\tilde{d}_1} + \tilde{\rho}\frac{\tilde{s}}{\tilde{d}_1}\frac{\hat{x}_2}{(\tilde{\alpha} + \hat{x}_2)} + \tilde{\rho}\frac{\hat{x}_3}{\tilde{\alpha} + \hat{x}_2} - \tilde{c}_1 \hat{x}_3 & -\tilde{d}_1 \end{pmatrix}.$$

We apply the parametric identification procedure based on the algorithm (1.15) with the vector $\alpha(t) = \left(\tilde{c}_1(t) \quad \tilde{c}_2(t) \quad \tilde{c}_3(t) \quad \tilde{r}_1(t) \quad \tilde{r}_2(t)\right)^{\mathrm{T}}$.

Figures 2.1 and 2.2 show the 3D graphs of the performance criterion (1.10) under different values of the estimated parameters.

For this system, the algorithm (1.15) takes the form

$$\frac{d}{dt}\alpha(t) = -M\left[\left\{\frac{\partial \hat{x}(t)}{\partial \alpha}\right\}^{\mathrm{T}} \varepsilon(t + \xi)\right],$$

$$\frac{d}{dt}k(t) = -M\left[\left\{\frac{\partial \hat{x}(t)}{\partial k}\right\}^{\mathrm{T}} \varepsilon(t + \xi)\right], \ \xi > \gamma,$$

$$\alpha(t_0) = \alpha_0, \ k(t_0) = k_0,$$

where $\alpha(t) = \left(\tilde{c}_1(t) \quad \tilde{c}_2(t) \quad \tilde{c}_3(t) \quad \tilde{r}_1(t) \quad \tilde{r}_2(t)\right)^{\mathrm{T}}$.

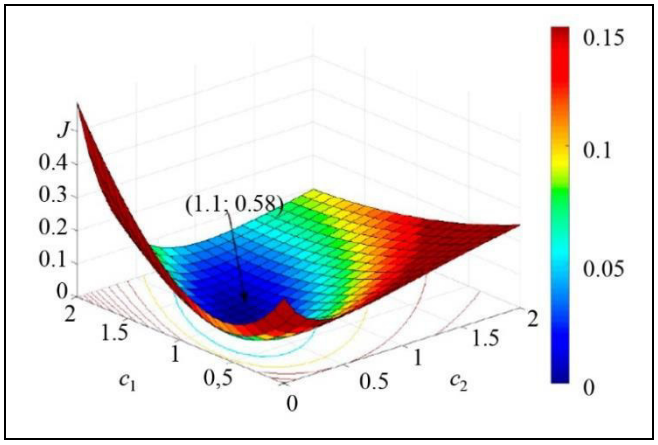

Fig. 2.1. The 3D graph of the criterion depending on the parameter estimates $\tilde{c}_1$ and $\tilde{c}_2$ under fixed values of the parameters $\tilde{r}_1$ and $\tilde{r}_2$ ($\tilde{c}_1 = 1.1$, $\tilde{c}_2 = 0.58$).

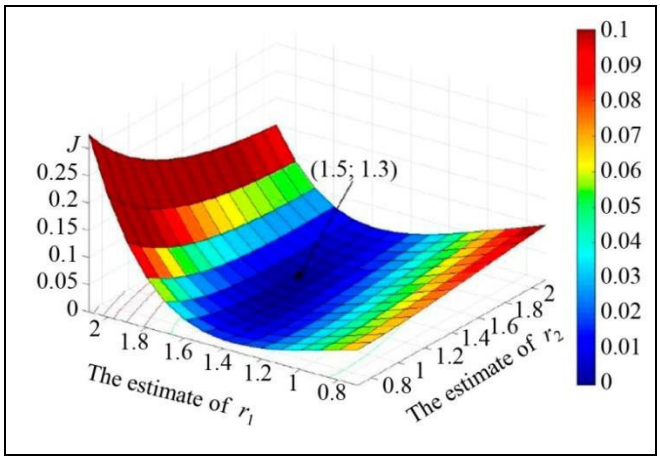

Fig. 2.2. The 3D graph of the criterion depending on the parameter estimates $\tilde{r}_1$ and $\tilde{r}_2$ under fixed values of the parameters $\tilde{c}_1$ and $\tilde{c}_2$ ($\tilde{r}_1 = 1.5, \tilde{r}_2 = 1.3$).

The sensitivity functions $\varsigma_a = \left\{\frac{\partial \hat{x}(t)}{\partial \alpha}\right\}^{\mathrm{T}} \in R^{5\times 3}$, $\zeta = \left\{\frac{\partial \hat{x}(t)}{\partial k}\right\}^{\mathrm{T}} \in R^{3\times 3}$ are calculated by the formulas

$$\frac{d}{dt}\varsigma_j(t) = \frac{\partial A(\hat{x}(t),\alpha(t))}{\partial \alpha_j}\hat{x}(t)$$

$$+\left[A(\hat{x}(t),\alpha(t)) - k(t)C\right]\left\{\frac{\partial \hat{x}(t)}{\partial \alpha_j}\right\}^{\mathrm{T}}, \quad j = 1,\ldots 5,$$

$$\frac{d}{dt}\zeta_l(t) = \frac{\partial A(\hat{x}(t),\alpha(t))}{\partial k_l}\hat{x}(t)$$

$$+\left[A(\hat{x}(t),\alpha(t)) - k(t)C\right]\left\{\frac{\partial \hat{x}(t)}{\partial k_l}\right\}^{\mathrm{T}} + \left\{\frac{\partial k(t)}{\partial k_l}\right\}^{\mathrm{T}} \varepsilon(t),$$

$$l = 1,\ldots,3.$$

Figure 2.3 shows the graphs of tunable model parameters under given values of the object parameters (see Table 2.2).

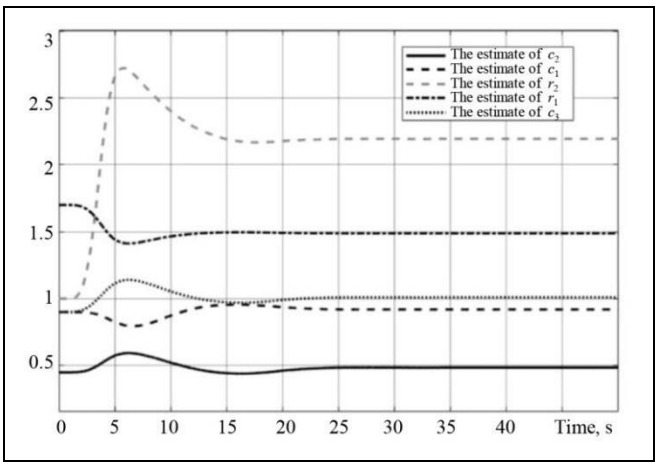

Fig. 2.3. The graphs of tunable model parameters $\left(\hat{c}_1(t) \quad \hat{c}_2(t) \quad \hat{c}_3(t) \quad \hat{r}_1(t) \quad \hat{r}_2(t)\right)^{\mathrm{T}}$.

The main operation of the identification algorithm falls on a time interval equal to the duration of the state transients; see Fig. 2.4.

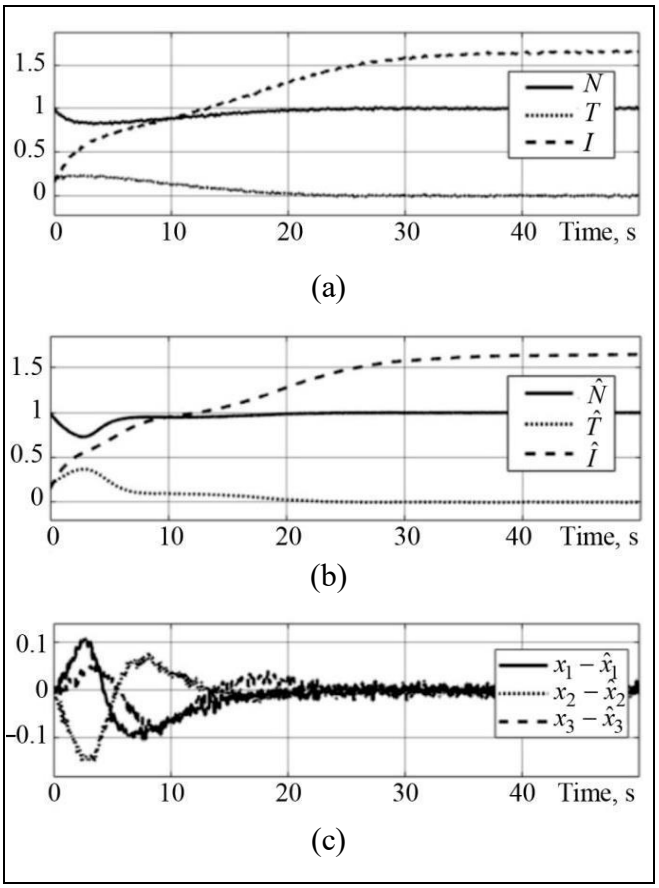

Fig. 2.4. Operation of the identification algorithm and state transients: (a) state parameters, (b) parameter estimates, and (c) estimation errors.

CONCLUSIONS

This paper has presented an identification method for a time-varying using a parametric optimization model. The problem has been considered in a Krein space, and the projection property of a linear transformation of the model output and identification error has been applied to develop the parametric optimization algorithm. A condition has been established for the successful tracking of the time-varying parameters of the object by the model parameters with this algorithm. The effectiveness of identification has been experimentally verified on a mathematical model of tumor cell growth.

Note that this parametric optimization algorithm of a nonlinear system in the identification problem can be used in control problems for uncertain objects of different nature, e.g., electrical and mechanical engineering systems, mobile objects, and non-technical systems arising in biology, medicine, chemistry, physics, economics, and many fields of science.

REFERENCES

1. Wensing, P.M., Kim, S., and Slotine, J.E., Linear Matrix Inequalities for Physically Consistent Inertial Parameter Identification: A Statistical Perspective on the Mass Distribution, *IEEE Robotics and Automation Letters*, 2017, vol. 3, no. 1, pp. 60–67.
2. Brunton, S.L., Proctor, J.L., and Kutz, J.N., Discovering Governing Equations from Data by Sparse Identification of Nonlinear Dynamical Systems, *Proceedings of the National Academy of Sciences*, 2016, vol. 113, no. 15, pp. 3932–3937.
3. Tabo, Z., Kalinda, C., Breuer, L., and Albrecht, C., Adapting Strategies for Effective Schistosomiasis Prevention: A Mathematical Modeling Approach, *Mathematics*, 2023, vol. 11, no. 12, art. no. 2609. DOI: https://doi.org/10.3390/math11122609.
4. Wu, L., Liu, F., Gu, H., and Wang, P., Adaptive Finite-Time Control of Stochastic Genetic Regulatory Networks with Time-Varying Delays, *Mathematics*, 2022, vol. 10, no. 21, art. no. 4071. DOI: https://doi.org/10.3390/math10214071.
5. Zhirabok, A.N., Shumsky, A.E., Zuev, A.V., and Sergiyenko, O., Identification of Faults in Nonlinear Dynamical Systems and Their Sensors Based on Sliding Mode Observers, *Automation and Remote Control*, 2022, vol. 83, no. 2, pp. 214–236.
6. Bobtsov, A.A., Nikolaev, N.A., Oskina, O.V., and Nizovtsev, S.I., Identification of Time-Varying Parameter of Noiseless Sinusoidal Signal, *Automation and Remote Control*, 2022, vol. 83, no. 7, pp. 1123–1135.
7. Afanas'ev, V.N., Kaperko, A.F., Kulagin, V.P., and Kolyubin, V.A., Method of Adaptive Filtering in the Problem of Restoring Parameters of Cosmic Radiation, *Automation and Remote Control*, 2017, vol. 78, no. 3, pp. 397–412.
8. Deng, X., Huang, Y., Xu, B., and Tao, L., Position and Attitude Tracking Finite-Time Adaptive Control for a VTOL Aircraft Using Global Fast Terminal Sliding Mode Control, *Mathematics*, 2023, vol. 11, no. 12, art. no. 2732. DOI: https://doi.org/10.3390/math11122732.
9. Afanas'ev, V.N., *Upravlenie nelineinymi neopredelennymi dinamicheskimi ob"ektami* (Control of Nonlinear Uncertain Dynamic Objects), Moscow: LENAND, 2015. (In Russian.)
10. Isermann, R. and Minchef, M., *An Identification of Dynamic Systems. An Introduction with Applications*, Berlin–Heidelberg: Springer, 2011.
11. Farza, M., Bouraoui, I., Menard, T., et al., Adaptive Observers for a Class of Uniformly Observable Systems with Nonlinear Parametrization and Sampled Outputs, *Automatica*, 2014, vol. 50, no. 11, pp. 2951–2960.
12. Letov, A.M., *Dinamika poleta i upravlenie* (Flight Dynamics and Control), Moscow: Nauka, 1969. (In Russian.)
13. Petrov, B.N. and Krut'ko, P.D., Algorithmic Design of Optimal Controllers under Incomplete Information about the Object's State and Disturbances, *Izv. Akad. Nauk SSSR. Tekh. Kibern.*, 1972, no. 6, pp. 188–199. (In Russian.)
14. Tsypkin, Ya.Z., *Adaptation and Learning in Automatic Systems*, Mathematics in Science and Engineering, vol. 73, Academic Press, 1971.
15. Zhang, Q., Adaptive Observer for Multiple-Input-Multiple-Output (MIMO) Linear Time Varying Systems, *IEEE Trans. on Automatic Control*, 2002, vol. 47, no. 3, pp. 525–529.
16. Toth, R., Willems, J., Heuberger, P., and Van den Hof, P., The Behavioral Approach to Linear Parameter Varying Systems, *IEEE Trans. Automatic Control*, 2011, vol. 56, no. 11, pp. 2499–2514.
17. Hassibi, B., Sayed, A.H., and Kailath, T., *Indefinite Quadratic Estimation and Control: A Unified Approach to H^2 and H^{inf} Theories*, Philadelphia: SIAM, 1999.
18. Iohvidov, I.S., Krein, M.G., and Longer, H., *Introduction to the Spectral Theory of Operators in Spaces with Indefinite Metric*, Berlin: Academie Verlag, 1982.
19. Lakeev, A.V., Rusanov, V.A., and Kozerev, V.A., On Realization of Quasi-Linear Systems Described by Stationary Differential Equations in Hilbert Space, *Control Sciences*, 2013, no. 1, pp. 7–18. (In Russian.)
20. dePillis, L.G. and Radunskaya, A.E., The Dynamics of an Optimally Controlled Tumor Model: A Case Study, *Mathematical and Computer Modelling*, 2003, vol. 37, no. 11, pp. 1221–1244.
21. Itik, M., Salamci, M.U., and Banks, S.P., Optimal Control of Drug Therapy in Cancer Treatment, *Nonlinear Analysis*, 2009, vol. 71, pp. 1473–1486.
22. Kadiri, M., Louaked, M., and Trabelsi, S., Optimal Control and Parameters Identification for the Cahn–Hilliard Equations Modeling Tumor Growth, *Mathematics*, 2023, vol. 11, no. 7, art. no. 1607. DOI: https://doi.org/10.3390/math11071607.
23. Batmani, Y. and Khaloozadech, H., Optimal Chemotherapy in Cancer Treatment: State Dependent Riccati Equation Control and Extended Kalman Filter, *Optimal Control Applications and Methods*, 2012, vol. 34, pp. 562–577.
24. Babaei, N. and Salamci, M.U., Personalized Drug Administration for Cancer Treatment Using Model Reference Adaptive Control, *Journal of Theoretical Biology*, 2015, vol. 371, pp. 24–44.
25. Romanovskii, Yu.M., Stepanova, N.V., and Chernavskii, D.S., *Matematicheskoe modelirovanie v biofizike* (Mathematical Modeling in Biophysics), Moscow: Nauka, 1975. (In Russian.)

This paper was recommended for publication by N.N. Bakhtadze, a member of the Editorial Board.

Received October 23, 2022, and revised February 23, 2023. Accepted March 14, 2023.

Author information

Afanas'ev, Valery Nikolaevich. Dr. Sci. (Eng.), HSE Tikhonov Moscow Institute of Electronics and Mathematics, Moscow, Russia
✉ afanval@mail.ru
ORCID iD: https://orcid.org/0000-0001-8979-2451

Frolova, Natal'ya Alekseevna. Postgraduate, Moscow State University, Moscow, Russia
✉ matveeva.nataljja@physics.msu.ru

Cite this paper

Afanas'ev, V.N. and Frolova, N.A., Parametric Optimization of a Nonlinear Model in Cancel Cell Growth Identification. *Control Sciences* **4**, 2–11 (2023). http://doi.org/10.25728/cs.2023.4.1

Original Russian Text © Afanas'ev, V.N., Frolova, N.A., 2023, published in *Problemy Upravleniya*, 2023, no. 4, pp. 3–13.

Translated into English by *Alexander Yu. Mazurov*,
Cand. Sci. (Phys.–Math.),
Trapeznikov Institute of Control Sciences,
Russian Academy of Sciences, Moscow, Russia
✉ alexander.mazurov08@gmail.com

DOI: http://doi.org/10.25728/cs.2023.4.2

MODELS OF JOINT DYNAMICS OF OPINIONS AND ACTIONS IN ONLINE SOCIAL NETWORKS. PART III: Binary Models

D.A. Gubanov and D.A. Novikov

Trapeznikov Institute of Control Sciences, Russian Academy of Sciences, Moscow, Russia

✉ dmitry.a.g@gmail.com, ✉ novikov@ipu.ru

Abstract. Based on *VKontakte* data, we study the influence of various factors on the dynamics of opinions and actions both at the macro level ("public opinion") and at the micro level (opinions and actions of individual agents). This paper concludes the multi-part study. Identification results are presented for binary models (threshold models and models with latent variables) that describe the dynamics of agents' opinions and actions in a social network. These models are used to estimate the influence of various factors on agents' opinions and actions (public opinion, the agent's individual opinions and actions, the opinions and actions of the social environment, and the mechanisms of the agent's trust in information sources and information content). Finally, linear models are compared with threshold models and qualitative findings of the multi-part study are drawn.

Keywords: social network, agent, opinion, action, social influence, cognitive dissonance, trust in information.

INTRODUCTION

In part I of this study [1], primary analysis results were presented for the joint dynamics of opinions and actions[1] of agents on the example of their attitude toward wearing medical masks in the *VKontakte* online social network during the first year of the COVID-19 pandemic (the period from March 2020 to February 2021 inclusive). In part II of this study [2], the results were used to identify formal linear models of the joint dynamics of opinions and actions, and the following questions were partially answered:

1) How consistent are the opinions and actions of agents with each other?

2) Do agents change their opinions and actions over time?

3) Who are these (opinion- and action-changing) agents? Do they differ from others in their socio-demographic characteristics?

4) Which models better describe the dynamics of the opinions and actions of agents (linear, threshold, etc.)?

5) Are the influence of actions on opinions (*cognitive dissonance*) and the converse effect significant?

6) Under which factors do the opinions and actions of agents change? Among such factors, we considered:

- the agent's previous opinions or (and) actions;
- social influence:

  – *public opinion* (the averaged shares of certain opinions and actions of the entire social network, i.e., the so-called *macro model*, where the network is conventionally treated as one agent);

  – the opinions or (and) actions of the agent's environment (the agents with the friendship relation to a given agent), i.e., the averaged and (or) individual ones (the so-called *micro model*);
- some unobservable (*latent*) characteristics of the agent.

7) Does an agent's change in the opinion (action) depend on his trust in the source of information? Does it depend on the content of that information?

[1] *An opinion* was conventionally interpreted as the "tone" of an agent's comment, as assessed by an automatic classifier; *an action* was conventionally interpreted as the tone of a comment with an agent's like.

This paper will answer Questions nos. 4–7 based on binary models. The presentation is organized as follows. Section 1 briefly considers key factors for the analysis and modeling of network interactions. In Section 2, we present identification results for binary micro models of the joint dynamics of opinions and actions. Qualitative findings of the multi-part study and promising lines of further research are given in the Conclusions.

1. AN OUTLINE OF KEY FACTORS TO MODEL AND ANALYZE NETWORK INTERACTIONS

Recall the formalization of the factors necessary to analyze and identify the models of the joint dynamics of opinions and actions; for details, see the papers [3, 4]. Let the network participants be *agents* from a set $N = \{1, 2, ..., n\}$. They commit some *acts*[2] from a fixed set $K = \{1, 2, ..., k\}$ at certain time instants t of an interval T. Our considerations are restricted to the following types of acts ($K = \{1, 2\}$):

– publishing a comment on a post or another comment,

– liking a comment.

We denote by Δ the set of acts.[3] Each act $a \in \Delta$ is described by three parameters: the agent who committed it, the type of the act, and the time instant when it was committed. We introduce the following functions to characterize acts:

- $f_a: \Delta \to N$, associating with each act $a \in \Delta$ the agent $i \in N$ who committed it;
- $f_t: \Delta \to T$, associating with each act $a \in \Delta$ the time instant $t \in T$ when it was committed;
- $f_k: \Delta \to K$, associating with each act $a \in \Delta$ its type $j \in K$.

On the set of acts, we define a binary partial-order relation of the form "a causes b": $a \to b$. If $a \to b$, $a \neq b$, and there does not exist $c \in \Delta$ such that $a \to c$ and $c \to b$, then a is *the direct cause of* b: $a \downarrow b$. The binary relation $a \to b$ is supposed to hold in the following cases:

- a is a comment and b is a like to it.
- a is a comment and b is a comment on it.
- a and b coincide.

For each agent $i \in N$, we define the set of all his acts $\delta_i = \{a \in \Delta \mid f_a(a) = i\}$ and the set of his friends $N_i \subseteq N$. (The formal "friendship" relation in an online social network implies that an agent can receive information about the comments posted by his friends, the likes they give, etc.).

Opinions and actions. When modeling the joint dynamics of opinions and actions, we conventionally interpret the agent's *opinion* as his attitude to wearing medical masks, expressed in a comment. *The agent's opinion* in a comment $b \in \Delta$ ($f_k(b) = 1$) is formally defined in three ways as follows:

- $r' \in \{0, 1, 2\}$, where the classification results 0, 1, and 2 correspond to "against masks" (or "–"), "for masks" (or "+"), and "neutral/irrelevant" (or "="). This result is determined using the stochastic vector $(p_-, p_+, p_=)$ calculated by the classifier.
- $r'' = \dfrac{p_+}{p_+ + p_-} \in [0, 1]$, the confidence that the comment reflects the "for masks" opinion. Note that $r' = 0$ or $r' = 1$ for this comment.
- $r = \dfrac{p_+ - p_-}{p_+ + p_-} \in [-1, 1]$, where $r = 1$ and $r = -1$ indicate strong confidence in expressing the "for masks" and "against masks" opinions, respectively. Note that either $r' = 0$ or $r' = 1$ for this comment.

Let a like to some comment be *an action* as well; its assessment coincides with that of the corresponding comment liked: $y' \in \{0, 1, 2\}$, $y'' \in [0,1]$, and $y \in [-1,1]$. For example, for a like $a \in \Delta$, $y'(a) = r'(b)$, where b is the corresponding comment liked (i.e., $b \downarrow a$). To simplify further notations, we adopt the conventions $r'(a) = y'(a)$, $r''(a) = y''(a)$, and $r(a) = y(a)$. Assume that the instant of liking coincides with the instant of publishing the corresponding comment liked.

2. BINARY MODELS OF JOINT DYNAMICS OF OPINIONS AND ACTIONS

The basic model in this study is the mathematical model of the joint dynamics of agents' opinions and actions proposed in [5]. This model became a foundation for building simpler and identifiable models, such as linear models [2]. Linear and binary micro models consider the dynamics of the opinions and actions of agent $i \in N$ committing "for" and "against" acts during a time interval τ:

- $\delta_i^{\pm}(\tau) = \{a \in \delta_i \mid f_t(a) \in \tau,\ r'(a) \in \{0, 1\}\}$ is the set of his acts,
- $\delta_{i,1}^{\pm}(\tau) = \{a \in \delta_i^{\pm}(\tau) \mid f_k(a) = 1\}$ is the set of his comments, and

[2] The term "action" used in [4] is replaced here by "act" to avoid confusion with actions in models of the joint dynamics of opinions and actions.

[3] The set of relevant comments on wearing medical masks (see Section 2) and their likes.

• $\delta^{\pm}_{i,2}(\tau)=\left\{a\in\delta^{\pm}_{i}(\tau)\,|\,f_k(a)=2\right\}$ is the set of his likes.

Agent i is subjected to the following factors:

• *The influence of the entire network*, given by

$$\circ\ \bar{r}_{-i}(\tau)=\frac{\sum\limits_{a\in\Delta(\tau)|f_k(a)=1,r'(a)\in\{0,1\}} r(a)}{\left|\{a\in\Delta(\tau)\,|\,f_k(a)=1,r'(a)\in\{0,1\}\}\right|}\in[-1,1],$$

$$\circ\ \bar{y}_{-i}(\tau)=\frac{\sum\limits_{a\in\Delta(\tau)|f_k(a)=2,r'(a)\in\{0,1\}} r(a)}{\left|\{a\in\Delta(\tau)\,|\,f_k(a)=2,r'(a)\in\{0,1\}\}\right|}\in[-1,1].$$

The network influence is mass or background for the agent: all opinions and actions of the network are considered regardless of the agent's knowledge of them.

• *The influence of the agent's own actions and opinions on himself*, given by

$$\circ\ \bar{r}_{i}(\tau)=\frac{\sum\limits_{a\in\delta^{\pm}_{i,1}(\tau)} r(a)}{\left|\delta^{\pm}_{i,1}(\tau)\right|},$$

$$\circ\ \bar{y}_{i}(\tau)=\frac{\sum\limits_{a\in\delta^{\pm}_{i,2}(\tau)} r(a)}{\left|\delta^{\pm}_{i,2}(\tau)\right|}.$$

• The indirect influence of friends on the agent's opinion (action) $h\in[-1,1]$, given by

$$\circ\ \bar{r}_{N_i}(\tau)=\sum_{j\in N_i,\ \delta^{\pm}_{j,1}(\tau)\neq\varnothing} e_{ij}\frac{\sum\limits_{a\in\delta^{\pm}_{j,1}(\tau)} E_i\left(h,\ r(a)\right)r(a)}{\left|\delta^{\pm}_{j,1}(\tau)\right|},$$

$$\circ\ \bar{y}_{N_i}(\tau)=\sum_{j\in N_i,\ \delta^{\pm}_{j,2}(\tau)\neq\varnothing} e_{ij}\frac{\sum\limits_{a\in\delta^{\pm}_{j,2}(\tau)} E_i\left(h,\ r(a)\right)r(a)}{\left|\delta^{\pm}_{j,2}(\tau)\right|},$$

where $e_{ij}\in[0,\ 1]$ is the trust of agent i in his friend j, $\sum\limits_{j\in N_i} e_{ij}=1$, and E_i denotes the information trust function of agent i (his trust in the information content with the range [0, 1]). Here, the influence on the agent's opinion (or action) is estimated at the beginning of the interval τ.

As a result, the change in the opinion of agent $i\in N$ between successive time instants $(m-1)$ and m (on the time interval $\tau=[t_{m-1},t_m)$) is determined by the influence of the entire network ($\bar{r}^{m-1}_{-i}=\bar{r}_{-i}(\tau)$, $\bar{y}^{m-1}_{-i}=\bar{y}_{-i}(\tau)$), the influence of the agent's own actions ($\bar{y}^{m-1}_{i}=\bar{y}_{i}(\tau)$), and the influence of his friends ($\bar{r}^{m-1}_{N_i}=\bar{r}_{N_i}(\tau)$, $\bar{y}^{m-1}_{N_i}=\bar{y}_{N_i}(\tau)$). In turn, the change in the action of agent $i\in N$ between successive time instants $(l-1)$ and l (on the time interval $\tau=[t_{l-1},t_l)$) is determined by the influence of the entire network ($\bar{r}^{l-1}_{-i}=\bar{r}_{-i}(\tau)$, $\bar{y}^{l-1}_{-i}=\bar{y}_{-i}(\tau)$), the influence of the agent's own opinions ($\bar{r}^{l-1}_{i}=\bar{r}_{i}(\tau)$), and the influence of his friends ($\bar{r}^{l-1}_{N_i}=\bar{r}_{N_i}(\tau)$, $\bar{y}^{l-1}_{N_i}=\bar{y}_{N_i}(\tau)$). The corresponding binary micro models of the joint dynamics of opinions and actions will be built *for significant agents*.[4]

2.1. Threshold Models

Besides the linear models, the second "classical" approach to describing the dynamics of collective behavior involves *threshold* micro models. In such models, an agent performs a certain action or agrees with a certain opinion only when social pressure is higher (lower) than his individual threshold [6–13]. Threshold models reflect the effects known in social psychology, according to which an individual's inclination to conformity threshold behavior is a predictor of his decisions.

Assume that agents in a social network are either *conformists* or *anti-conformists* undergoing social pressure $u\in[-1,\ 1]$. Conventionally, conformists succumb to the pressure, while *anti-conformists* express opinions and perform actions opposite to the pressure. The following threshold model is a special case of the basic model:

– For a conformist, the opinion is given by

$$r^{m}_{i}=\begin{cases}1, & u^{m-1}_{-i}\geq\theta_{i,1}\\ -1, & u^{m-1}_{-i}<\theta_{i,1},\end{cases}\qquad(1)$$

where $m=1,\ 2\ldots$, and $\theta_{i,1}\in[-1,\ 1+\epsilon]$ denotes his individual opinion *threshold*; the action is given by

$$y^{l}_{i}=\begin{cases}1, & u^{l-1}_{-i}\geq\theta_{i,2}\\ -1, & u^{l-1}_{-i}<\theta_{i,2},\end{cases}\qquad(2)$$

where $l=1,\ 2\ldots,$ and $\theta_{i,2}\in[-1,\ 1+\epsilon]$ denotes his individual action threshold.

[4] The agents who showed the minimum network activity required for modeling. The criteria for selecting significant agents were described in part I of the study [1].

– For an anti-conformist, the opinion is given by

$$r_i^m = \begin{cases} -1, & u_{-i}^{m-1} \geq \theta_{i,1} \\ 1, & u_{-i}^{m-1} < \theta_{i,1}, \end{cases} \quad (3)$$

where $m = 1, 2\ldots$, and $\theta_{i,1} \in [-1, 1+\epsilon]$ denotes his individual opinion *threshold*; the action is given by

$$y_i^l = \begin{cases} -1, & u_{-i}^{l-1} \geq \theta_{i,2} \\ 1, & u_{-i}^{l-1} < \theta_{i,2} \end{cases}, \quad (4)$$

where $l = 1, 2\ldots,$ and $\theta_{i,2} \in [-1, 1+\epsilon]$ denotes his individual action threshold.

The quality of models (1)–(4) will be assessed using the *balanced accuracy* measure [14]

$$\frac{1}{2}\left(\frac{TP}{TP+FN} + \frac{TN}{TN+FP}\right) \quad (5)$$

with the following notations: TP is the number of agent's "for" opinions correctly determined by the model; FN is the number of agent's "for" opinions incorrectly determined by the model; TN is the number of agent's "against" opinions correctly determined by the model; finally, FP is the number of agent's "against" opinions incorrectly determined by the model. (This measure takes into account the imbalance of opinions expressed by agents; as a rule, one opinion prevails for an agent.)

Consider several threshold micro models in ascending order of their complexity:

(I) micro models where changes in opinions and actions are due to the influence of the network;

(II) unified micro models, which include the influence of the network and friends;

(III) personalized micro models (besides the influence of the network and friends, the agents' trust functions reflect their individual characteristics).

(I) Threshold micro models with network influence

In these models, the agent's opinion (action) at the current time instant depends on the background influence of the entire network at the previous time instant and his individual threshold. We define the influence of the network in two ways as follows:

- $u_{-i}^{m-1} = \bar{r}_{-i}^{m-1}$;
- $u_{-i}^{m-1} = \bar{y}_{-i}^{m-1}$.

In addition, consider the case of two (lower and upper) thresholds: $\breve{\theta}_i, \hat{\theta}_i \in [-1, 1+\varepsilon]$, where $\breve{\theta}_i \leq \hat{\theta}_i$. The opinion of a conformist at a time instant m is given by (cf. formula (1))

$$r_i^m = \begin{cases} 1, & u_{-i}^{m-1} \geq \hat{\theta}_{i,1} \\ -1, & u_{-i}^{m-1} < \breve{\theta}_{i,1} \\ r_i^{m-1}, & u_{-i}^{m-1} \in [\breve{\theta}_{i,1}, \hat{\theta}_{i,1}). \end{cases} \quad (6)$$

The opinion of an anti-conformist is given by (cf. formula (3))

$$r_i^m = \begin{cases} -1, & u_{-i}^{m-1} \geq \hat{\theta}_{i,1} \\ 1, & u_{-i}^{m-1} < \breve{\theta}_{i,1} \\ r_i^{m-1}, & u_{-i}^{m-1} \in [\breve{\theta}_{i,1}, \hat{\theta}_{i,1}). \end{cases} \quad (7)$$

The dynamics of actions are defined by analogy. Possible modifications of opinion dynamics models and the results of their parameter identification are presented in Tables 1 and 2, respectively.

The following conclusions can be drawn from Tables 1 and 2:

– On average, the quality of models (6) and (7) is satisfactory.

– Considering both conformists and anti-conformists significantly improves the average quality of the threshold models.

– Introducing two thresholds leads to a smaller quality gain.

Table 1

Identification results for threshold models of opinion dynamics

Types of agents	Type of influence	One threshold	Two thresholds
Conformists	Network opinions	Quality 0.73 (median 0.71)	Quality 0.79 (median 0.78)
	Network actions	Quality 0.72 (median 0.68)	Quality 0.78 (median 0.77)
Conformists and anti-conformists	Network opinions	Quality 0.83 (median 0.83)	Quality 0.86 (median 0.87)
	Network actions	Quality 0.83 (median 0.82)	Quality 0.86 (median 0.88)

Table 2

Identification results of threshold models of action dynamics

Types of agents	Type of influence	One threshold	Two thresholds
Conformists	Network opinions	Quality 0.73 (median 0.69)	Quality 0.76 (median 0.73)
	Network actions	Quality 0.71 (median 0.70)	Quality 0.75 (median 0.73)
Conformists and anti-conformists	Network opinions	Quality 0.78 (median 0.75)	Quality 0.81 (median 0.8)
	Network actions	Quality 0.76 (median 0.75)	Quality 0.80 (median 0.78)

(II) Unified threshold micro models

In such models, we estimate the change in the agent's opinions and actions depending on the influence of his friends:

- $u_{-i}^{m-1} = \overline{r}_{N_i}^{m-1}$;
- $u_{-i}^{m-1} = \overline{y}_{N_i}^{m-1}$.

Each agent does not "distinguish" between friends (treating friends as one meta-agent) and trusts the information source regardless of its content.

Unexpectedly, considering only the influence of friends deteriorates quality compared to the models with macro variables (Table 3).

Table 3

Identification results for dynamic models

Types of agents	Type of influence	Models of opinion dynamics	Models of action dynamics
Conformists and anti-conformists	Opinions of friends	Quality 0.66 (median 0.61)	Quality 0.66 (median 0.62)
	Actions of friends	Quality 0.70 (median 0.67)	Quality 0.68 (median 0.65)

(III) Personalized threshold micro models

In personalized models, the best configuration of hyperparameters is chosen for each agent: the types of his trust functions for information and friends.

Like in part II [2], we consider the following common types of *information trust* functions $E(\cdot)$: $E_C(h,g)$ (*simpletons*), $E_\varepsilon^+(h,g)$ (*conservatives*), and $E_\varepsilon^-(h,g)$ (*innovators*). As a common type of the *friend trust* function $e(\cdot)$, we consider a "non-differentiating" function (the agent treats his friends as one meta-agent) and functions where the trust in a friend is proportional to:

– unity;
– the number of friends of this friend;
– the number of friends shared with this friend;
– unity if this friend is active (i.e., has an opinion or commits acts);
– the number of friends of this friend if he is active;
– the number of friends shared with this friend if he is active;
– the friend's activity by comments;
– the friend's activity by likes or his popularity.

The personalized description of friends' influence improves quality on average (Table 4) but still does not surpass the quality of models with macro variables (i.e., the models with network influence).

Table 4

Identification results for dynamic models

Types of agents	Type of influence	Models of opinion dynamics	Models of action dynamics
Conformists and anti-conformists	Opinions of friends	Quality 0.69 (median 0.62)	Quality 0.72 (median 0.68)
	Actions of friends	Quality 0.75 (median 0.70)	Quality 0.76 (median 0.75)

The preferable type of the information trust function. Consider the models with the influence of friends' opinions. As it turns out, for the majority of agents, the type of the information trust function is not important. "Pure" innovators form 12% of the agents (the models of opinion dynamics) and 27% of the agents (the models of action dynamics). Pure conservatives constitute 4% of the agents (the models of opinion dynamics) and 10% of the agents (the models of action dynamics). Note that there are no pure simpletons (Fig. 1).

Consider the models with the influence of friends' actions. In these models, the type of the information trust function does not matter for 44% of the agents (the models of opinion dynamics) and for 39% of the agents (the models of action dynamics); see Fig. 2.

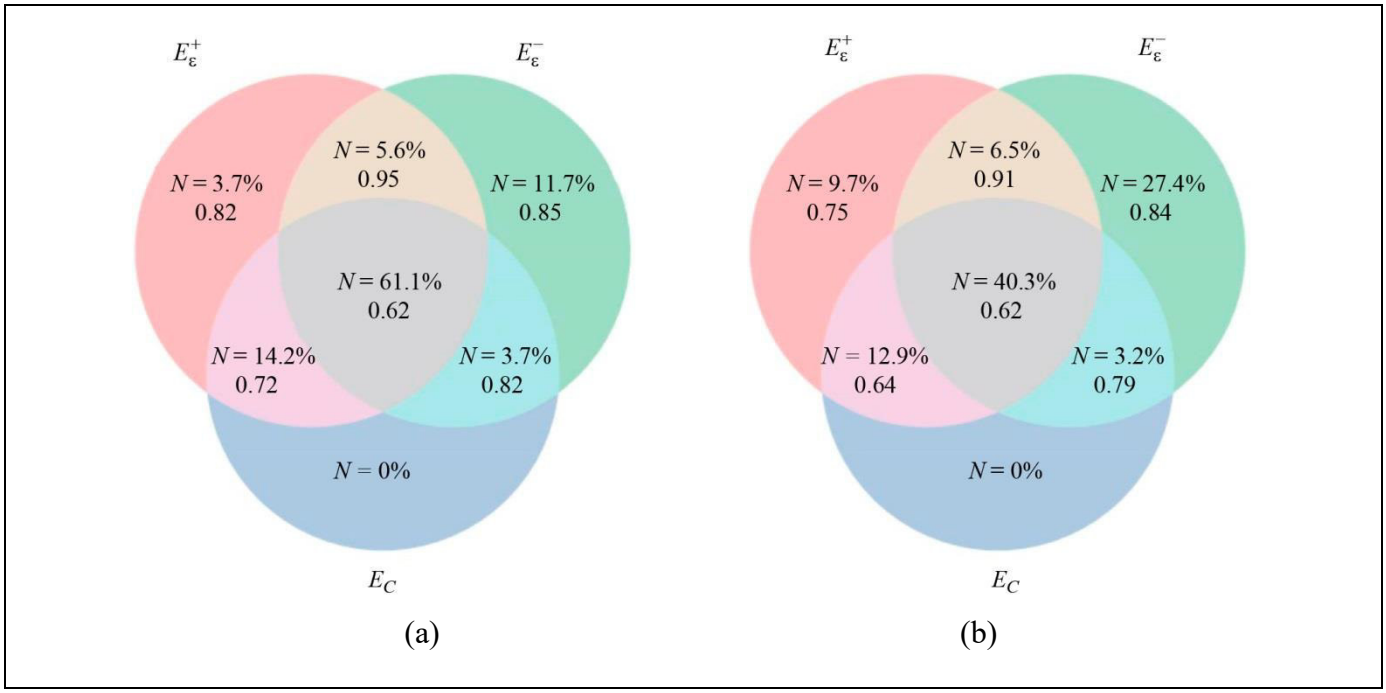

Fig. 1. The Euler–Venn diagram of preferability of information trust functions with the influence of friends' opinions: (a) the models of opinion dynamics and (b) the models of action dynamics.

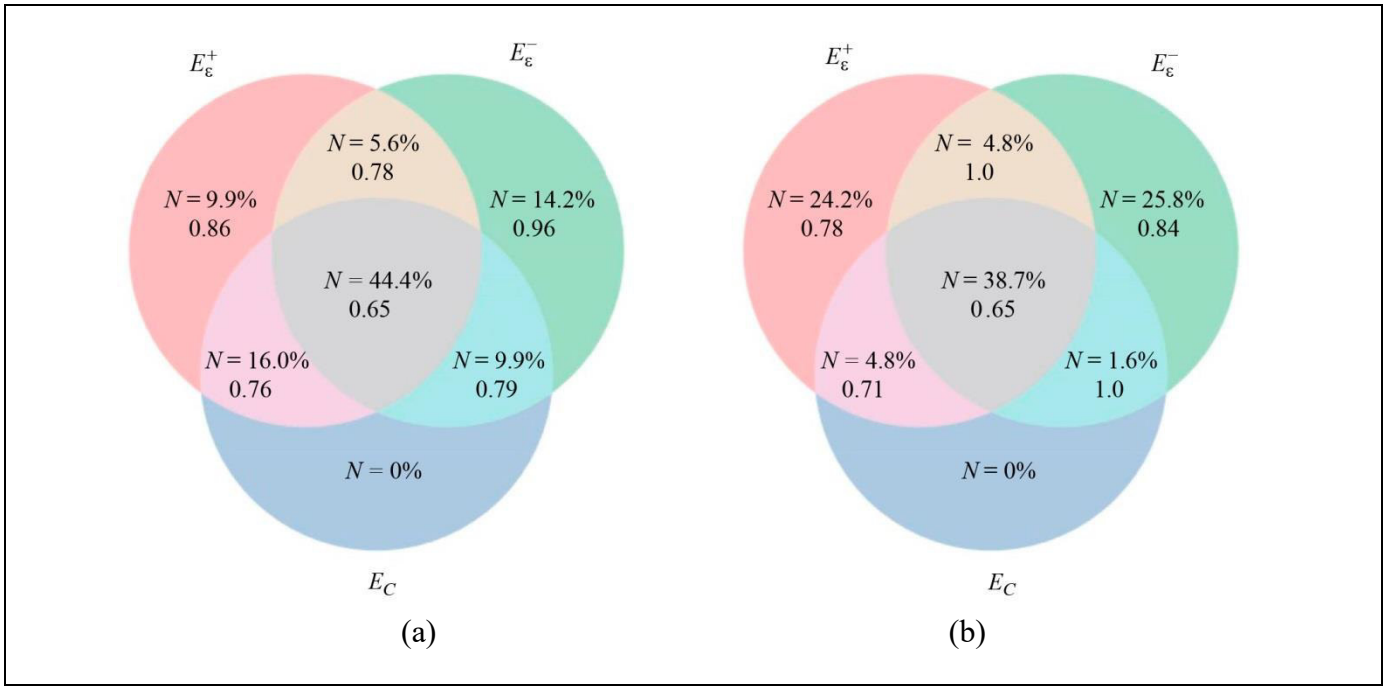

Fig. 2. The Euler–Venn diagram of preferability of information trust functions with the influence of friends' actions: (a) the models of opinion dynamics and (b) the models of action dynamics.

"Pure" innovators form 14% of the agents (the models of opinion dynamics) and 26% of the agents (the models of action dynamics). Pure conservatives constitute 10% of the agents (the models of opinion dynamics) and 24% of the agents (the models of action dynamics). Pure simpletons are absent as well.

The preferable type of the friend trust function. In general, the type of the friend trust function is not important for agents. Also, for a significant share of the agents, trusting friends as a meta-agent or trusting them separately with the same level give identical quality results (Figs. 3 and 4).

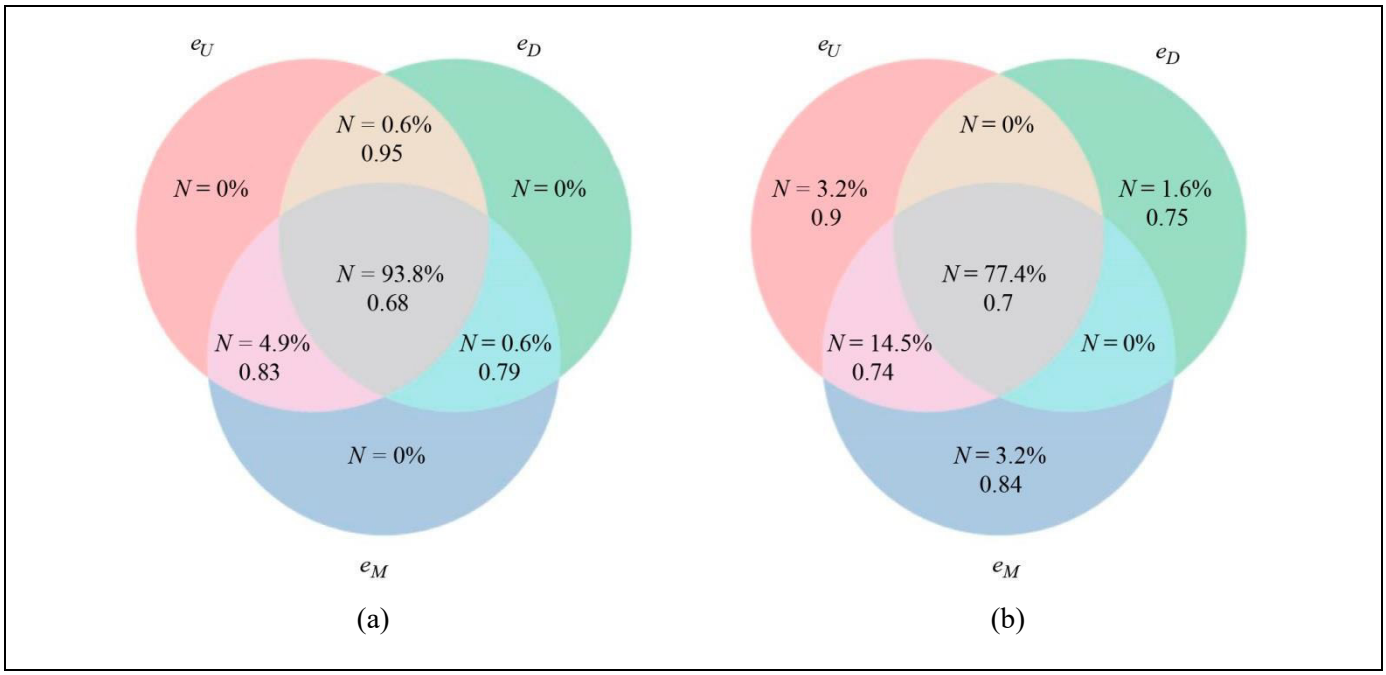

Fig. 3. The Euler–Venn diagram of preferability of friend trust functions with the influence of friends' opinions: (a) the models of opinion dynamics and (b) the models of action dynamics.

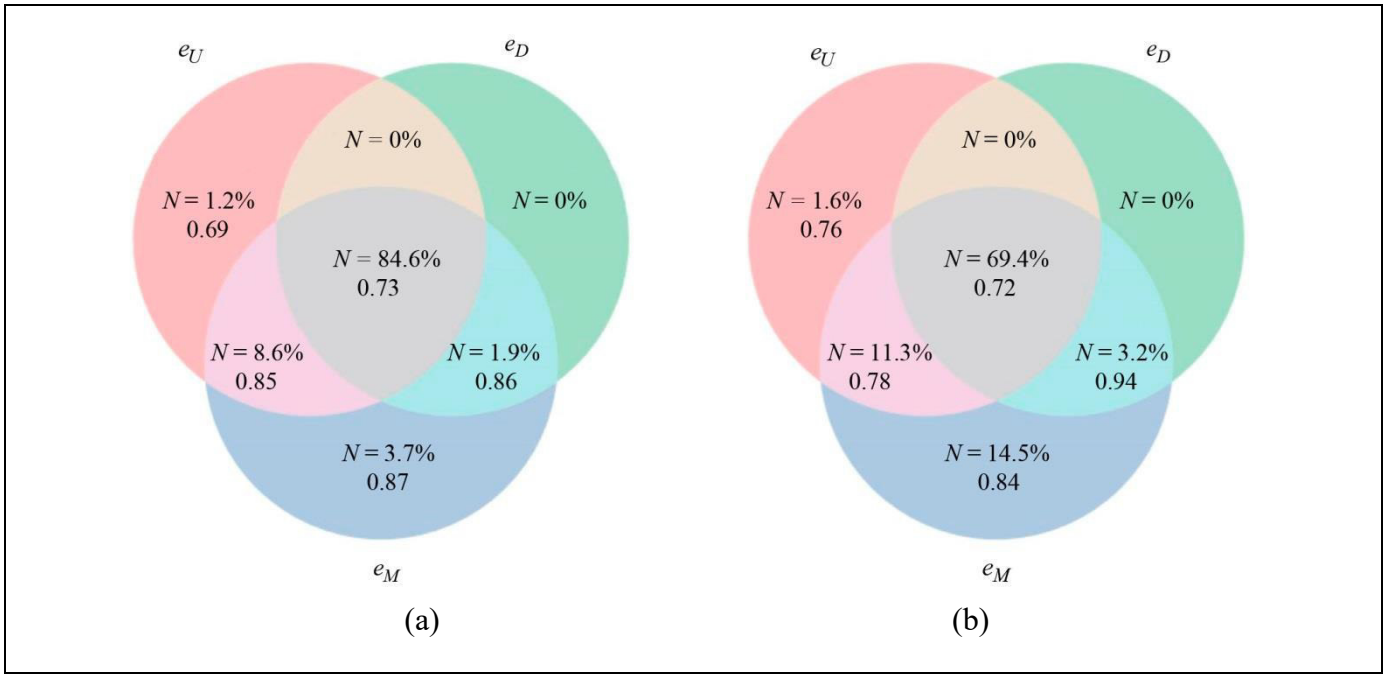

Fig. 4. The Euler–Venn diagram of preferability of friend trust functions with the influence of friends' actions: (a) the models of opinion dynamics and (b) the models of action dynamics.

2.2. Comparison of Linear and Threshold Models

To answer Question no. 4 (linear vs. threshold models, see the Introduction), it is necessary to use the same quality criterion. Threshold models consider discrete opinions (actions) agents; therefore, the forecasting results in linear models have to be preliminarily discretized in order to calculate the quality (5). Assume that if the forecast is greater than 0, its discrete value is 1; otherwise, –1.

Table 5 presents the average quality of the linear and threshold models (over the set of agents).

Table 5

Quality comparison: linear vs. threshold models

Class of models	Type of models	Quality of models	
		Opinion dynamics	Action dynamics
Linear models	Network influence	0.62	0.58
	Unified	0.70	0.62
	Personalized	0.80	0.77
Threshold models	Network influence	0.78	0.76
	Unified	0.70	0.68
	Personalized	0.75	0.76

Note. Table 5 presents the best results of the threshold models. For example, if the unified models with the influence of friends' actions demonstrate higher results than those with the influence of friends' opinions, then only the former results are given therein.

We emphasize in contrast to the linear models with the complete set of explanatory variables, the threshold models use only one of the following explanatory variables: network actions, network opinions, friends' actions, or friends' opinions. Despite this peculiarity, the threshold models have comparable quality (in the case of threshold models with network influence, even a significantly higher quality).

2.3. Models with Hidden States and Observed Actions

An alternative to the approach above (the separation of opinions (comments) and actions (likes)) is the introduction of hidden variables (opinions) and their identification by observed "actions" (comments and likes) within hidden Markov models, Bayesian networks, etc. For example, see the papers [15, 16].

Consider a model with the agent's *state* as a hidden (latent) variable taking a value $\theta_t \in [0, 1]$ at a time instant t. Suppose that the state is not directly observable but determines the agent's observed binary "*actions*" $x_t \in \{0; 1\}$ (the tones of his comments and the comments liked by him) in the following probabilistic way: at each time instant when the agent performs such an action, this action is independently equal to 1 (unit action, "for" wearing masks) with a probability θ_t and to 0 with the probability $(1 - \theta_t)$ (zero action, "against" wearing masks). In other words, the action is a random variable described by the Bernoulli distribution with the density

$$p(x,\theta) = \theta^x (1-\theta)^{1-x}. \qquad (8)$$

Given the vector of observed actions $x = (x_1, x_2, \ldots, x_T)$ for T sequential time instants, the optimal current state estimate (by the maximum likelihood criterion) has the form

$$\theta(t) = \frac{1}{t}\sum_{\tau=1}^{t} x_\tau.$$

Let the agent's state have changed once from a known initial value θ^1 to a known final value θ^2. In this case, the change point t_p is a posteriori estimated by the cumulative sums method as

$$t_p = \inf\left\{t : S_{t-1} \geq S_\tau,\ \tau = \overline{2,T}\right\},$$

where

$$S_t = t \ln\frac{1-\theta^1}{1-\theta^2} + \sum_{\tau=1}^{t} x_\tau \ln\frac{\theta^1(1-\theta^2)}{\theta^2(1-\theta^1)}.$$

(For details, see the expression (2.3.3) in [17].)

If the initial and final values are unknown, the change point t_p is a posteriori estimated as [18]

$$t_p = \arg\max_{t=\overline{1,T-1}} d(x,t), \qquad (9)$$

where $d(x,t) = t(T-t)\left[\frac{1}{t}\sum_{\tau=1}^{t} x_\tau - \frac{1}{T-t}\sum_{\tau=t+1}^{T} x_\tau\right]^2$.

Whenever the one-time change is not justified, the latent variables can be estimated using the moving average method:

$$\theta_\Delta(t) = \frac{1}{\Delta}\sum_{\tau=t-\Delta}^{t} x_\tau.$$

Here, the window Δ is tuned depending on the available experimental data.

Now we proceed to the identification of hidden variables (the states of agents) based on the available information about their actions in the social network. The procedure (9) allows finding the single change point for a sequence of agent's actions in the network. Consider the agents who have performed at least 10 zero or unit actions with at least one unit action and one zero action. In total, there are about 2000 such agents (4% of the total number of agents who performed unit or zero actions). For each agent of this group, we determine the change point t_p and the corresponding estimates θ^1 and θ^2. First, the values $D = \max_{t=\overline{1,T-1}} d(x,t)$ and $\tilde{D} = D/T^2$ are calculated. Then the quality of detecting the single change point is assessed using the value $\tilde{D}$ and the variation of the maximum likelihood:

$$L_+ = \max_{t=\overline{1,T-1}}\left(\max_\theta L\left(x_{\overline{1,t}},\theta\right) + \max_\theta L\left(x_{\overline{t+1,T}},\theta\right)\right) - \max_\theta L\left(x_{\overline{1,T}},\theta\right),$$

where $L\left(x_{\overline{a,b}},\theta\right)=\sum_{\tau=a}^{b}\left[x_\tau\ln(\theta)+(1-x_\tau)\ln(1-\theta)\right]$ is the logarithmic likelihood function on the interval $\overline{a,b}$.

The following results were obtained. Figure 5 shows the distribution of the normalized change points (normalization by T). Clearly, in many cases, the change point is shifted to the start of the agents' activity.

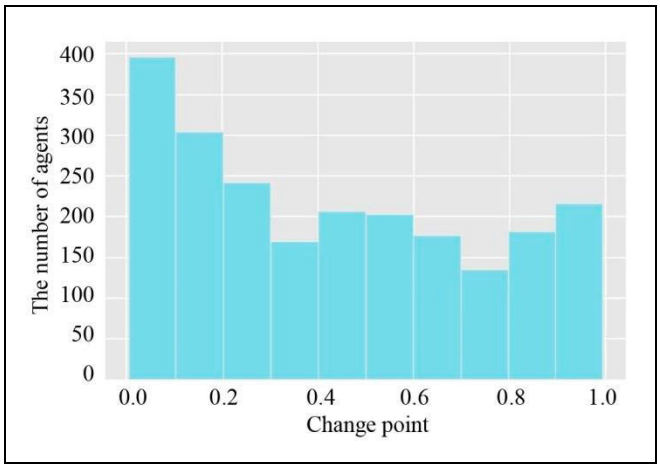

Fig. 5. The distribution of change points.

Next, Figure 6 demonstrates a histogram of the distribution of the differences between θ^1 and θ^2 (in absolute terms). For 18% of the users, the hidden state changes insignificantly (by at most 0.2); for half of the users, by at least 0.5. Thus, the state of the bulk of users undergoes a significant change. (Of course, the change point must "meaningfully" separate the sequence of actions for each agent.)

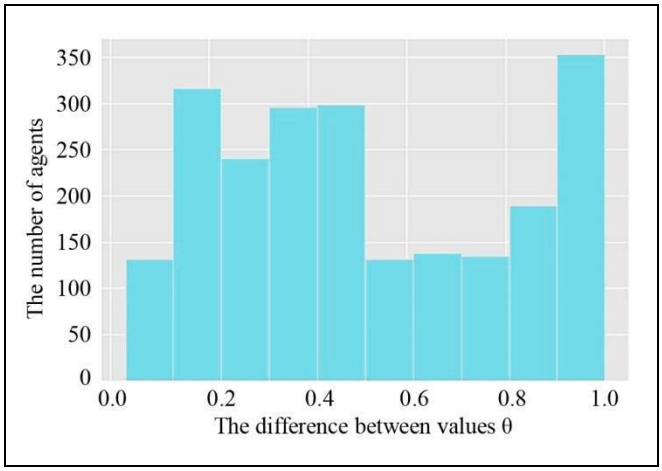

Fig. 6. The distribution of the difference $|\theta^1-\theta^2|$.

Figure 7 shows a histogram of the distribution of the value L_+. For a quarter of the agents from the considered set, the likelihood value improves at least by 3.25.

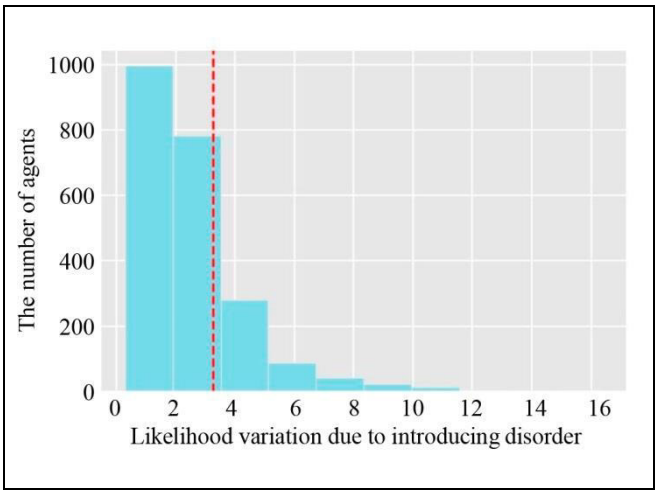

Fig. 7. The distribution of the likelihood variation due to introducing change point.

Finally, Fig. 8 presents a histogram of the distribution of the value $\tilde{D}$. For one quarter of the agents, $\tilde{D}$ is not smaller than 0.06. This value can be used as a threshold to scissor "bad" cases.

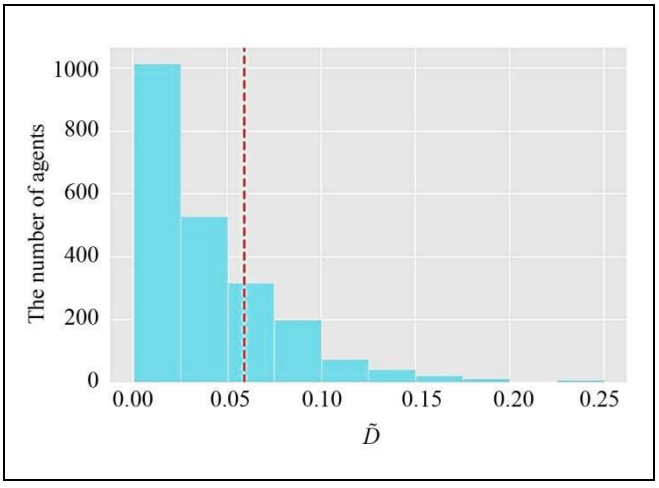

Fig. 8. The distribution of the value $\tilde{D}$.

The values L_+ and $\tilde{D}$ are well correlated with each other: their Spearman's correlation coefficient is 0.64. In addition, the values $|\theta^1-\theta^2|$ and L_+ as well as $|\theta^1-\theta^2|$ and $\tilde{D}$ correlate well with each other (0.65 and 0.83, respectively). The quality of the disorder will be assessed mainly using the value L_+.

Figure 9 shows a scatter diagram (more precisely, a heat map) for the identified hidden parameters of the network agents before and after the disorder.

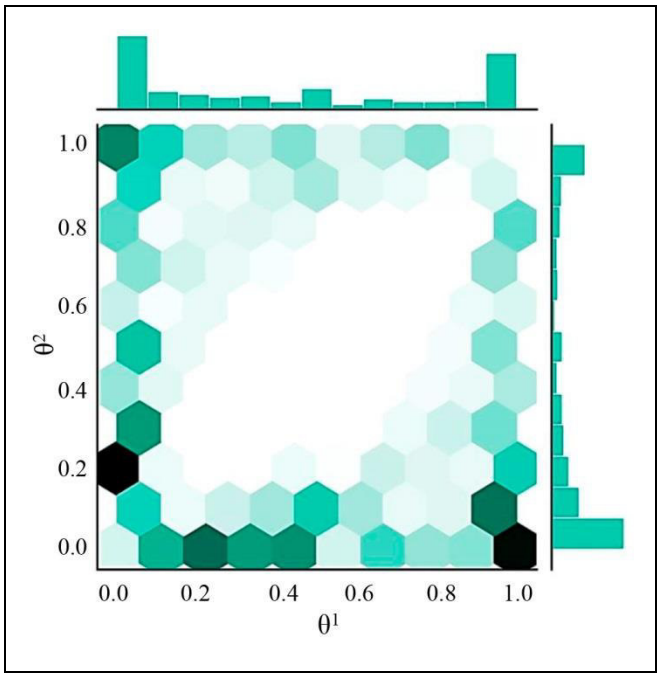

Fig. 9. The heat map of the parameters θ^1 and θ^2 (the agent's hidden state before and after disorder). The darker the color of the hexagon is, the more agents it contains.

The diagonal of this diagram is "empty": the agents change their state.

As an example, Fig. 10a demonstrates a time series of agent's actions for which $L_+ = 11.09$ (the likelihood gain due to introducing disorder). The zero and unit values are indicated by large dots; the disorder time, by a dashed red line. The found values of the agent's hidden state are given to the left and right of the disorder time. Figure 10b shows the graph of the agent's function $d(t)$ as well as the values D (its maximum) and $\tilde{D}$ (its normalized maximum).

The disorder detection method (9) works well for homogeneous sequences (with relatively clear switching from 0 to 1 and vice versa) but worse for sequences where θ^1 and θ^2 are close or zero and unit actions alternate. Therefore, we form the following heuristic criteria to identify agents with a single disorder:

- The change point is in the sequence $1 < t_p < T - 1$.
- The sequence contains at least two "for" actions and two "against" actions.
- The variance of the value $\theta_{\Delta=2}(t)$ before and after the disorder does not exceed 0.12.
- The estimate of the state θ changes at least by 0.1.
- The likelihood variation is $L_+ > 2.86$.

The criterion thresholds were obtained by the expertise of the sequences of agents in descending order of their criterion values. A total of 320 agents with a single disorder were found.

Linear micro models and the agent's hidden state

Consider the micro models of the joint dynamics of opinions and actions for significant agents (see part II [2]) and include the agent's hidden state in them.

- **The model with the variable θ.** For each agent, we find the change point and calculate the hidden state before and after it ($\theta = \theta^1$ and $\theta = \theta^2$, respectively). Let us conduct a series of computational experiments as follows. In each experiment, a sequence of agents' actions is generated by model (8) with hidden states and observed actions; then the degree of its similarity to the observed sequence is assessed. The resulting estimates are averaged to obtain the quality of the model with the variable θ.
- **The inertial model with θ.** We add the variable θ in the inertial model and estimate the quality of the new model.
- **The unified model with θ.** We add the variable θ in the unified model and estimate the quality of the new model.
- **The personalized model with θ.** We add the variable θ in the personalized model and estimate the quality of the new model.

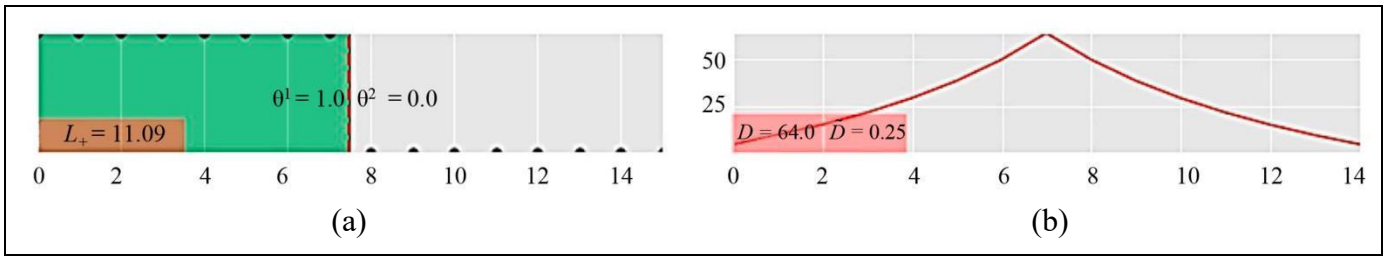

Fig. 10. (a) the time series of agent's actions and (b) the graph of $d(x, t)$.

As it turns out, the balanced accuracy measure of the model with the variable θ is 0.70 (opinion model) and 0.64 (action model). Table 6 summarizes the estimated quality gain of the linear micro models due to introducing the variable θ.

Table 6

Quality gain of linear micro models due to introducing the variable θ

Type of models	Relative error reduction for opinion model	Relative error reduction for action model
Inertial models	– 59%	– 56%
Unified models	– 17%	– 7%
Personalized models	– 17%	– 8%

The maximum quality gain occurs for the inertial model (an error reduction of 56–59%); the contribution of the latent state is smaller for the unified model (7–17%) and for the personalized model (8–17%). In general, introducing the latent variables gives approximately an additional "net" quality gain of 2% for the models of opinion and action dynamics.

CONCLUSIONS

This multi-part study has been devoted to the joint dynamics of the opinions and actions of *VKontakte* users (on the example of their attitudes towards wearing medical masks during the first year of the COVID-19 pandemic). Based on the results, we have verified mathematical models of the relationship between changes in the opinions and actions of agents. The most important outcomes are as follows (see the previous parts [1, 2]).

In part I of the study [1], the opinions of *VKontakte* users have been identified and then a primary analysis of the joint dynamics of opinions and actions in the network has been carried out. Among other things, the polarization of positions (opinions and actions) in the network and the gradually increasing share of "against" positions have been discovered. The analysis of network interactions has shown that there are no echo chambers in the network and agents are exposed to the information influence of different positions of the social environment and, as a consequence, can change their opinions. The consistency and mutual influence of agents' opinions and actions have been revealed (see Questions nos. 1 and 5 in the Introduction). In addition, the so-called *significant agents* have been found and characterized; they changed their opinions during the period under consideration (see Questions nos. 2 and 3).

In part II [2] and this paper, formal models of opinion and action dynamics have been identified and investigated (see Question no. 6). Different modifications of macro models have been considered where the "public" opinion and action in the network (i.e., the share of "for" or "against" opinions and actions) at the current time instant depends on the opinions and actions at the previous one. Also, different modifications of the micro models (linear and threshold models) have been considered; they take into account the influence of the entire network, the influence of the agent's friends, and his personal characteristics. According to the identification results of these macro models, there exists a relationship between actions and opinions in the network.

Micro models have been considered only for significant agents. The quality of such models is acceptable and improves as they become more complex. In the class of linear micro models, the largest error is given by the inertial model (Fig. 11); moderate errors, by the model with macro variable(s) (with 1–4 variables; see Fig. 11) and the unified model (see "Unif." in Fig. 11); the smallest error, by the personalized model (see "Pers." in Fig. 11), in which each agent can have an individual trust function. The contribution of the latent variables for linear models is about 2% (see "Pers.+θ" in Fig. 11).

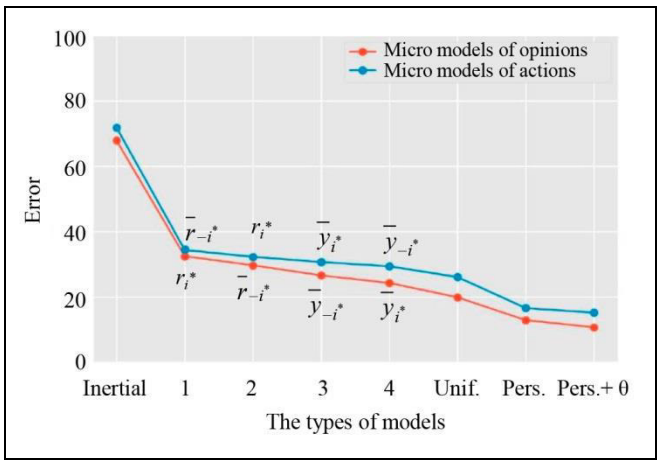

Fig. 11. The quality of linear micro models of agents' opinions and actions.

Among the threshold micro models (see Question no. 4), the models with network influence show the best quality, followed by personalized and unified models with the influence of friends. Considering anti-conformity significantly improves the quality of the models on average; however, introducing the second threshold does not produce the same effect. In the case of personalized threshold models, the type of information trust functions is not important for a high share of agents (about 40%); the share of those trusting information that diverges from their opinion is greater than the share of those trusting information that coincides with their opinion; meanwhile, there are almost no agents trusting information regardless of its content. Also, the choice of friend trust functions is not determinant in threshold models (see Question no. 7).

The threshold and linear models demonstrate approximately the same quality. But threshold models involve fewer parameters and seem to be preferable (see Question no. 4).

The "promotional" version of outcomes of this multi-part study can be formulated as follows. A very small proportion of people (about 1%) change their opinions (beliefs, actions, etc.). These dynamics are largely influenced by their own initial beliefs[5] (conditionally, about 67% of influence on average; see Fig. 12), less by the social environment (about 15% of influence of the opinions and actions of other network agents) and their own actions (about 3% of influence, the contribution of cognitive dissonance), by latent factors (about 2% of influence), and other (off-model and (or) random) factors (about 13% of influence). At the same time, people often focus on information that strongly differs from their current beliefs.

A promising line for further research is to analyze more complex mechanisms of changing the opinions and actions of social network agents, e.g., with the agent's "memory," the influence of exogenous factors on the network, and even more "subtle" effects: the relationship of the agent's opinion on a current issue with his opinions on related issues (e.g., COVID-19 aspects), the influence of arguments and emotions in network messages (actions) on the agent's opinion, the influence of individual characteristics of the agent (e.g., the degree of rationality), etc.

[5] Note separate and very important and interesting questions as follows. Where do these "initial beliefs" come from? How are they formed? Indeed, this multi-part study considers the period from the very beginning of the COVID-19 pandemic (March 2020): before it, few people on Earth thought about the benefits of wearing medical masks.

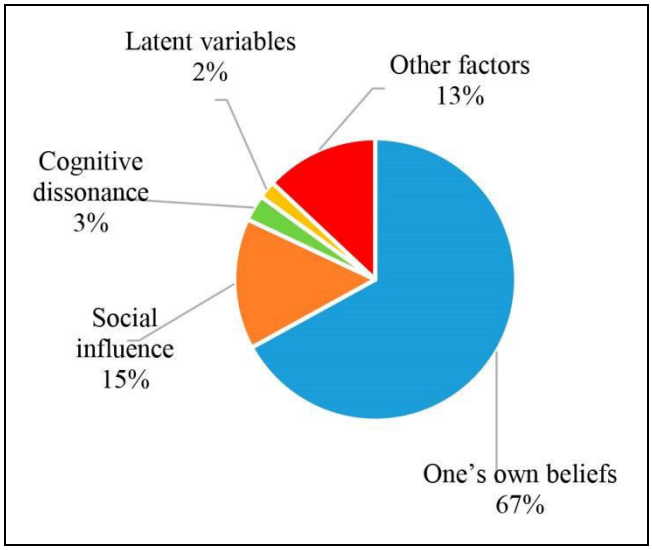

Fig. 12. The influence of different factors on agent's opinions.

REFERENCES

1. Gubanov, D.A. and Novikov, D.A., Models of Joint Dynamics of Opinions and Actions in Online Social Networks. Part I: Primary Data Analysis, *Control Sciences*, 2023, no. 2, pp. 31–45.
2. Gubanov, D.A. and Novikov, D.A., Models of Joint Dynamics of Opinions and Actions in Online Social Networks. Part II: Linear Models, *Control Sciences*, 2023, no. 3, pp. 31–54.
3. Gubanov, D.A. A Study of Formalizations of User Influence in Actional Model / Proceedings of the 13th International Conference "Management of Large-Scale System Development" (MLSD). Moscow, Russia: IEEE, 2020, pp. 1–5. URL: https://ieeexplore.ieee.org/document/9247658.
4. Gubanov, D.A. and Chkhartishvili, A.G., Meta-agent and User Influence Levels in a Social Network, *Control Sciences*, 2016, no. 6, pp. 12–17. (In Russian.)
5. Novikov, D.A., Dynamics Models of Mental and Behavioral Components of Activity in Collective Decision-Making, *Large-Scale Systems Control*, 2020, vol. 85, pp. 206–237. (In Russian.)
6. Breer, V.V., Novikov, D.A., and Rogatkin, A.D., *Mob Control: Models of Threshold Collective Behavior*, Studies in Systems, Decision and Control, vol 85, Cham: Springer, 2017.
7. Gubanov, D.A., Novikov, D.A., and Chkhartishvili, A.G., *Social Networks: Models of Information Influence, Control and Confrontation*, Cham: Springer, 2019.
8. Flache, A., Mäs, M., Feliciani, T., et al., Models of Social Influence: Towards the Next Frontiers, *The Journal of Artificial Societies and Social Simulation*, 2017, vol. 20, no. 4. DOI: 10.18564/jasss.3521.
9. Granovetter, M., Threshold Models of Collective Behavior, *The American Journal of Sociology*, 1978, vol. 83, no. 6, pp. 1420–1443.
10. Karimi, F. and Holme, P., Threshold Model of Cascades in Empirical Temporal Networks, *Physica A: Statistical Mechanics and Its Applications*, 2013, vol. 392, no. 16, pp. 3476–3483.

11.Kempe, D., Kleinberg, J., and Tardos, E., Maximizing the Spread of Influence through a Social Network, *Theory of Computing*, 2015, vol. 11, no. 4, pp. 105–147.
12.Schelling, T., *Micromotives and Macrobehaviour*, New York, London: Norton & Co Ltd, 1978.
13.Semenov, A., Veremyev, A., Pasiliao, E.L., and Boginski, V., Double-Threshold Models for Network Influence Propagation, *Computational Data and Social Networks: 9th International Conference* (*CSoNet 2020*), Dallas, 2020, pp. 512–523.
14.Brodersen, K., Ong, C., Stephan, K., and Buhmann, J., The Balanced Accuracy and Its Posterior Distribution, *Proceedings of the 20th International Conference on Pattern Recognition*, Istanbul, 2010, pp. 3121–3124.
15.Elliott, R.J., Aggoun, L., and Moore, J.B., *Hidden Markov Models: Estimation and Control*, Luxembourg: Springer Science & Business Media, 2008.
16.Koller, D. and Friedman, N., *Probabilistic Graphical Models: Principles and Techniques*, MIT Press, 2009.
17.Nikiforov, I.V., *Posledovatel'noe obnaruzhenie izmeneniya svoistv vremennykh ryadov* (Sequential Detection of Changes in Time Series Properties), Moscow: Nauka, 1983. (In Russian.)
18.Darkhovskii, B.S. and Brodskii, B.E., A Posteriori Detection of the "Disorder" Time of a Random Sequence, *Theory of Probability & Its Applications*, 1981, vol. 25, no. 3, pp. 624–628.

This paper was recommended for publication by F.T. Aleskerov, a member of the Editorial Board.

Received December 28, 2022, and revised March 27, 2023. Accepted April 5, 2023.

Author information

Gubanov, Dmitry Alekseevich. Dr. Sci. (Eng.), Trapeznikov Institute of Control Sciences, Russian Academy of Sciences, Moscow, Russia
✉ dmitry.a.g@gmail.com
ORCID iD: https://orcid.org/0000-0002-0099-3386

Novikov, Dmitry Aleksandrovich. Academician, Russian Academy of Sciences; Trapeznikov Institute of Control Sciences, Russian Academy of Sciences, Moscow, Russia
✉ novikov@ipu.ru
ORCID iD: https://orcid.org/0000-0002-9314-3304

Cite this paper

Gubanov, D.A. and Novikov, D.A., Models of Joint Dynamics of Opinions and Actions in Online Social Networks. Part III: Binary Models. *Control Sciences* **4**, 12–24 (2023). http://doi.org/10.25728/cs.2023.4.2

Original Russian Text © Gubanov, D.A., Novikov, D.A., 2023, published in *Problemy Upravleniya*, 2023, no. 4, pp. 14–27.

Translated into English by *Alexander Yu. Mazurov*, Cand. Sci. (Phys.–Math.),
Trapeznikov Institute of Control Sciences,
Russian Academy of Sciences, Moscow, Russia
✉ alexander.mazurov08@gmail.com

DOI: http://doi.org/10.25728/cs.2023.4.3

IDENTIFICATION-BASED SPEED CONTROL OF AN OVERHEAD CRANE WITH A REDUCED CARGO TRANSFER MODEL[1]

S.P. Kruglov and S.V. Kovyrshin

Irkutsk State Transport University, Irkutsk, Russia

✉ kruglov_s_p@mail.ru, ✉ sergkow@mail.ru

Abstract. This paper considers an automatic control approach for an overhead crane trolley under the current parametric uncertainty of the crane, transported cargo, and exogenous disturbances. It generates a given trolley speed, which corresponds to the modern hardware implementation of control of cranes with asynchronous motors and frequency converters. The approach is based on a control scheme with a current parametric identification algorithm, an implicit reference model, and "simplified" adaptability conditions to track cargo movements directly. This algorithm involves a recursive least-squares method with the forgetting factor. Unlike previous publications on the topic, the idea is to use a reduced model of the "crane–cargo" object when moving the cargo along one horizontal axis. In this case, it is necessary to estimate only two parameters; moreover, the construction of the control algorithm becomes simpler and the closed-loop control system has a better performance. The stability of the closed-loop control system is proved and requirements for the parameters of the assigned reference motion are found. Due to the self-tuning property of the control system, the approach can be obviously generalized to construct an overhead crane control system along two horizontal axes and three axes (with simultaneous vertical movement of the cargo). A model example is given to demonstrate the implementability of this crane control system based on modern controllers and sensors.

Keywords: automatic control of overhead crane, adaptive control system, parametric identification algorithm, current parametric uncertainty, stability of the closed-loop control system.

INTRODUCTION

Automatic control of cranes with suspended cargo, particularly overhead cranes, is very important due to their mass use and the need to increase the productivity of crane operations and safety, to reduce operating costs, etc. A crane control system is required to move the cargo to a given point with the maximum speed and accuracy, eliminating the pendulum swinging of the suspended cargo. This phenomenon arises due to different factors: inertial swinging at the motion start and stop, wind gusts affecting the cargo, sea waves on ship cranes, etc.

As a rule, modern cranes are characterized by numerous operating modes, a large variation of the parameters of the transported cargo and suspension-length, and the probability of exogenous disturbances. Therefore, the operation of a crane control system is often associated with the current uncertainty of its characteristics as well as the characteristics of the transported cargo and exogenous disturbances.

Many studies on the automatic control of an overhead crane are based on a priori information about the parameters of the crane and the cargo or require the preliminary tuning of the control system. For example, see the papers devoted to the use of PID and PD controllers [1–3] and sliding mode control systems [4–8]. But such systems cannot, in principle, implement high-quality control of the crane in numerous operation modes with a single tuning. A priori information about a controlled object is required when designing optimal control (e.g., see the publications [9, 10]). Much research considers the application of fuzzy logic and neurocontrollers (e.g., see the papers [11, 12]).

[1] **Funding.** This work was supported by the Russian Science Foundation, project no. 23-29-00654; https://rscf.ru/project/23-29-00654/.

However, fuzzy control strategies are rather difficult to tune and neglect uncertain factors. On the other hand, neurocontrollers need significant time for training.

There exist approaches to designing an adaptive crane control system based on the Lyapunov function (e.g., see the papers [13, 14]). Here, the control law parameters are tuned using the gradient algorithm, which leads to the problem of selecting the discrete tuning parameters for a particular case.

The authors [15, 16] proposed an adaptive control approach for an overhead crane trolley based on the direct tracking of horizontal cargo movements with forming a control force or a given speed. Control by a given speed corresponds to modern crane control approaches using asynchronous motors and frequency converters. The approach is based on a control scheme with a current parametric identification algorithm, an implicit reference model, and "simplified" adaptability conditions [17]. The solution allows constructing a relatively simple control law for an overhead crane under the current parametric uncertainty of the crane, transported cargo, and exogenous disturbances.

This paper is a logical continuation of the studies [15, 16]; unlike them, the idea is to use a reduced model of the "crane–cargo" object when moving the cargo along one horizontal axis. In this case, the design of identification and control algorithms becomes simpler and the closed-loop control system has a better performance. The stability of the closed-loop control system with the generated control law is proved and requirements for the parameters of the assigned reference motion are found.

1. PROBLEM STATEMENT

Consider a single-pendulum model of an overhead crane moving cargo along one horizontal axis. We will neglect the weight of the cable on which the cargo is suspended and the resistance during its movements. Figure 1 shows the diagram of this overhead crane.

Figure 1 has the following notations: m_{T} and m_{c} are the masses of the crane trolley and transported cargo, respectively; r_{c} is the radius of the cargo inertia; l is the length of the cargo suspension (the distance between the attachment point of the suspension on the trolley and the cargo's center of gravity; x is the horizontal movement of the trolley from an assigned position; $\dot{x} = v$ is the trolley speed and v_{giv} is a given value of this speed; f_{con} is the control force generated by the drive of the crane trolley; $f_{\text{fri}} = k_{\text{fri}} v$ is the friction force counteracting trolley movements with the viscous friction coefficient k_{fri}; f_{w} is the wind force

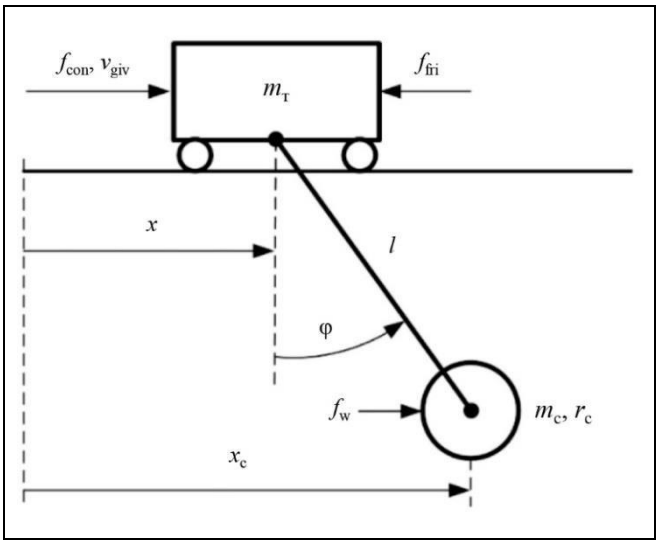

Fig. 1. The diagram of an overhead crane moving a cargo along one axis.

applied to the center of the cargo mass; φ is the deviation angle of the cargo suspension from the vertical axis; $x_{\text{c}} = x + l\sin\varphi$ is the horizontal movement of the cargo. (Without loss of generality, we adopt this friction model, which is obvious for control by speed.) Assume that the motion of the trolley with the cargo is subjected to an exogenous disturbance. It represents a stepwise change in the friction force and wind gusts with an arbitrary instant of occurrence and a limited intensity.

The motion dynamics of the object presented in Fig. 1 are studied well enough. Without considering the initial state in terms of linear and angular movements and their speed, it can be described by the following system of Euler–Lagrange equations (similar to the papers [2, 6] and others):

$$\begin{cases} \left(m_{\text{T}} + m_{\text{c}}\right)\ddot{x} + \left(m_{\text{c}} l\cos\varphi\right)\ddot{\varphi} = f_{\text{con}} - k_{\text{fri}}\dot{x} + m_{\text{c}} l\dot{\varphi}^2\sin\varphi \\ \left(m_{\text{c}} l\cos\varphi\right)\ddot{x} + m_{\text{c}}\left(l^2 + r_{\text{c}}^2\right)\ddot{\varphi} = -m_{\text{c}} gl\sin\varphi - lf_{\text{w}}\cos\varphi \\ \text{x}_{\text{c}} = x + l\sin\varphi, \end{cases} \quad (1)$$

where g denotes the free fall acceleration.

Since the cargo's deviation angle is small (in practice, no more than $10-20^{\circ}$), the angular velocity is also low. Considering the kinematics of motion, we suppose that $\sin\varphi \approx \varphi$, $\cos\varphi \approx 1$, and $\dot{\varphi}^2\sin\varphi \cong 0$. Therefore, system (1) can be linearized as follows:

$$\begin{cases} \ddot{x} \approx a_x^{f_{\text{con}}}\left(f_{\text{con}} - k_{\text{fri}}\dot{x}\right) + a_x^{\varphi}\varphi + a_x \\ \ddot{\varphi} \approx a_{\varphi}^{f_{\text{con}}}\left(f_{\text{con}} - k_{\text{fri}}\dot{x}\right) + a_{\varphi}^{\varphi}\varphi + a_{\varphi} \\ x_{\text{c}} \approx x + l\varphi, \end{cases} \quad (2)$$

where $a_x^{f_{\text{con}}} = \gamma^{-1} m_{\text{c}} \left(l^2 + r_{\text{c}}^2 \right)$, $a_x^{\varphi} = \gamma^{-1} g \left(m_{\text{c}} l \right)^2$, $a_x = \gamma^{-1} m_{\text{c}} \left[-\left(l^2 + r_{\text{c}}^2 \right) f_{\text{fri}} + l^2 f_{\text{w}} \right]$, $a_{\varphi}^{f_{\text{con}}} = -\gamma^{-1} m_{\text{c}} l$, $a_{\varphi}^{\varphi} = -\gamma^{-1} \left(m_{\text{r}} + m_{\text{c}} \right) m_{\text{c}} g l$, $a_{\varphi} = \gamma^{-1} l \left[m_{\text{c}} f_{\text{fri}} - \left(m_{\text{r}} + m_{\text{c}} \right) f_{\text{w}} \right]$, and $\gamma = m_{\text{c}} \left[m_{\text{r}} l^2 + \left(m_{\text{r}} + m_{\text{c}} \right) r_{\text{c}}^2 \right]$.

Let us substitute the first and second equations into the twice-differentiated third equality of system (2), express the signal $\left(f_{\text{con}} - k_{\text{fri}} \dot{x} \right)$ from the first equality of (2), and substitute it into the resulting formula. Consequently, the cargo's motion can be approximately described through the trolley speed as follows:

$$\ddot{x}_{\text{c}} \approx a_{\text{c}}^{\dot{v}} \dot{v} + a_{\text{c}}^{\varphi} \varphi + a_{\text{c}}, \tag{3}$$

where $a_{\text{c}}^{\dot{v}} = r_{\text{c}}^2 \big/ \left(r_{\text{c}}^2 + l^2 \right)$, $a_{\text{c}}^{\varphi} = l \left(a_{\varphi}^{\varphi} - a_x^{\varphi} a_{\varphi}^{f_{\text{con}}} \big/ a_x^{f_{\text{con}}} \right) = -g\mu$, $\mu = l^2 \big/ \left(l^2 + r_{\text{c}}^2 \right)$ is the dimensionless coefficient of the cargo's radius of inertia, and $a_{\text{c}} = l \left(a_{\varphi} - a_x a_{\varphi}^{f_{\text{con}}} \big/ a_x^{f_{\text{con}}} \right)$.

For further considerations, let $l^2 >> r_{\text{c}}^2$, which holds in most practical cases. Then $a_{\text{c}}^{\dot{v}} \approx 0$ and equation (3) can be rewritten as

$$\ddot{x}_{\text{c}} \approx a_{\text{c}}^{\varphi} \varphi + a_{\text{c}}. \tag{4}$$

This linearized cargo transfer model along one axis will be called reduced as compared to model (3), which was used in the paper [16] to design an adaptive crane control law. The reduced model contains only two unknown parameters. In addition to the arguments above, such a significant simplification of the dynamic model of cargo's linear movements is explained by the fact that it will be used to approximate these movements only.

The natural frequency of the cargo's angular oscillations $\left(\omega_0 \right)$ can be determined from equation (4). As is well known, natural oscillations satisfy the equation [18] $\ddot{\varphi} + \omega_0^2 \varphi = 0$. Equality (4) can be written as $\ddot{x} + l\ddot{\varphi} \approx a_{\text{c}}^{\varphi} \varphi + a_{\text{c}}$. The frequency ω_0 is found under $\ddot{x} \equiv 0$ and the absence of exogenous disturbances ($a_{\text{c}} \equiv 0$). Hence, considering equation (3), we obtain

$$\omega_0 \approx \sqrt{-a_{\text{c}}^{\varphi} / l} = \sqrt{\mu g / l}. \tag{5}$$

Under the current parametric uncertainty of the crane, cargo, and exogenous disturbances, it is required to construct a control law (a given speed of the crane trolley provided that $\dot{x} \cong v_{\text{giv}}$) for the trolley drive so that

$$x_{\text{c}} \to x_{\text{c giv}}, \ \dot{\varphi} \to 0, \tag{6}$$

where $x_{\text{c giv}}$ is the given position of the cargo (or its target point). Assume that there is approximate a priori information about the natural frequency of angular oscillations. As data sensors, we will adopt meters of the signals $\dot{\varphi}, \ddot{x}_{\text{c}}$, and x. Note that modern sensors provide the necessary functionality. For example, the first two signals can be measured by a micromechanical sensor located near the cargo with remote data transmission.

2. CONTROL ALGORITHM

Let the following equality be the desired (model) behavior of the second derivative $\left(\ddot{x}_{\text{c}}^{\text{m}} \right)$ of the cargo's linear movement that corresponds to the oscillatory process:

$$\ddot{x}_{\text{c}}^{\text{m}} = -2\omega_{\text{m}} \xi_{\text{m}} \dot{x} - \omega_{\text{m}}^2 \left(x_{\text{c}} - x_{\text{c giv}} \right), \tag{7}$$

where ω_{m} is a given natural frequency of the reference motion and ξ_{m} is the relative damping factor. This behavior will be called the reference motion; see the Appendix for the justification of such a solution vs. the usual reference model.

Equating the right-hand sides of equations (4) and (7), we find the control law of the crane trolley in the form of its given speed $\left(v_{\text{giv}} \right)$:

$$\dot{x} \approx v_{\text{giv}} = -T_{\text{m}}^{-1} \left[\left(x_{\text{c}} - x_{\text{c giv}} \right) + \omega_{\text{m}}^{-2} \left(a_{\text{c}}^{\varphi} \varphi + a_{\text{c}} \right) \right], \tag{8}$$

where $T_{\text{m}} = 2\xi_{\text{m}} / \omega_{\text{m}}$ is a given (model) time constant of the linear movement.

Based on Fig. 1, the cargo tracking error can be written as

$$x_{\text{c}} - x_{\text{c giv}} = x - x_{\text{giv}}, \tag{9}$$

where $x_{\text{giv}} = x_{\text{c giv}} - l\varphi_{\text{st}} = \text{const}$, assuming that φ_{st} is the steady-state constant value of the angle φ after control.

Equation (8) can be transformed to a dependence describing the dynamics of the closed-loop control system:

$$T_{\text{m}} \dot{x} + x \approx x_{\text{giv}} - \omega_{\text{m}}^{-2} \left(a_{\text{c}}^{\varphi} \varphi + a_{\text{c}} \right). \tag{10}$$

In the case of no angular motion $\left(\varphi \equiv 0 \right)$ and no disturbance $\left(a_{\text{c}} \equiv 0 \right)$, it follows from (10) that $x \to x_{\text{giv}}$ aperiodically with the time constant T_{m} (which explains the name of this parameter). Generally speaking, the aperiodic motion of the crane trolley is disturbed by the angular motion and the component a_{c} [19].

According to formulas (4) and (10), if the steady state $\dot{x} \to 0, \dot{\varphi} \to 0, \dot{x}_c \to 0$ is reached in the closed-loop control system, the only possibility is $\varphi \to \varphi_{st} = -a_c / a_c^{\varphi}$ and $x \to x_{giv}$; hence, by formula (9), we have $x_c \to x_{c\,giv}$.

Proposition. *Under* $\omega_m < \omega_0$, *the closed-loop control system* (2), (4), (8) *satisfies* $\dot{x} \to 0, \dot{\varphi} \to 0, \dot{x}_c \to 0$ *as* $t \to +\infty$, *where* t *denotes the current time. Hence, the control objective* (6) *is achieved.*

P r o o f. For simple considerations, let $x_{c\,giv} = \text{const}$. (According to the reasoning below, it can be also assumed that $x_{c\,giv} \approx \text{const}$.) We choose the Lyapunov function

$$\Lambda = 0.5\left[\dot{x}_c^2 + \omega_m^2 \left(x_c - x_{c\,giv}\right)^2\right] \geq 0.$$

Note that $\Lambda = 0$ only for $\dot{x}_c = 0$ and $x_c = x_{c\,giv}$. Due to the equated right-hand sides of (4) and (7), the derivative of the Lyapunov function is $\Lambda' = -2\omega_m \xi_m \dot{x}\dot{x}_c$. Hence, for the Lyapunov function to decrease in time, it suffices to fulfill the condition $\text{sign}(\dot{x}) = \text{sign}(\dot{x}_c)$ on almost the entire oscillation period. Let us analyze it.

Considering the third equality of (2), equation (7) with $\ddot{x}_c^m$ replaced by $\ddot{x}_c$ (the closed-loop control system with control law (8)) can be written as

$$\ddot{x} + 2\xi_m \omega_m \dot{x} + \omega_m^2 (x - x_{c\,giv}) \approx -l(\ddot{\varphi} + \omega_m^2 \varphi).$$

Adding to the right-hand side of this equality the zero expression $\ddot{\varphi} + \omega_0^2 \varphi = 0$ multiplied by l yields

$$\ddot{x} + 2\xi_m \omega_m \dot{x} + \omega_m^2 \left(x - x_{c\,giv}\right)$$
$$\approx \left(\omega_0^2 - \omega_m^2\right) l\varphi \approx \left(\omega_0^2 - \omega_m^2\right)\left(x_c - x\right).$$

Differentiating this equality and performing further transformations, we obtain

$$\dddot{x} + 2\tilde{\xi}_m \omega_0 \ddot{x} + \omega_0^2 \dot{x} \approx \left(\omega_0^2 - \omega_m^2\right)\dot{x}_c,$$

where $\tilde{\xi}_m = \xi_m \omega_m / \omega_0$ is the resulting relative damping factor.

According to the theory of automatic control, the trolley's dynamics in the variable $\dot{x}$ correspond to an oscillatory link with the natural frequency $\omega_0^{\dot{x}} = \omega_0 \sqrt{1 - \tilde{\xi}_m^2}$ of the output signal and with the convergence property $\dot{x} \to \left[\left(\omega_0^2 - \omega_m^2\right) / \omega_0^2\right] \dot{x}_c$ [19].

Let us impose the condition $\omega_m < \omega_0$. Then the natural frequencies of the output signal of the closed-loop control system and the assigned reference motion (7) ($\omega_0^{\dot{x}}$ and $\omega_0^m = \omega_m \sqrt{1 - \xi_m^2}$) will be related as follows:

$$\omega_0^{\dot{x}} = \omega_0 \sqrt{1 - \left(\xi_m \omega_m / \omega_0\right)^2} = \omega_m \sqrt{\left(\omega_0 / \omega_m\right)^2 - \xi_m^2} > \omega_0^m.$$

Since the control law (8) aims at changing the variable x_c by properties (7), the natural frequency ω_0^m of the reference output signal will dominate in the motion in $\dot{x}_c$. In other words, in the closed-loop control system, the transients in $\dot{x}$ are faster than in $\dot{x}_c$. Therefore, $\dot{x}$ has the same sign on almost the entire period of oscillations: $\text{sign}(\dot{x}) \cong \text{sign}(\dot{x}_c)$.

Thus, if $\omega_m < \omega_0$, then the Lyapunov function will decrease in time. Due to its properties, we have $\dot{x}_c \to 0$ $(\ddot{x}_c \to 0)$ and $x_c \to x_{c\,giv}$. It follows from formulas (8) and (4) that $\dot{x} \to 0$. In view of the dependence $x_c \approx x + l\varphi$, it also follows that $\dot{\varphi} \to 0$. ♦

As a rule, the desired motion of the cargo to the target point is a process close to aperiodic, without overshoot and with the smallest possible time. Note that the parameters T_m or ω_m should be chosen considering the maximum implementable speed of the drive and the required cargo movement. In view of these provisions, the properties of the maximum speed of the oscillatory motion, the proof of the proposition above, the parameters of the assigned reference motion (7) should satisfy the following requirements [19]:

$$\omega_m < \omega_0,\ \xi_m = 0.8,\ \omega_m \overset{\xi_m = 0.8}{\leq} 2.3 v_{max} \Big/ \left|x_{c\,giv} - x_{c_0}\right|, \quad (11)$$
$$T_m = 1.6/\omega_m,$$

where v_{max} is the maximum speed of the crane trolley implemented by the drive and x_{c_0} is the initial position of the cargo.

The control law (8) is based on the exact values of the parameters a_c^{φ} and a_c of the controlled object (4). In practice, however, with numerous types of transported cargos, suspension lengths, and exogenous disturbances at the current time instant, they are usually unknown. If it were possible to measure $\ddot{x}_c$, then this variable would be used in the control law (8) instead of $\left(a_c^{\varphi}\varphi + a_c\right)$ based on equation (4). As a rule, the measurements of the variable $\ddot{x}_c$ are very noisy, which reduces the control performance. A conventional low-frequency filter introduces a phase delay, which also deteriorates control.

To solve the above problems, we approximate $\ddot{x}_c$ based on current parametric identification for low-frequency filtering without phase shift. This idea is part of the approach called the "simplified" adaptability conditions [17].

Therefore, the control law is constructed using the current estimates of these parameters instead of formula (8):

$$\dot{x} \approx v_{\text{giv}} = -T_{\text{m}}^{-1}\left[\left(x_{\text{c}} - x_{\text{c giv}}\right) + \omega_{\text{m}}^{-2}\left(\hat{a}_{\text{c}}^{\varphi}\varphi + \hat{a}_{\text{c}}\right)\right], \quad (12)$$

where the hat symbol indicates the current estimates of the corresponding parameters yielded by the current parametric identification algorithm. For example, it is possible to apply the recurrent least-squares method with the forgetting factor [20]:

$$\begin{cases} \hat{\boldsymbol{\theta}}_i = \hat{\boldsymbol{\theta}}_{i-1} + \mathbf{P}_i\mathbf{y}_i\varepsilon_i, \ \varepsilon_i = \ddot{x}_{\text{r}_i} - \mathbf{y}_i^{\text{T}}\hat{\boldsymbol{\theta}}_{i-1} \\ \mathbf{P}_i = \left[\mathbf{P}_{i-1} - \mathbf{P}_{i-1}\mathbf{y}_i\mathbf{y}_i^{\text{T}}\mathbf{P}_{i-1}\left(1 + \mathbf{y}_i^{\text{T}}\mathbf{P}_{i-1}\mathbf{y}_i\right)^{-1}\right]\Big/\beta \\ \mathbf{P}_0 = \vartheta\mathbf{E}_2, \ \beta < 1, \ \beta \to 1, \end{cases} \quad (13)$$

where $i = 1, 2, 3, \ldots$ denotes the ith time instant with a step Δt; $\hat{\boldsymbol{\theta}} = \left[\hat{a}_{\text{c}}^{\varphi}, \hat{a}_{\text{c}}\right]^{\text{T}}$ is the vector of the estimates of the desired parameters; $\mathbf{y} = \left[\varphi, 1\right]^{\text{T}}$ is the vector of the factor variables; ε is the identification residual; $\mathbf{P}_i$ is the matrix gain of the algorithm of dimensions 2 × 2; β is the assigned forgetting factor of previous measurements to track the time-varying desired parameters; ϑ is a large positive number determining the initial rate of variation of the parameter estimates; finally, $\mathbf{E}_2$ is an identity matrix of dimensions 2 × 2. The least-squares estimation procedure has good approximation properties, which is generally recognized.

In the Appendix, we show that the identification residual of algorithm (13) with the linearly independent elements of the vector-function $\mathbf{y}_i$ on a sliding time interval with a sufficiently small step Δt converges very quickly to the neighborhood of zero (even in the first steps of the algorithm) and remains therein. Meanwhile, the parameter estimates can be far from the true values [17]. In the paper [21], this result was also established under more stringent operating conditions of the closed-loop control system.

Thus, algorithm (13) ensures the condition

$$\ddot{x}_{\text{c}} \cong \hat{\ddot{x}}_{\text{c}} = \hat{a}_{\text{c}}^{\varphi}\varphi + \hat{a}_{\text{c}}, \quad (14)$$

i.e., approximates the variable $\ddot{x}_{\text{c}}$ even under inaccurate parameter estimates.

In other words, the estimates can be substituted into the control law (12) from the very beginning of the identification algorithm. Also, the control objective is achieved for the current parameter estimates and $\hat{\ddot{x}}_{\text{c}}$ (in approximate terms); see the proof above.

Concluding the theoretical part of this paper, we emphasize that all the considerations involve the condition $l^2 >> r_{\text{c}}^2$ and equation (4). According to model studies, the control system with the control law (12) and the identification algorithm (13) demonstrates high performance without this condition (e.g., if $l = r_{\text{c}}$). This result is explained, in particular, by the good approximation properties of the identification algorithm (13) with condition (14) even for the moderately incorrect reduced model (4).

3. A MODEL EXAMPLE

A model example to analyze the properties of the closed-loop control system was constructed based on the dependencies (1), (12), and (13) using formulas (5), (7), and (11). Numerical simulation was carried out in Matlab/Simulink/SimMechanics. Differential equations were solved by the Runge–Kutta method of the fourth and fifth orders with a step of 0.01 s.

Consider control of the trolley of a typical medium-sized crane with the following parameters: $m_{\text{r}} = 450$ kg, $m_{\text{c}} = 100 - 10\,000$ kg, $l = 3 - 10$ m, $r_{\text{c}} = 0.2 - 5$ m, $k_{\text{fri}} = 0.3$ N s/m, $x_{\text{c giv}} = 10$ m. The servo drive generating the speed of the crane trolley $\left(\dot{x}\right)$ according to a given value $\left(v_{\text{giv}}\right)$ is described by an aperiodic link with the unit gain and a time constant of 0.1 s. It has additional nonlinearities: a time delay of 0.03 s and the output signal constraints $v_{\max} = 0.67$ m/s and $|\dot{v}| \le 3$ m/s^2. Many of these parameters match the standard [22] and the variety of typical cargo.

Assume that a step wind disturbance with an intensity of 10% of the cargo weight affects the cargo at the time instant 50 s. (This disturbance is smoothed by an aperiodic link with a time constant of 1 s.)

The angular velocity $\dot{\varphi}$ and acceleration $\ddot{x}_{\text{c}}$ were measured using an MPU-6050 micromechanical sensor located near the cargo with wireless data transmission. The data contain the centered Gaussian noise with RMS errors of 0.1 deg/s (angular velocity) and 0.1 m/s^2 (acceleration) [23]. The signal φ was obtained by integrating the measured angular velocity. The linear movement of the trolley $\left(x\right)$ was determined by an encoder with the same noise with an RMS error of 0.01 m. The cargo position was determined from the measured signals x and φ and the suspension length estimate $(\hat{l})$: $x_{\text{c}} = x + \hat{l}\varphi$.

In the studies described here, $\hat{l} = l$: due to the dependences presented above, if this estimate has an error, the crane control algorithm will generate a constant inaccuracy of cargo positioning only under an exogenous disturbance. When organizing an automated crane control system, the operator can easily compensate this effect. By the expression (5), the error in determining the parameter ω_0 based on $\hat{l}$ to set ω_{m} remains small even under large errors of $\hat{l}$.

For example, an error of up to 30% in the estimate $\hat{l}$ gives an error of up to 16% in the value ω_0.

The identification algorithm (13) has the following parameter values: $\Delta t = 0.01$ s, $\vartheta = 10$, and $\beta = 0.998$. (The control law (12) is implemented with the same time step.) In the crane operation modes, its natural frequency varies in the range $\omega_0 = 0.9 - 1.8\ \text{s}^{-1}$. In view of (11), the parameters of the control law (12) are $\omega_\text{m} = 0.15\ \text{s}^{-1}$, $\xi_\text{m} = 0.8$, and $T_\text{m} = 10.7$ s.

The behavior of the closed-loop control system in the variables x and x_c was compared with the variable x_m, which is the output of the dynamic link corresponding to the reference motion (7): $\ddot{x}_\text{m} = -2\omega_\text{m}\xi_\text{m}\dot{x}_\text{m} - \omega_\text{m}^2(x_\text{m} - x_{\text{c giv}})$ (with the parameters specified above).

Figure 2 shows the results of the study under the average values of the crane operation parameters: $m_\text{c} = 3\,000$ kg, $l = 5$ m, and $r_\text{c} = 2$ m. Other parameter values from the ranges (see above) give almost the same curves (the difference is units of percent). The only exception is high-frequency transients near the time instants $t = 0$ and $t = 50$ s in the variables v, φ, , and $\hat{\ddot{x}}_\text{c}$ under a large ratio r_c/l. In any case, their duration does not exceed 5 s. The stable response of the closed-loop control system under various parameters of the crane, cargo, and an exogenous disturbance indicates better performance characteristics of the control system under the current uncertainty compared to the approach proposed in the papers [15, 16] (the model of the object (3) with three unknown parameters). For example, in these works, there was a small (but more significant than indicated above) variation of the transient time and its character.

In addition, Fig. 2 shows the graphs of the variable $\ddot{x}_\text{c}$ and its estimate $\hat{\ddot{x}}_\text{c}$ (14) based on the current parameter estimates using algorithm (13). Clearly, the identification algorithm provides excellent low-frequency smoothing without phase shift (even without the condition $l^2 >> r_\text{c}^2$, i.e., when the reduced cargo model is "not quite correct."

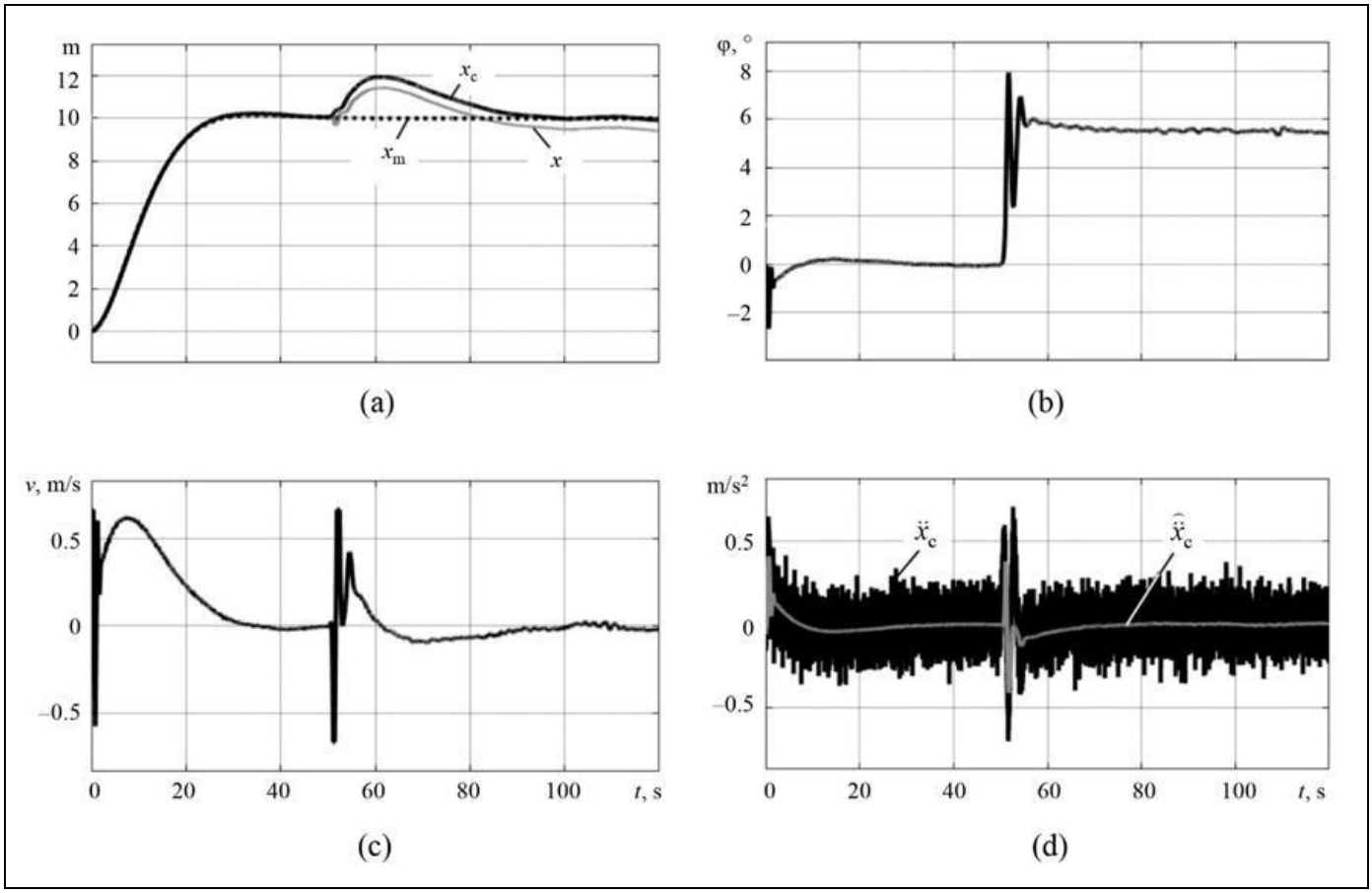

Fig. 2. The analysis results of the crane control system: (a) linear movements of the trolley and cargo compared to the variable $x_\text{м}$, (b) the deviation angle of the cargo suspension, (c) the trolley speed generated by the servo drive, and (d) the second derivative of the cargo's linear movement measured by the sensor and its estimate.

Note that the impact of the third condition in (11) was also analyzed. If this condition is violated, when the crane trolley cannot provide the required speed, the cargo coordinate simply lags behind the reference curve on the sections of motion associated with the transients. When approaching the steady state, the identity with the reference motion is restored. In practice, such small lags during transients are not critical.

The theoretical calculations presented above were fully confirmed by simulations. With a large variety of cargo parameters, its motion is close to the behavior of the assigned reference motion with reaching the target point. A step wind disturbance is successfully compensated. All these results are established under the current parametric uncertainty. Similar properties were obtained for other crane parameters without changing the control algorithm.

CONCLUSIONS

This paper has considered the automatic control of an overhead crane trolley to transport the cargo to a given point and damp its angular oscillations under the current parametric uncertainty of the crane, cargo, and exogenous disturbances. The approach involves a linearized dynamic model of cargo movements depending on the trolley speed, containing two unknown parameters, and the control algorithm based on "simplified" adaptability conditions.

To implement the proposed approach, it is necessary to select the parameters of the reference motion (7) considering conditions (11) and then design the current identification algorithm (13) and the control law (12). The reference motion parameters are selected using a priori information about the natural frequency of the crane suspension, determined by formula (5) based on the suspension length. Due to conditions (11), it suffices to know this frequency approximately. Also, the suspension length is necessary to calculate the cargo's horizontal coordinate. The inaccuracy in determining the suspension length affects only the constant positioning error of the cargo under an exogenous disturbance. The latter can be easily compensated by the crane operator in an automated control system. In the case of a fully automated control system (e.g., a remote crane control system), an additional sensor will be required to determine the suspension length.

A modern micromechanical sensor located near the cargo with wireless data transmission that determines acceleration and angular velocity has been proposed as a cargo motion sensor. An alternative is to place such a wired sensor on the crane trolley.

This paper has been devoted to the problem of horizontal motion along one axis. However, due to the self-tuning of the control system, the results can be generalized to the case of control on two horizontal axes and even on three axes with simultaneous vertical motion of the cargo.

In future, the overhead crane control algorithm will be investigated on an experimental setup.

APPENDIX

J u s t i f i c a t i o n of the reference motion (7).

In the case of control by the cargo coordinate, the reference model cannot be used instead of model (7) in the conventional sense (when the output variable of the scalar reference model corresponds to the controlled variable). This conclusion is immediate from the following arguments:

$$\ddot{x}_{\mathrm{m}} \approx -2\omega_{\mathrm{m}}\xi_{\mathrm{m}}\dot{x}_{\mathrm{m}} - \omega_{\mathrm{m}}^2\left(x_{\mathrm{m}} - x_{\mathrm{c\,giv}}\right),$$

where x_{m} corresponds to the variable x_{c}; then the desired second derivative of the cargo's linear movement (denoted by $\ddot{x}_{\mathrm{c}}^{\mathrm{m}}$, above) takes the form

$$\ddot{x}_{\mathrm{c}}^{\mathrm{m}} \approx -2\omega_{\mathrm{m}}\xi_{\mathrm{m}}\dot{x}_{\mathrm{c}} - \omega_{\mathrm{m}}^2\left(x_{\mathrm{c}} - x_{\mathrm{c\,giv}}\right),$$

and the control law (8) becomes

$$\dot{x} \approx v_{\mathrm{giv}} = -T_{\mathrm{m}}^{-1}\left[\left(x_{\mathrm{c}} - x_{\mathrm{c\,giv}}\right) + \omega_{\mathrm{m}}^{-2}\left(a_{\mathrm{c}}^{\varphi}\varphi + a_{\mathrm{c}}\right)\right] - l\dot{\varphi}.$$

Due to the last term in the control law $\mathrm{sign}(\dot{x}) = -\mathrm{sign}(\dot{\varphi})$, we obtain internal instability (see Fig. 1) in the formation of a given speed, i.e., an analog of nonminimum-phase systems (unstable by the input). ♦

P r o o f of the convergence of the identification residual in algorithm (13).

Let us eliminate the trivial cases $\mathbf{y}_i = 0$ from consideration. Assume also that the norm of the estimate vector is bounded. We multiply the first equality of (13) by the nonzero vector $\mathbf{y}_i^{\mathrm{T}}$ on the left and add the term $\left(\varepsilon_{i+1} - \varepsilon_i\right)$ to the left- and right-hand sides of the result. Then straightforward manipulations yield

$$\left(\ddot{x}_{\mathrm{c}_{i+1}} - \ddot{x}_{\mathrm{c}_i}\right) - \left(\mathbf{y}_{i+1} - \mathbf{y}_i\right)^{\mathrm{T}}\hat{\boldsymbol{\theta}}_i = \varepsilon_{i+1} - (1-\eta_i)\,\varepsilon_i,$$

where $\eta_i = \mathbf{y}_i^{\mathrm{T}} P_i \mathbf{y}_i$ and $0 < \eta_i < 1$.

Since $P_i^{-1} = \sum_{k=1}^{i} \left(\vartheta^{-1} + y_i y_i^{\mathrm{T}} \right) \beta^{i-k}$, this restriction of η_i is easily proved by direct calculations for the scalar value $\mathbf{y}$. In the multidimensional case, it can be established by considering the range of the eigenvalues of the matrix P_i based on the Rayleigh relation. Note that the matrix P_i^{-1} is nonsingular under the linearly independent elements of the vector-function $\mathbf{y}_i$ on the sliding time interval of the algorithm "memory."

The right-hand (left-hand) side of the presented equality describes the "proper motion" of the identification residual (its "disturbance," respectively). The proper motion of this discrete system is stable due to the range of the value η_i. The norm of the disturbance takes lower values for smaller steps Δt. Indeed, when Δt decreases, the norms of the parenthesized vectors on the left-hand side of the equality become smaller even in the closed-loop control system: under the accepted conditions, according to formula (4), the trolley speed formed by the control law does not actually affect the variable $\ddot{x}_{\mathrm{c}}$, and the angle φ within the vector $\mathbf{y}$ is related to this speed through the integral (i.e., very weakly). This fact follows from the third equality in system (2). The elements φ_i and 1 of the vector-function $\mathbf{y}_i$ are linearly independent on a moving time interval, at least on transients.

Hence, as the step Δt decreases, the stable proper motion of the identification residual generates an increasingly narrow domain of attraction near zero [19]. ♦

REFERENCES

1. Mescheryakov, V.N. and Kolmykov, V.V., Methods for Determining Parameters of Cargo Transported by Overhead Cranes with Automatic Swinging Suppression System, *Fundamental Research*, 2015, no. 7, part 1, pp. 79–84. (In Russian.)
2. Rogova, N.S. and Yurkevich, V.D., Design of Control for Cargo Movement by Overhead Crane, *Sb. Nauchn. Tr. NGTU*, 2015, no. 3(81), pp. 43–54. (In Russian.)
3. Korytov, M.S., Sherbakov, V.S., and Shershneva, E.O., Justification of Values Factor Controller Vibration Damping Shipping Overhead cranes, *The Russian Automobile and Highway Industry Journal*, 2017, no. 1(53), pp. 12–19. (In Russian.)
4. Antipov, A.S. and Krasnova, S.A., Stabilization System of Convey-Crane Position via Sigmoidal Function, *Mekhatronika, Avtomatizatsiya, Upravlenie*, 2019, vol. 20, no. 10, pp. 609–614. (In Russian.)
5. Chen, Z.M., Meng, W.J., and Zhang, J.G., Intelligent Anti-swing Control for Overhead crane, *Journal of Central South University*, 2012, vol. 19, no. 10, pp. 2774–2781.
6. Qian, D. and Yi, J., *Hierarchical Sliding Mode Control for Under-actuated Cranes. Design, Analysis and Simulation*, Springer, 2015.
7. Wu, X., Xu, K., Lei, M., and He, X., Disturbance-Compensation-Based Continuous Sliding Mode Control for Overhead Cranes with Disturbances, *IEEE Transactions on Automation Science and Engineering*, 2020, vol. 17(4), pp. 2182–2189.
8. Qian, Y., Hu, D., Chen, Y., and Fang, Y., Programming-Based Optimal Learning Sliding Mode Control for Cooperative Dual Ship-Mounted Cranes Against Unmatched External Disturbances, *IEEE Transactions on Automation Science and Engineering*, 2023, vol. 20(2), pp. 969–980.
9. Kabanov, S.A., Nikulin, E.N., Yakushev, B.E., and Yakusheva, D.B., Optimal Control over Cargo Movement with Overhead crane, *Journal of Instrument Engineering*, 2011, vol. 54, no. 5, pp. 56–65. (In Russian.)
10. Romasevych, Y.O., Loveikin, V.S., Khoroshun, A.S., et al., Synthesis of Optimal Feedback Control of the Crane–Load System, *International Applied Mechanics*, 2022, vol. 58, pp. 199–207.
11. Petrenko, Y.N., Alavi, S.E., and Aleksandrovsky, S.V., Operational Investigation of Overhead Crane with Fuzzy Logic Anti-Swing Controller Using 3-D Simulation, *ENERGETIKA. Proceedings of CIS Higher Education Institutions and Power Engineering Associations*, 2011, no. 3, pp. 20–25. (In Russian.)
12. Drag, L., Model of an Artificial Neural Network for Optimization of Payload Positioning in Sea Waves, *Ocean Engineering*, 2016, vol. 115, pp. 123–134.
13. Sun, N., Fang, Y., and Chen, H., Adaptive Antiswing Control for Cranes in the Presence of Rail Length Constraints and Uncertainties, *Nonlinear Dynamics*, 2015, vol. 81, pp. 41–51.
14. Zhang, M., Ma, X., Rong, X., et al., Adaptive Tracking Control for Double-Pendulum Overhead Cranes Subject to Tracking Error Limitation, Parametric Uncertainties and External Disturbances, *Mechanical Systems and Signal Processing*, 2016, vol. 76–77, pp. 15–32.
15. Kruglov, S.P., Aksamentov, D.N. A Method of Adaptive Control of an Overhead Crane with Direct Tracking of the Load Movement, *Mekhatronika, Avtomatizatsiya, Upravlenie*, 2020, vol. 21, no. 12, pp. 682–688. (In Russian.)
16. Kruglov, S.P. and Aksamentov, D.N. Adaptive Control of the Overhead Crane by the Trolley Speed, *Proceedings of TUSUR University*, 2022, vol. 25, no. 1, pp. 86–92. (In Russian.)
17. Kruglov, S.P., *Adaptivnaya avtomatizatsiya pilotirovaniya samoletom na bol'shikh uglakh ataki na osnove uproshchennykh uslovii adaptiruemosti* (Adaptive Automation of Aircraft Piloting at Large Angles of Attack Based on Simplified Adaptability Conditions), Irkutsk: Irkutsk Branch of Moscow State Technical University of Civil Aviation, 2012. (In Russian.)
18. Sivukhin, D.V., *Obshchii kurs fiziki. Tom I. Mekhanika* (General Course of Physics. Vol. I: Mechanics), Moscow: Fizmatlit, 2005. (In Russian.)
19. Pervozvanskii, A.A., *Kurs teorii avtomaticheskogo upravleniya* (Course of Automatic Control Theory), St. Petersburg: Lan', 2015. (In Russian.)
20. Ljung, L., *System Identification: Theory for the User*, New Jersey: Prentice Hall, 1991.
21. Kruglov, S.P., Adaptive Control of a Non-minimal-phase Scalar Object of the Second Order with the Maintenance of the Preset Transient Characteristics, *Science Bulletin of the NSTU*, 2016, vol. 65, no. 4, pp. 33–53 (In Russian.)
22. *GOST* (State Standard) *3332-54: General-Purpose Electric Overhead Cranes with Load Capacity from 5 to 50 Tons of Medium and Heavy Operating Modes*, 1974. (In Russian.)
23. Zhmud, V.A., Kuznetsov, K.A., Kondratyev, N.O., et al., Accelerometer and Gyroscope MPU6050: The First Inclusion on

STM32 and the Study of Its Indications in Statics, *Automatics & Software Enginery*, 2018, no. 3 (25), pp. 9–22 (In Russian.)

This paper was recommended for publication by S.A. Krasnova, a member of the Editorial Board.

Received June 29, 2023,
and revised July 13, 2023.
Accepted July 18, 2023.

Author information

Kruglov, Sergey Petrovich. Dr. Sci. (Eng.), Irkutsk State Transport University, Irkutsk, Russia
✉ kruglov_s_p@mail.ru
ORCID iD: https://orcid.org/0000-0001-9241-3352

Kovyrshin, Sergey Vladimirovich. Cand. Sci. (Eng.), Irkutsk State Transport University, Irkutsk, Russia
✉ sergkow@mail.ru
ORCID iD: https://orcid.org/0000-0001-5564-0951

Cite this paper
Kruglov, S.P., Kovyrshin, S.V., Identification-Based Speed Control of an Overhead Crane with a Reduced Cargo Transfer Model. *Control Sciences* **4**, 25–33 (2023). http://doi.org/10.25728/cs.2023.4.3

Original Russian Text © Kruglov, S.P., Kovyrshin, S.V., 2023, published in *Problems of Upravleniya*, 2023, no. 4, pp. 28–37.

Translated into English by *Alexander Yu. Mazurov*,
Cand. Sci. (Phys.–Math.),
Trapeznikov Institute of Control Sciences,
Russian Academy of Sciences, Moscow, Russia
✉ alexander.mazurov08@gmail.com

DOI: http://doi.org/10.25728/cs.2023.4.4

AIRCRAFT MOTION CONTROL ALGORITHMS FOR AIRBORNE GEOPHYSICAL SURVEY

A.M. Garakoev[1] and A.I. Gladyshev[2]

[1]Trapeznikov Institute of Control Sciences, Russian Academy of Sciences, Moscow, Russia
[2]Section on Defense Problems of the Ministry of Defense of the Russian Federation at the RAS Presidium, Moscow, Russia

[1]✉ garac@ipu.ru, [2] ✉ tolyagladyshev@yandex.ru

Abstract. In an airborne geophysical survey, the control of moving objects requires forming optimal program (reference) trajectories. Optimality criteria differ depending on the tasks to be performed. The most obvious criterion is the time in which an object reaches its final position from an initial position. Problems with such a criterion are known as time-optimal control problems. This paper considers two control problems of this class related to the performance of a flight task by an aircraft during an airborne geophysical survey. Such a survey is traditionally carried out over a network of parallel routes. Accordingly, the first mode is to start the next survey route. The second mode is to approach the current straight segment of the route. The corresponding time-optimal control problems are posed and solved. The resulting solutions are the reference trajectories for the start and approach modes. The solutions are formally analyzed and methods for forming optimal trajectories and the corresponding controls implementing these trajectories are described. The onboard software implementation of these algorithms is described.

Keywords: Dubins' car, time-optimal control problem, optimal control, Pontryagin's maximum principle.

INTRODUCTION

Trajectory planning in automatic control is applied in various technical systems, e.g., manned and unmanned vehicles, robotic complexes, etc. One qualitative optimality criterion is the minimum time to pass a planned trajectory by a moving object.

A system known as the Dubins' car [1, 2] is often considered when planning optimal shortest-length trajectories. Such a model is described by a nonlinear system of third-order differential equations. Two state variables characterize the location of a controlled object on the plane whereas the third variable the direction (angle) of the velocity vector. The velocity value is assumed to be constant. The scalar control action under geometric constraints determines the instantaneous turning radius.

For the first time, this system was considered by A.A. Markov in 1887 [3]. The Dubins' car is studied as a controlled object with the simplest model of motion in the horizontal plane. In terms of geometry, the Dubins' trajectory is the shortest curve of bounded curvature connecting two points on the plane in the Euclidean space. In 1957, L. Dubins proved [4] that the time-optimal trajectory is composed of segments of circular arcs of maximum curvature and straight lines.

Motion control along a trajectory composed of fragments arises in many applications: control of manipulators on automated assembly lines, monitoring of thermal and power networks, the aerial survey of some territory over a network of parallel routes, etc. In this paper, Dubins' trajectories are considered for aircraft control in an airborne geophysical survey.

This task requires two main control modes to be switched sequentially:

– start the next segment of the trajectory (the next route) with a given course;

– approach the current straight segment of the route with the minimum lateral deviation.

There exist different approaches to solving this problem. For a manned object, navigational information for the pilot is generated by software systems based on certain control algorithms. A widespread approach is to demonstrate on graphic displays a map with path lines and the current location of the con-

trolled object [5, 6]. The disadvantages of such flight support systems are excessive information for the pilot and the absence of control algorithms. Within some approaches, control commands are generated for manned aviation to optimize the start and improve the passage of a straight segment [7, 8]. One approach described therein is to design a new program trajectory at each time instant corresponding to new navigational information and to use a PID controller to demonstrate the deviation from the program trajectory to the pilot. The papers [7, 8] were mainly focused on the algorithmic component of the control process. Many parameters were considered that directly or indirectly affect the quality of navigational information. The information is displayed on the trajectory control indicator, which is common for the pilot.

This paper is devoted to aircraft motion control algorithms for an airborne geophysical survey. To implement these algorithms, a program trajectory is calculated at each time instant, and the deviation from this trajectory is displayed on the Pilot's Indicator. The program trajectories are obtained by solving two time-optimal control problems: when the aircraft starts the next route and when it approaches the current straight segment of the route. Altitude control goes beyond the scope of this paper. As a rule, the pilot carries out a geophysical survey with terrain flow, and aircraft altitude control is a separate complex problem [9].

1. MOTION EQUATIONS

Figure 1 shows the general form of a piecewise fragmentary trajectory in geographic coordinates. Fragments (2–3) and (4–5) correspond to the start mode whereas fragments (1–2), (3–4), and (5–6) to the approach mode (stabilization on the route).

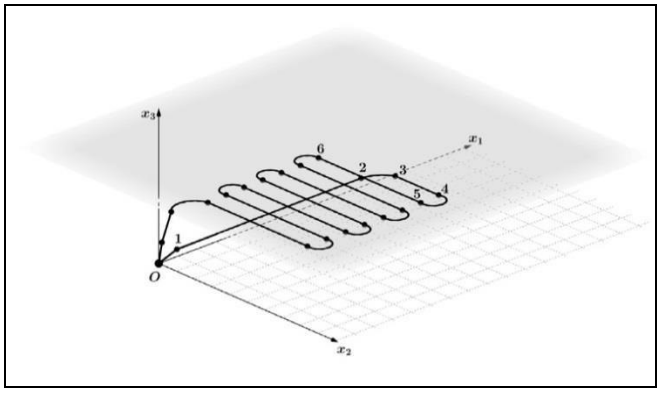

Fig. 1. One example of a fragmentary trajectory.

Consider a simplified problem statement. The main assumptions are as follows. First, the flight altitude is not analyzed in this paper: the problem is solved in projection on the horizontal plane. Second, at the current stage of research, the variation of the horizontal velocity of the object is neglected. Finally, the aircraft is controlled through the momentary action of constant vertical angular acceleration to change the direction of motion. For an aircraft, it corresponds to a momentary deviation of the ailerons by a fixed angle. When a given roll angle is reached, control is terminated.

In the case of a coordinated turn, when the sum of centripetal and gravitational accelerations is compensated by the wing lift, the roll angle under a fixed velocity is uniquely related to the turning radius.

We introduce the following notations: T is the time (in s); x_1 and x_2 are the object's local Cartesian coordinates (in m); φ is the course (track angle) of the object's motion (in rad); ω is the rate of course change (in rad/s); V is the absolute value of the object's horizontal velocity (in m/s); finally, U is the control action (in rad/s^2).

Under the accepted assumptions and notations, the aircraft's motion equations [8] can be written as

$$\begin{cases} \dot{x}_1 = V\cos\varphi \\ \dot{x}_2 = V\sin\varphi \\ \dot{\varphi} = \omega \\ \dot{\omega} = U. \end{cases} \quad (1)$$

Let us reduce the system of equations (1) to a dimensionless form. For this purpose, we introduce the following scaling factors: $V^* = V = 50$ m/s is the characteristic speed of an aircraft (e.g., the Antonov An-3); $\gamma^* = 0.35$ rad (approximately 20 deg) is the maximum value of the roll angle. We express the radius R^* of a coordinated turn.

According to the scheme in Fig. 2, this radius satisfies the relation

$$\tan\gamma^* = \frac{\left|\vec{F}_{\text{cf}}\right|}{\left|\vec{F}_{\text{grav}}\right|} = \frac{m\omega^{*2}R^*}{mg} = \frac{V^{*2}}{gR^*} \Rightarrow R^* = \frac{V^{*2}}{g\tan\gamma^*}, \quad (2)$$

where m is the aircraft's mass; g is the gravity acceleration; $\left|\vec{F}_{\text{cf}}\right|$ is the absolute value of centrifugal force; $\left|\vec{F}_{\text{grav}}\right|$ is the absolute value of gravity. Therefore, $R^* \approx \frac{2500}{10\cdot 0.36} \approx 700$ m. Now, the time constant of the trajectory motion can be calculated as $T_1 = \frac{R^*}{V^*} \Rightarrow T_1 = \frac{700}{50} \approx 14$ s. The course angle changes by one radian in this time. Also, consider the time constant for the fourth equation of system (1), i.e., the

roll angle setting time $T_2 \sim 1$ s. The value T_2 was chosen experimentally for performing flights on aircraft such as An-2, An-3, Cessna, and others.

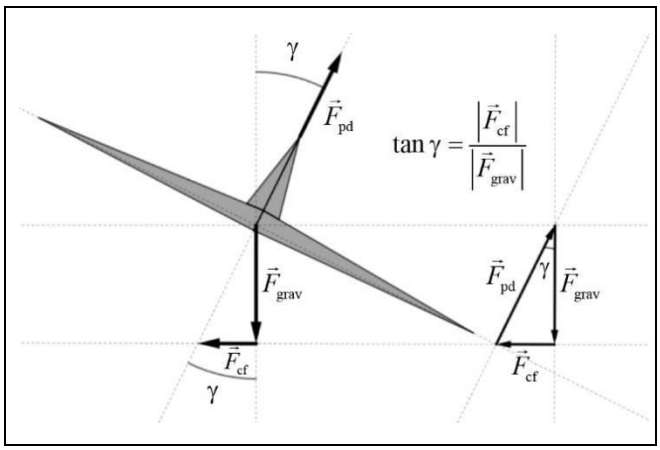

Fig. 2. Forces acting on the aircraft.

Obviously, the characteristic values of the angular velocity and the angular acceleration are $\omega^* = \frac{V^*}{R^*} = \frac{1}{T_1} \Rightarrow \omega^* = \frac{1}{14} \sim 0.07$ rad/s and $U^* = \frac{\omega^*}{T_2} = \frac{1}{T_1 T_2} \Rightarrow U^* = \frac{1}{1 \cdot 14} \sim 0.07$ rad/s^2, respectively.

Note that the value U in equation (1) is nonzero only at the instants of varying the angular velocity, i.e., on time intervals $\Delta T \le T_2$.

Thus, the solution of system (1) for the course angle φ is a linear function on time intervals of the order of T_1 or higher and a quadratic function on short transient segments.

We introduce the dimensionless quantities

$$t = \frac{T}{T^*},\ x = \frac{x_1}{R^*},\ y = \frac{x_2}{x_2^*},\ w = \frac{\omega}{\omega^*},\ u = \frac{U}{U^*},$$

where $T^* = T_1$ or T_2; then system (1) takes the form

$$\begin{cases} \dot{x} = \dfrac{T^*}{T_1}\cos\varphi \\ \dot{y} = \dfrac{T^*}{T_1}\sin\varphi \\ \dot{\varphi} = \dfrac{T^*}{T_1} w \\ \dot{w} = \dfrac{T^*}{T_2} u. \end{cases} \tag{3}$$

Applying the theory of motion separation [10], system (3) can be considered in "fast" ($T^* = T_2$) and "slow" ($T^* = T_1$) time. "Fast" time makes sense only on the control interval where $u = \pm 1$. Indeed, with the small parameter $\varepsilon = \frac{T_2}{T_1} \sim 0.07$, the object is stationary in the zero approximation, and only the dimensionless angular velocity w varies:

$$\dot{x} = \dot{y} = \dot{\varphi} = 0,\ \ \dot{w} = u.$$

In "slow" time, the small parameter occurs only in the last equation of system (3):

$$\begin{cases} \dot{x} = \cos\varphi \\ \dot{y} = \sin\varphi \\ \dot{\varphi} = w \\ \dot{w} = 0. \end{cases} \tag{4}$$

Thus, the original system of motion equations (1) has been reduced to the one (4) of lower dimension with the control action w, limited to the values $[-1, 1]$. In dimensional time, it corresponds to angular velocities ranging from –0.07 to +0.07 rad/s.

According to Poincaré's theorem [8], the solution of system (4) on the time interval T_1 will differ from that of system (1) by a value of the order of ε. The optimal trajectory will be permanently calculated based on the current coordinates updated several times per second. Consequently, this difference will not affect the further solution of the control problem.

2. TIME-OPTIMAL CONTROL PROBLEM

2.1. Motion Equations

Consider system (4) in the dimensional version, which corresponds to problem (1) without the last equation:

$$\begin{cases} \dot{x}_1 = V\cos\varphi \\ \dot{x}_2 = V\sin\varphi \\ \dot{\varphi} = \omega, \end{cases} \tag{5}$$

where $\omega \in [-\omega_{max}, \omega_{max}]$ is the control action.

2.2. Time-Optimal Control in the Start Mode

First of all, we introduce new variables (y_1, y_2, y_3) for system (5) so that the origin of coordinates O coincides with the initial point of the start route, the Oy_1 axis coincides with the direction of this

route, and the Oy_2 axis complements the coordinate system to the right orthonormalized pair; the parameter y_3 specifies the deviation angle of the motion direction from the route direction (in rad):

$$\begin{cases} y_1 = x_1 \cos\varphi_0 + x_2 \sin\varphi_0 - x_{10} \\ y_2 = -x_1 \sin\varphi_0 + x_2 \cos\varphi_0 - x_{20} \\ y_3 = \varphi - \varphi_0, \end{cases} \quad (6)$$

where (x_{10}, x_{20}) are the coordinates of the initial point O of the route and φ_0 is the course of the route.

With the change of variables (6), system (5) takes the form

$$\begin{cases} \dot{y}_1 = V \cos y_3 \\ \dot{y}_2 = V \sin y_3 \\ \dot{y}_3 = \omega. \end{cases} \quad (7)$$

The performance criterion for the object's motion is given by

$$J = \int_{t_0}^{t_f} 1 dt \to \min. \quad (8)$$

In view of the expressions (7) and (8), we consider the time-optimal control problem in the start mode:

$$\begin{cases} \dot{y}_1 = V \cos y_3 \\ \dot{y}_2 = V \sin y_3 \\ \dot{y}_3 = \omega, \end{cases} \quad \begin{cases} y_1(0) = y_1^0 \\ y_2(0) = y_2^0 \\ y_3(0) = y_3^0, \end{cases} \quad \begin{cases} y_1(t_f) = 0 \\ y_2(t_f) = 0 \\ y_3(t_f) = 0. \end{cases} \quad (9)$$

Here, the parameters $\{y_1^0, y_2^0, y_3^0\}$ describe a given initial state of the object and t_f is the start time subject to minimization.

It is required to find an optimal control action $\omega^+(t)$ and the corresponding trajectory $y^+(t)$ such that the controlled object moves from the given initial state to the origin of coordinates in the minimum time t_f [11].

To solve problem (9) using Pontryagin's maximum principle, we introduce the vector of conjugate variables $(\psi_1(t), \psi_2(t), \psi_3(t))$ and write the Hamiltonian and the adjoint system of equations [11]:

$$H = \psi_1 V \cos y_3 + \psi_2 V \sin y_3 + \psi_3 \omega,$$

$$\begin{cases} \dot{\psi}_1 = 0 \\ \dot{\psi}_2 = 0 \\ \dot{\psi}_3 = \psi_1 V \sin y_3 - \psi_2 V \cos y_3, \end{cases} \quad (10)$$

where $\dot{\psi}_i = \dfrac{d\psi_i}{dt} = -\dfrac{\partial H}{\partial y_i}$, $i = 1, 2, 3$.

According to the maximum principle for the time-optimal control problem, it is necessary that there exists a solution $\psi(t) \not\equiv 0$ of system (10) such that $\max\limits_{\omega} H(\psi, y^+, \omega) = H(\psi, y^+, \omega^+) \equiv \text{const} \geq 0$ [11].

Obviously, the first equation of system (10) implies $\psi_1(t) \equiv \psi_1^* = \text{const}$ and the second equation implies $\psi_2(t) \equiv \psi_2^* = \text{const}$. We adopt the change of variables $\psi_1^*, \psi_2^* : \psi_1^* = \rho\cos\alpha, \psi_2^* = \rho\sin\alpha.$ Then $\rho = \sqrt{\psi_1^{*2} + \psi_2^{*2}}$ and $\tan\alpha = \dfrac{\psi_2^*}{\psi_1^*}$. With this change, the Hamiltonian takes the form

$$H = \rho V \cos(y_3 - \alpha) + \psi_3 \omega. \quad (11)$$

The conditions for the time-optimal control problem are as follows: a) $H \equiv \text{const}$; b) $H = \max\limits_{\omega}$.

If $\rho = 0$, then $H = \psi_3 \omega$, where $\psi_3 \neq 0$. Therefore, $\omega^+(t) = \text{sign}\,\psi_3 = \begin{cases} \omega_{\max}, \psi_3 > 0 \\ -\omega_{\max}, \psi_3 < 0 \end{cases}$ since for $|\omega| < \omega_{\max} \Rightarrow \psi_3 \cdot \text{sign}\,\psi_3 > \psi_3 \omega \Rightarrow \psi_3 = C = \text{const}$. Conditions a) and b) are satisfied.

For $\rho \neq 0$ in formula (11), the control action is

$$\omega^+(t) = \begin{cases} \omega_{\max}, \psi_3 > 0 \\ 0, \psi_3 = 0 \\ -\omega_{\max}, \psi_3 < 0. \end{cases}$$

Here, $\psi_1^* \neq 0$ and (or) $\psi_2^* \neq 0 \Rightarrow \psi_3^* = \psi_1^* y_2^+(t) - \psi_2^* y_1^+(t) + C$, $C = \text{const}$, where $y_1^+(t), y_2^+(t)$ is the optimal trajectory.

The value $\omega^+(t) = 0$ is also a solution of the time-optimal control problem: if $\omega(t) = 0$ in formula (11), the maximum value $H = \rho V \cos(y_3 - \alpha) = \text{const}$ is achieved at $(y_3 - \alpha) = \pm\dfrac{\pi}{2}$ as well. This solution corresponds to $\psi_3^* = 0$, describing straight-line motion [12] because ψ_1^*, ψ_2^*, and C are constants:

$$\psi_1^* y_2^+ - \psi_2^* y_1^+ + C = 0. \quad (12)$$

The control actions satisfying the maximum principle may vary only on the straight line (12), which is called the switching line. The motion outside the straight line will be a circular arc.

The solution of the time-optimal control problem for the object described by equations (7) is the solution of the Dubins' problem [4]. The resulting time-optimal trajectories will be called Dubins' trajectories.

In Fig. 3, the optimal trajectory consists of three fragments. The first one is arc L_aA of a circle centered at C_1; the second one is segment AB joint with arc L_aA at the point of tangency with the circle centered at C_1; the third one is arc BO of a circle centered at C_2. The values y_i^0, $i=1, 2, 3$, are the initial conditions of problem (8): y_1^0 is the initial value of the pitch deviation from the start of the route, y_2^0 is the initial value of the roll deviation, and y_3^0 is the initial deviation of the object's course from the route direction. The switching line represents the straight-line segment AB. The first switch occurs when passing from fragment L_aA to AB. The second one occurs when passing from AB to BO. The start route is limited to segment OD.

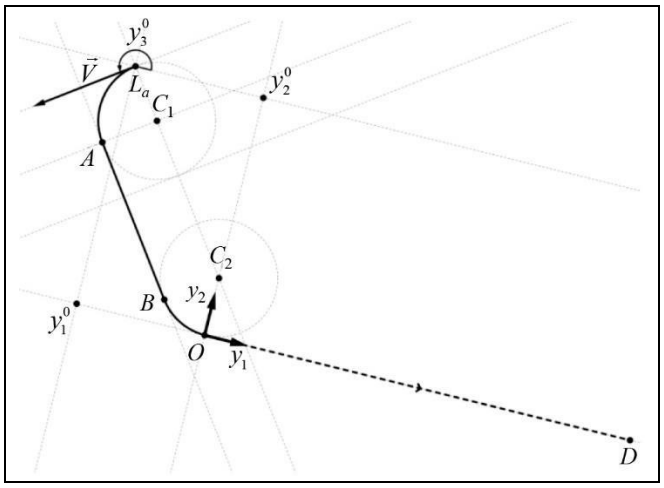

Fig. 3. A trajectory in the start mode.

2.3. Time-Optimal Control in the Approach Mode

The approach problem is as follows. If the aircraft has left the survey route, it must be returned to the corresponding straight line as quickly as possible. It does not matter at which point along the straight line the return will occur. Problem (9) is solved for a smaller dimension: y_2 is the deviation from the straight line (in m), and y_3 is the angle of course deviation from the route direction (in rad):

$$\begin{cases} \dot{y}_2 = V\sin y_3 \\ \dot{y}_3 = \omega, \end{cases} \quad \begin{cases} y_2(0) = y_2^0 \\ y_3(0) = y_3^0, \end{cases} \quad \begin{cases} y_2(t_f) = 0 \\ y_3(t_f) = 0. \end{cases} \tag{13}$$

We write the Hamiltonian for the expression (13):

$$H = \psi_2 V\sin y_3 + \psi_3\omega. \tag{14}$$

The corresponding adjoint system of equations is

$$\begin{cases} \dot{\psi}_2 = 0 \\ \dot{\psi}_3 = \psi_2 V\cos y_3. \end{cases} \tag{15}$$

Hence, $\psi_2(t) \equiv \psi_2^* = \text{const}$.

Analyzing equation (14), we observe that if $\psi_2^* = 0 \Rightarrow \psi_3^* = \text{const} \neq 0$, then $\omega^+(t) = \text{sign}\,\psi_3 = \begin{cases} \omega_{\max}, \psi_3 > 0 \\ -\omega_{\max}, \psi_3 < 0 \end{cases}$ since $\psi(t) \not\equiv 0$. If $\psi_3^* \equiv 0$ with $\psi_2^* \neq 0$, then by the second equation of system (15) the control action is

$$\omega^+(t) = \begin{cases} \omega_{\max}, \psi_3 > 0 \\ 0, \psi_3 = 0 \\ -\omega_{\max}, \psi_3 < 0. \end{cases}$$

The case $\omega^+ = 0$ occurs only for $y_3 = \pm\dfrac{\pi}{2}$.

Note that the expression (14) is equivalent to formula (11) for $\alpha = \dfrac{\pi}{2}$ and $\psi_2 = \rho$. Thus, the approach problem is a particular case of the start problem.

Figure 4 shows two start trajectories. As in the start mode, the first optimal trajectory has two switches. The second one has one switch (at point A when passing from fragment L_aA to fragment AB).

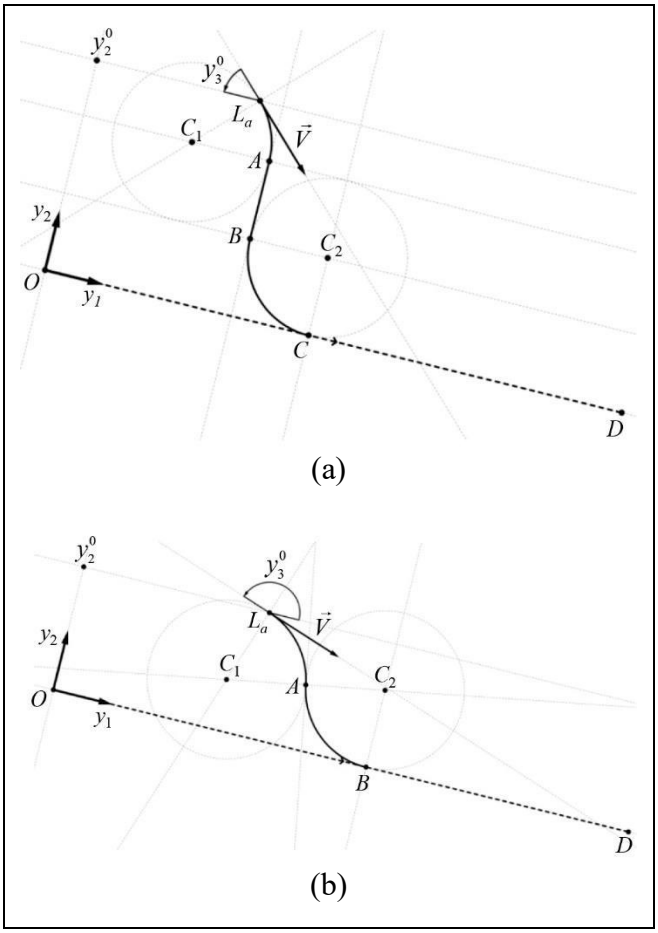

Fig. 4. Examples of trajectories in the start mode: (a) with two switches and (b) with one switch.

2.4. Numerical Solution of the Time-Optimal Control Problem

We introduce the following notations: *C* is a circular arc, and *S* is a straight segment. According to the theorem proved in the paper [13], the Dubins' trajectory has the types *CSC* and *CCC* or a subset of these types. An arc *C* with $\dot{y}_3 > 0$ is that of left turn *L* (left arc); an arc *C* with $\dot{y}_3 < 0$ is that of right turn *R* (right arc). Considering the turning direction, the Dubins' trajectory can be characterized by one of the types from the set

$$\{LRL, RLR, LSL, LSR, RSL, RSR\},$$

or a subset of one of these types, e.g., *LR*, *RL*, *RS*, *L*, etc. In total, we have 15 possible variants. The approach proposed in the paper [13] for obtaining the shortest (optimal) Dubins' trajectory is to parameterize the time-optimal control problem in terms of the final time t_f and switching times.

Let L_{ξ_1} be a left arc of length $V\xi_1$, R_{ξ_2} be a right arc of length $V\xi_2$, and S_{ξ_3} be a segment of length $V\xi_3$. Also, for an arc L_{ξ_4}, we introduce the length $V\xi_4$; for an arc R_{ξ_5}, the length $V\xi_5$. The resulting sequence has the form

$$L_{\xi_1} R_{\xi_2} S_{\xi_3} L_{\xi_4} R_{\xi_5}.$$

On the one hand, a trajectory of the type *RLR* can be obtained when $\xi_1 = \xi_3 = 0$, $\xi_2, \xi_4, \xi_5 > 0$. On the other hand, a trajectory of the type *LR* can be obtained when $\xi_3 = \xi_4 = \xi_5 = 0$ and $\xi_1, \xi_2 > 0$, or $\xi_1 = \xi_2 = \xi_3 = 0, \xi_4, \xi_5 > 0$. Let the initial time be $t_0 = 0$ and the final time be $t_5 = t_f$. Also, we define the switching times t_j, $j = 1,\ldots,4$, such that

$$\xi_j = t_j - t_{j-1},\ j = 1,\ldots, 5.$$

Note that the control action is $\omega^+(t) = \omega_{\max}$ along an arc *L* and $\omega^+(t) = -\omega_{\max}$ along an arc *R*. Along a segment *S*, we have $\omega^+(t) = 0$. In view of these considerations, the numerical approach to solving the time-optimal control problems will be as follows. For $t_{j-1} \le t \le t_f$,

$$y_3(t) = y_3(t_{j-1}) + \omega^+(t)(t - t_{j-1}) \quad \text{if } j = 1,\ldots, 5,$$

$$y_1(t) = \begin{cases} y_1(t_{j-1}) + V\left(\sin y_3(t) - \sin y_3(t_{j-1})\right)/\omega^+(t) \\ \text{if } j = 1, 2, 4, 5 \\ y_1(t_{j-1}) + V\cos y_3(t)(t - t_{j-1}) \\ \text{if } j = 3, \end{cases}$$

$$y_2(t) = \begin{cases} y_2(t_{j-1}) + V\left(\cos y_3(t) - \cos y_3(t_{j-1})\right)/\omega^+(t) \\ \text{if } j = 1, 2, 4, 5 \\ y_2(t_{j-1}) + V\sin y_3(t)(t - t_{j-1}) \\ \text{if } j = 3, \end{cases}$$

where

$$\omega^+(t) = \begin{cases} \omega_{\max} & \text{if } j = 1, 4 \\ -\omega_{\max} & \text{if } j = 2, 5 \\ 0 & \text{if } j = 3. \end{cases}$$

The time-optimal control problem is reduced to the optimization problem

$$\begin{cases} \min t_f = \sum_{j=1}^{5} \xi_j \\ y_1^0 + \dfrac{V}{\omega_{\max}}\left(-\sin y_3^0 + 2\sin y_3^1 - 2\sin y_3^2 \right. \\ \quad \left. + 2\sin y_3^4\right) + V\xi_3 \cos y_3^2 = 0 \\ y_2^0 + \dfrac{V}{\omega_{\max}}\left(\cos y_3^0 - 2\cos y_3^1 + 2\cos y_3^2 \right. \\ \quad \left. - 2\cos y_3^4 + 1\right) + V\xi_3 \sin y_3^2 = 0 \\ \xi_j \ge 0 \text{ for } j = 1,\ldots, 5, \end{cases} \tag{16}$$

where $y_3^1 = y_3^0 + \omega_{\max}\xi_1$, $y_3^2 = y_3^1 - \omega_{\max}\xi_2$, and $y_3^4 = y_3^2 + \ +\omega_{\max}\xi_4$. Substituting y_3^1, y_3^2, y_3^4 into problem (16), we obtain a finite-dimensional nonlinear optimization problem.

This numerical solution approach to time-optimal control problems was described in detail in the paper [13]. In particular, the problems and possible trajectories were generally analyzed.

Note that Dubins' trajectories cannot be implemented in the trajectory control of real moving objects. Here, they are used as program trajectories only.

3. CONTROL THROUGH PILOT'S INDICATOR

The described approach to forming aircraft program trajectories during an airborne geophysical sur-

vey is used in the NavDat hardware-software complex [7, 14, 15]. The Pilot's Indicator receives the difference between the angular velocity for the program trajectory and the real current trajectory of the aircraft based on a satellite navigation system (SNS). SNS data can be used to obtain the exact time, coordinates (latitude and longitude), altitude, and velocity of a moving point.

The angular velocity is given by

$$\omega = \frac{V}{R},$$

where V denotes the horizontal velocity and R is the radius of a coordinated turn.

For program and real current trajectories, the value V is taken from SNS data. The radius R is set for the program trajectory and is calculated for the current trajectory by formula (2) with the limitation on the roll angle of the aircraft.

In the approach mode, the NavDat program uses a PID controller based on the current lateral deviation. Consequently, the controller must be retuned if the aircraft velocity varies significantly.

In this paper, the control algorithm in the approach mode is designed in the same way as in the start mode. The only parameter of the algorithm to be tuned is the maximum angular velocity of the object, which is directly related to the maximum admissible roll angle.

The requirements for lateral deviations from the survey route are specified as follows. For surveys with an inter-route distance of 100 m (the survey scale is 1:10 000), the admissible lateral deviation is 15–25 m; for inter-route distances of 1000 m (1:100 000), the admissible lateral deviation is 100–200 m [16].

To avoid an excessive pilot's workload, the idea is to calculate the program trajectory in the approach mode using the minimum admissible value of the roll angle instead of its limiting value (limiting angular velocity). In this case, the approach program trajectory can be constructed without crossing the boundaries of the aircraft flight corridor (Fig. 5.).

Figure 5 shows two trajectories with one switch and one common initial point L_a. The first one is the optimal trajectory formed by the arcs of circles centered at C_1 and C_2. The switch occurs at point A when moving from fragment L_aA to fragment AB. The second one is an admissible trajectory formed by arcs of circles of greater radius than in the first case. The switch occurs at point C at the conjunction of sections L_aC and CF.

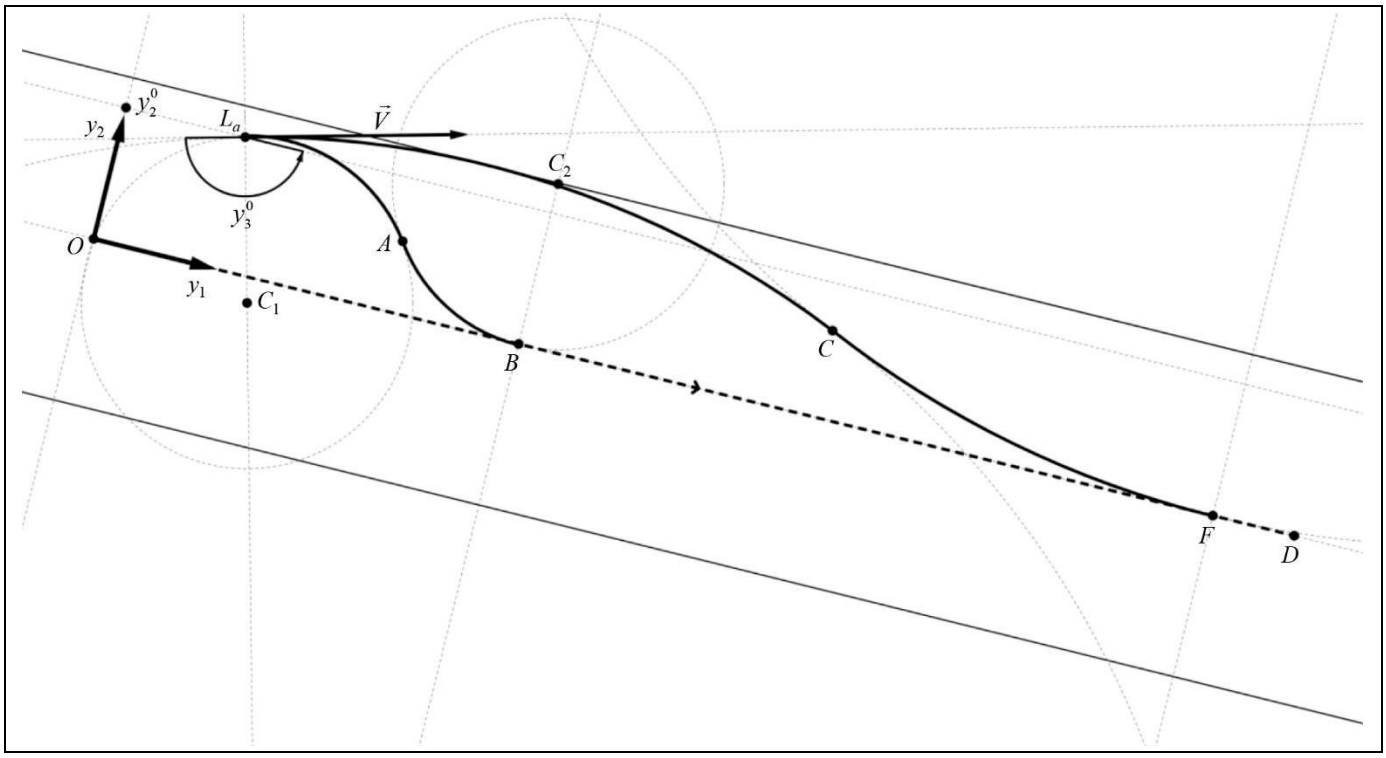

Fig. 5. An admissible approach.

Figure 6 shows a pad with the Pilot's Indicator, original software installed on it. The display is divided into three windows. The first window contains a crosshair indicator informing the pilot about the current position relative to the program trajectory. The second window is a navigation panorama with routes and other necessary data. The third window (a list on the left) provides the status of devices connected to the NavDat hardware and software complex.

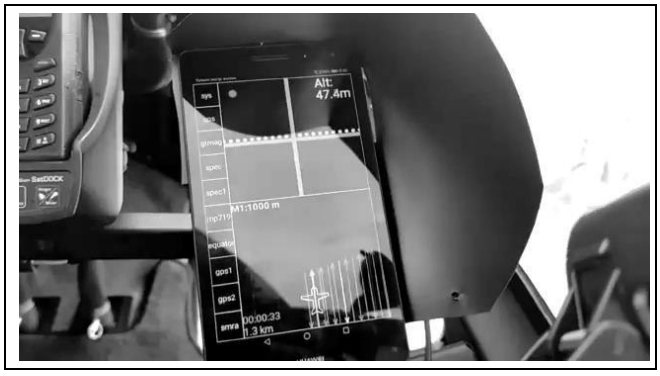

Fig. 6. Pilot's Indicator.

CONCLUSIONS

Optimal trajectory planning methods for moving objects are widely used in various systems. In systems with multi-mode motion, it is necessary to consider the constraints when passing from one motion mode to another. The resulting time-optimal control problems with constraints are solved within classical approaches, such as Pontryagin's maximum principle.

This paper has considered a model of object motion in the plane, known as the Dubins' car, for an aircraft carrying out an airborne geophysical survey in the start and approach modes. The optimal trajectories and controls implementing these trajectories in the two modes have been designed and formally analyzed. The methodology described above is unified and can be applied to form optimal trajectories in both modes mentioned.

A transition from optimal control to flight task-permissible control has been proposed to reduce the pilot's workload.

The corresponding methods have been adopted to modify the NavDat software, which forms an optimal program trajectory and guides the aircraft along a given route. After calculations, all the necessary data are displayed on the Pilot's Indicator in a rather convenient form.

REFERENCES

1. Nguyen, T.K., Pham, D.H., Nguyen, Q.C., et al., An Optimal Smooth-Path Motion Planning Method for a Car-Like Mobile Robot, *Journal of Technical Education Science*, 2023, vol. 75A, pp. 20–30.
2. Kumar, D.P., Darbha, S., Manyam, S.G., and Casbeer, D., The Weighted Markov-Dubins Problem, *IEEE Robotics and Automation Letters*, 2023, vol. 8, no. 3, pp. 1563–1570.
3. Markov, A.A., Some Solution Examples for a Special Class of Problems on the Greatest and Least Quantities, *Soobshch. Khar'kovsk. Mat. Obshch.*, 1887, vol. 1, pp. 250–276. (In Russian.)
4. Dubins, L.E., On Curves of Minimal Length with a Constraint on Average Curvature and with Prescribed Initial and Terminal Positions and Tangents, *American Journal of Mathematics*, 1957, vol. 79, no. 3, pp. 497– 516.
5. Zhodzishsky, P.Yu. and Puhvatov, V.A., Improvement of Airborne Geophysical Studies Efficiency, *Geoprofi*, 2010, no. 2, pp. 23–25. (In Russian.)
6. Trigubovich, G.M., Shevchuk, S.O., Kosarev, N.S., and Nikitin, V.N., Complex Technology of Navigation and Geodetic Support of Airborne Electromagnetic Surveys, *Gyroscopy and Navigation*, 2017, vol. 8, no. 3, pp. 226–234.
7. Karshakov, E.V., Aircraft Control Algorithms Features in Case of Airborne Surveying, *Control Sciences*, 2012, no. 3, pp. 71–76. (In Russian.)
8. Volkovitsky, A.K. and Garakoev, A.M., Algorithms for Controlling Movement along a Fragmentary Trajectory, *Trudy 16-oi Mezhdunarodnoi konferentsii "Ustoichivost' i kolebaniya nelineinykh sistem upravleniya" (konferentsiya Pyatnitskogo)*, (Proceedings of the 16th International Conference on Stability and Oscillations of Nonlinear Control Systems (Pyatnitskiy's Conference) (STAB-2022), Moscow, 2022, pp. 101–105. (In Russian.)
9. Karshakov, E.V., Shevchenko, A.M., and Garakoev, A.M., Formation of a Director Index to Assist the Pilot in Conducting Airborne Geophysical Survey, *International Workshop on Navigation and Motion Control (NMC 2020)*, Samara, 2020, pp. 1–10.
10. Novozhilov, I.V., *Fraktsionnyi analiz* (Fractional Analysis), Moscow: Faculty of Mechanics and Mathematics, Moscow State University, 1995. (In Russian.)
11. Aleksandrov, V.V., Parusnikov, N.A., Lemak, S.S., and Zlochevskii, S.I., *Vvedenie v dinamiku upravlyaemykh sistem* (An Introduction to the Dynamics of Controlled Systems), Moscow: Moscow State University, 1993. (In Russian.)
12. Patsko, V.S. and Fedotov, A.A., Reachable Set at a Certain Time for a Dubins Car in the Case of a One-Sided Turn, *Trudy Inst. Mat. Mekh. UrO RAN*, 2018, vol. 24, no. 1, pp. 143–156. (In Russian.)
13. Kaya, C.Y., Markov–Dubins Path via Optimal Control Theory, *Comput. Optim. Appl.,* 2017, vol. 68, pp. 719–747. DOI: https://doi.org/10.1007/s10589-017-9923-8.
14. Volkovitsky, A.K., Karshakov, E.V., and Pavlov, B.V., The Structure of the Control Algorithms of Aircraft Navigating, *Izv. SFedU. Eng. Sci.*, 2013, no. 3 (140), pp. 217–225. (In Russian.)
15. URL: https://geotechnologies.ru/ru/products/navdat_ru.html.
16. *Instruktsiya po magnitorazvedke (nazemnaya magnitnaya s"emka, aeromagnitnaya s"emka, gidromagnitnaya s"emka)* (Instruction on Magnetic Survey (Ground Magnetic Survey, Airborne Magnetic Survey, and Hydromagnetic Survey), the USSR Ministry of Geology, Leningrad: Nedra, 1981. (In Russian.)

This paper was recommended for publication by L.B. Rapoport, a member of the Editorial Board.

Received February 7, 2023,
and revised May 18, 2023.
Accepted June 21, 2023.

Author information

Garakoev, Amir Musaevich. Junior Researcher, Trapeznikov Institute of Control Sciences, Russian Academy of Sciences, Moscow, Russia
✉ garac@ipu.ru
ORCID iD: https://orcid.org/0000-0003-1886-4934

Gladyshev, Anatoly Ivanovich. Dr. Sci. (Eng.), Chairman of Section on Defense Problems of the Ministry of Defense of the Russian Federation at the RAS Presidium, Moscow, Russia
✉ tolyagladyshev@yandex.ru
ORCID iD: https://orcid.org/0000-0002-8362-0293

Cite this paper
Garakoev, A.M., Gladyshev, A.I., Aircraft Motion Control Algorithms for Airborne Geophysical Survey. *Control Sciences* **4**, 34–42 (2023). http://doi.org/10.25728/cs.2023.4.4

Original Russian Text © Garakoev, A.M., Gladyshev, A.I., 2023, published in *Problemy Upravleniya*, 2023, no. 4, pp. 38–47.

Translated into English by *Alexander Yu. Mazurov*,
Cand. Sci. (Phys.–Math.),
Trapeznikov Institute of Control Sciences,
Russian Academy of Sciences, Moscow, Russia
✉ alexander.mazurov08@gmail.com

DOI: http://doi.org/10.25728/cs.2023.4.5

INTER-ORBITAL SPACECRAFT TRANSFER OPTIMIZATION: CHOOSING INITIAL APPROXIMATIONS BASED ON CORRELATION ANALYSIS OF KEY PARAMETERS

E.V. Savvina

✉ petrakowae@mail.ru

Abstract. This paper presents a new approach to choosing initial approximations in inter-orbital transfer optimization problems for a spacecraft with a chemical booster and fixed thrust. The approach involves correlations between the values of key problem parameters. It is implemented using numerical methods, mathematical modeling, and programming. Relevant publications on the subject area (methods for finding initial approximations in optimization problems) are systematically studied and several mathematical relationships are identified. As a result, laws are specified to facilitate the choice of initial approximations in order to ensure convergence and achieve the optimum. The results of a computational experiment confirm the applicability and effectiveness of this approach in typical optimization problems (an optimal spacecraft trajectory design between near-Earth orbits as one example).

Keywords: optimal control, spacecraft trajectory optimization, maximum principle, mathematical modeling, nonlinear programming, statistical analysis.

INTRODUCTION

In optimal control, choosing initial approximations is a relevant and significant problem. Here, a correct approach ensures faster convergence of a numerical method for solving the boundary-value problem and successfully yields an optimal solution [1–3]. However, there are difficulties in selecting such an approach due to the branching of optimal solutions and the high sensitivity of the residuals of the boundary-value problem to its parameter variations [4].

Currently, there exist many practical methods to simplify the process of finding initial approximations, e.g., the homotopy of maximum thrust [5], edge normalization [6], and others. In some cases, such methods may have a significant positive effect; in particular, see rendezvous solutions developed to find initial approximations for indirect methods [3, 7, 8]. According to the literature survey, relevant studies in this area focus on particular problems. At the same time, more and more efforts of the global research community are applied to develop algorithms that will be effective in choosing initial approximations [1–3, 5, 6].

This paper presents research on the statistical analysis of data vectors obtained in the course of mathematical modeling. The analysis is aimed at identifying and analyzing correlations between the values of key parameters of a typical optimization problem. The analysis results are then interpreted to refine the optimization algorithm: we specify several laws to facilitate the choice of initial approximations in order to ensure convergence of the numerical solution method and achieve the optimum for typical problems. The results of a computational experiment confirm the applicability and effectiveness of this approach in typical optimization problems (an optimal spacecraft trajectory design between near-Earth orbits as one example).

1. THE ALGORITHM FOR SOLVING TYPICAL PROBLEMS

1.1. Mathematical Formalization of the Optimal Inter-Orbital Spacecraft Transfer Problem

Consider the problem of designing an optimal spacecraft transfer trajectory between near-Earth elliptical orbits with coinciding apsidal lines. This problem

statement is used at the first stage to verify the hypothesis that there exist relationships between the values of the conjugate variables vector in the optimal solution. The next stage of the analysis involves a similar study for a set of problems with orbits lying on different planes. Such orbits are in potential demand when forming an orbital service system. (For example, we mention geostationary orbits, solar-synchronous orbits, and the Molniya orbit.)

The general problem statement is as follows. We consider a spacecraft on a given initial near-Earth orbit. The spacecraft includes a chemical booster with some known characteristics. This booster must transfer the spacecraft to a working near-Earth orbit with specified characteristics.

It is required to find a rational transfer scheme between the orbits. As an optimality criterion, we choose the spacecraft mass inserted into the working orbit: the mass is maximized. The transfer time is not limited.

We fix the following parameters and conditions for all cases under consideration: the mass of the spacecraft at the initial instant is 5000 kg; the thrust of the rocket engine is 5 kN (unregulated, the number of switching on is unlimited); the specific impulse is 330 s. The spacecraft transfer is limited to one revolution. The orbits belong to the same plane, and their apsidal lines coincide.

We vary the following parameters: the perigee altitude of the initial orbit and its apogee altitude; the perigee altitude of the final orbit and its apogee altitude.

Parameters of the transfer scheme, which should be selected: the moment of the spacecraft motion start from the reference orbit; the duration of active and passive sections of the trajectory and their location on the transfer trajectory; the pitch angle program on each active section; the end point on the transfer.

Spacecraft transfer model

The mathematical model of the spacecraft motion includes the vector of its phase coordinates with five components: the radial velocity V_r, the normal velocity V_n, the radius r and the polar angle β, spacecraft mass m. Then, the spacecraft motion can be described by a system of differential equations (DE)

$$\begin{aligned}
\dot{V}_r &= \frac{P\sin(\varphi)}{m}\delta - \frac{\mu}{r^2} + \frac{V_n^2}{r},\\
\dot{V}_n &= \frac{P\cos(\varphi)}{m}\delta - \frac{V_r V_n}{r},\\
\dot{r} &= V_r,\\
\dot{\beta} &= \frac{V_n}{r},\\
\dot{m} &= -q\delta.
\end{aligned} \tag{1}$$

The notations are as follows:
P is the engine thrust; μ is the Earth's gravitational parameter; q is the mass flow rate of the engine (a known value); δ is the thrust function taking only two values: $\delta = 1$ (ignition) and $\delta = 0$ (cutoff); finally, φ is the pitch angle of the spacecraft. Note that $\delta(t)$ and $\varphi(t)$ are the control functions to be optimized.

Pontryagin's maximum principle, the boundary-value problem

We introduce the vector of conjugate variables, further called the conjugate vector:

$$\lambda = \begin{pmatrix} \lambda_{V_r} \\ \lambda_{V_n} \\ \lambda_r \\ \lambda_\beta \\ \lambda_m \end{pmatrix}. \tag{2}$$

The Hamiltonian is given by

$$\begin{aligned}
H = {} & \lambda_{V_r}\left(\frac{P\sin(\varphi)}{m}\delta - \frac{\mu}{r^2} + \frac{V_n^2}{r}\right)\\
& + \lambda_{V_n}\left(\frac{P\cos(\varphi)}{m}\delta - \frac{V_r V_n}{r}\right)\\
& + \lambda_r V_r + \lambda_\beta \frac{V_n}{r} - \lambda_m q\delta.
\end{aligned} \tag{3}$$

According to the maximum principle, the chosen control law maximizes the Hamiltonian, i.e., the optimal control functions ($\delta(t)$ and $\varphi(t)$) can be found from the maximum conditions for the Hamiltonian [9].

In addition, it is possible to show that

$$\cos(\varphi_{\text{opt}}) = \frac{\lambda_{V_n}}{\lambda_V},\ \sin(\varphi_{\text{opt}}) = \frac{\lambda_{V_r}}{\lambda_V},$$

where

$$\lambda_V = \sqrt{\lambda_{V_r}^2 + \lambda_{V_n}^2},$$

$$\delta_{\text{opt}} = \begin{cases} 1 \text{ if } \Psi > 0 \\ 0 \text{ if } \Psi < 0, \end{cases}$$

$$\Psi = \frac{P}{m}\lambda_V - \lambda_m q \text{ or } \Psi = \frac{W}{m}\lambda_V - \lambda_m.$$

Here, Ψ denotes the engine switching function and W is the exhaust velocity. The subscript "opt" means that the corresponding relations are derived by maximizing the Hamiltonian.

The obtained pitch angle program is as follows:

$$\varphi = \begin{cases} \arccos\left(\dfrac{\lambda_{V_n}}{\sqrt{\lambda_{V_n}^2+\lambda_{V_r}^2}}\right) \text{ if } \lambda_{V_r} > 0 \\ -\arccos\left(\dfrac{\lambda_{Vn}}{\sqrt{\lambda_{V_n}^2+\lambda_{V_r}^2}}\right) \text{ if } \lambda_{V_r} \le 0. \end{cases}$$

Considering the optimal control laws (the pitch angle program and the optimal thrust function), the equations of system (1) take the form

$$\begin{gathered} \dot V_r = \frac{P\lambda_{V_r}}{m\lambda_V}\delta_{\text{opt}} - \frac{\mu}{r^2} + \frac{V_n^{\,2}}{r}, \\ \dot V_n = \frac{P\lambda_{V_n}}{m\lambda_V}\delta_{\text{opt}} - \frac{V_r V_n}{r}, \\ \dot r = V_r, \\ \dot\beta = \frac{V_n}{r}, \\ \dot m = -q\delta_{\text{opt}}. \end{gathered} \tag{4}$$

Due to the maximum principle, the conjugate variables satisfy the system of differential equations

$$\begin{gathered} \frac{d\lambda_{V_r}}{dt} = -\frac{\partial H}{\partial V_r} = \lambda_{V_n}\frac{V_n}{r} - \lambda_r, \\ \frac{d\lambda_{V_n}}{dt} = -\frac{\partial H}{\partial V_n} = -\lambda_{V_r}\frac{2V_n}{r} + \lambda_{V_n}\frac{V_r}{r} - \lambda_\beta\frac{1}{r}, \\ \frac{d\lambda_r}{dt} = -\frac{\partial H}{\partial r} = \lambda_{V_r}\left(-\frac{2\mu}{r^3}+\frac{V_n^2}{r^2}\right) \\ +\lambda_{V_n}\left(-\frac{V_r V_n}{r^2}\right) + \lambda_\beta\frac{V_n}{r^2}, \\ \frac{d\lambda_\beta}{dt} = -\frac{\partial H}{\partial\beta} = 0. \end{gathered} \tag{5}$$

In the first stage of the analysis, we fix the start and end points of the transfer with motions at the initial orbit perigee and the final orbit apogee, respectively.

The boundary-value problem of the maximum principle

It is required to find the components of the conjugate vector at the start point, $\lambda_{V_r}(t_0), \lambda_{V_n}(t_0)$, $\lambda_r(t_0), \lambda_\beta(t_0), \lambda_m(t_0)$, and a transfer time t_f that satisfy one initial condition (6) and five final conditions (7):

$$\begin{gathered} H(t_0) = 0 \\ \text{or} \\ \left(\lambda_V(t_0)\frac{P}{m(t_0)} - \lambda_m(t_0)q\right)\delta(t_0) \\ +\lambda_{V_r}(t_0)\left(-\frac{\mu}{r(t_0)^2}+\frac{V_n(t_0)^2}{r(t_0)}\right) \\ +\lambda_{V_n}(t_0)\left(-\frac{V_r(t_0)V_n(t_0)}{r(t_0)}\right) \\ +\lambda_r(t_0)V_r(t_0) + \lambda_\beta(t_0)\frac{V_n(t_0)}{r(t_0)} = 0; \end{gathered} \tag{6}$$

$$\begin{gathered} V_r(t_f) = 0, \\ V_n(t_f) = \sqrt{\frac{\mu}{p_f}}(1-e_f), \\ r(t_f) = \frac{p_f}{1-e_f}, \\ \beta(t_f) = \pi, \\ \lambda_m(t_f) = 1, \end{gathered} \tag{7}$$

where p_f and e_f are the focal parameter and eccentricity of the final transfer orbit.

Now we introduce transversality conditions to unbind the start and end points of the transfer from the initial orbit apogee and final orbit perigee, respectively.

The transversality conditions at the start and end points of the transfer trajectory

The transversality condition expresses the perpendicularity of the vector λ (2) to all tangent vectors of the boundary manifold. Thus, the optimality conditions for the start point are given by the perpendicularity of the vector λ (2) and the tangent vector. The transversality conditions were derived in the paper [9] (the implementation and results of the initial stage of this study). In the case under consideration, this condition can be written as follows:

$$\lambda_{V_r}(t_0)\frac{e_0\cos(\upsilon_0)}{\sqrt{p_0}}-\lambda_{V_n}(t_0)\frac{e_0\sin(\upsilon_0)}{\sqrt{p_0}}$$

$$+\lambda_r(t_0)\frac{p_0e_0\sin(\upsilon_0)}{\left(1+e_0\cos(\upsilon_0)\right)^2}$$

$$+\lambda_\beta(t_0)\cdot 1+\lambda_m(t_0)\cdot 0=0.$$

Consequently,

$$\lambda_\beta(t_0)=-\lambda_{V_r}(t_0)\frac{e_0\cos(\upsilon_0)}{\sqrt{p_0}}$$

$$+\lambda_{V_n}(t_0)\frac{e_0\sin(\upsilon_0)}{\sqrt{p_0}}-\lambda_r(t_0)\frac{p_0e_0\sin(\upsilon_0)}{\left(1+e_0\cos(\upsilon_0)\right)^2},$$

where e_0 is the initial orbit eccentricity, υ_0 is the true anomaly of the start point, and p_0 is the focal parameter of the initial orbit.

The condition for optimizing the end point is obtained by analogy:

$$\lambda_\beta(t_f)=-\lambda_{V_r}(t_f)\frac{e_f\cos(\beta_f)}{\sqrt{p_f}}$$

$$+\lambda_{V_n}(t_f)\frac{e_f\sin(\beta_f)}{\sqrt{p_f}}-\lambda_r(t_f)\frac{p_fe_f\sin(\beta_f)}{\left(1+e_f\cos(\beta_f)\right)^2},$$

where β_f is the polar angle at the end point of the transfer.

1.2. Data Preparation for Correlation Analysis Based on Iterating the Parameter Values

Consider five statements with the following values of varying orbital parameters:

1. 400-km perigee altitude and 1400-km apogee altitude (the initial orbit), and 1900-km perigee altitude and 9900-km apogee altitude (the final orbit).

2. 400-km perigee altitude and 1400-km apogee altitude (the initial orbit), and 2000-km perigee altitude and 10 000-km apogee altitude (the final orbit).

3. 400-km perigee altitude and 1400-km apogee altitude (the initial orbit), and 2100-km perigee altitude and 10 100-km apogee altitude (the final orbit).

4. 500-km perigee altitude and 1500-km apogee altitude (the initial orbit), and 2000-km perigee altitude and 10 000-km apogee altitude (the final orbit).

5. 600-km perigee altitude and 1600-km apogee altitude (the initial orbit), and 2000-km perigee altitude and 10 000-km apogee altitude (the final orbit).

The preliminary search range for problem statements 1–5 was formed based on the solution of the reference problem (statement 4 in subsection 1.1). This range was used to iterate the parameter values and obtain value sets for further statistical (correlation) analysis. The search range and the data sample for further analysis and solution within problem statements 1–5 were described in the paper [9].

Table 1 shows the resulting values of the required characteristics (problem statements 1–5) that ensure the optimal transfer.

Thus, the iterative search inside the selected parameter ranges improved the result for the reference problem (statement 4) by 365 g relative to the solution previously obtained using the random search [1].

This stage of the study was presented in detail in the paper [9].

Table 1

The optimal transfer characteristics in problem statements 1–5 (analysis within the data grid)

Characteristics	Statement 1	Statement 2	Statement 3	Statement 4	Statement 5
υ_0	-0.608528181266	-0.687262955509	-0.58694862445	-0.58063271537992	-0.67460422765
λ_{V_r}	-0.065265825615	-0.075257944004	-0.06564653582	-0.06466045327036	-0.06339073139
λ_{V_n}	1.3623340777782	1.3653869345017	1.364158466294	1.36474044140864	1.357648817782
λ_r	1.4200011568480	1.4207257561587	1.421069918027	1.42243156356652	1.40764863211
T_f	6.7321648922778	7.0228415355241	12.30599404742	12.48386539989280	5.855669428846
β_f	3.1311300732552	3.166796288751	5.127686975088	5.33807657900554	2.859452408788
m_f, kg	3227.339	3182.552	3181.12	3204.153	3247.748

2. CORRELATIONS BETWEEN KEY PROBLEM PARAMETERS

2.1. Special Mathematical and Algorithmic Support for Data Analysis and Processing

The presence and significance of mathematical relationships between the problem parameters that ensure convergence of the numerical method for solving the boundary-value problem and optimization of the resulting solution are checked using a *Python* program [11]. This program is a special mathematical and algorithmic support tool for the data analysis and processing system. It is implemented based on *pandas*, *scipy*, and *numpy*, the libraries for data analysis and mathematical programming.

The program algorithm includes the following steps.

1. Data are loaded; parameters for the analysis and their relationships are selected.
2. Normality is tested based on frequency statistics to verify the absence of large deviations from the mean values in the data. It can be performed by many methods, e.g., the Shapiro–Wilk test [12–14] or the Kolmogorov–Smirnov test [13, 15]. The program involves the Shapiro–Wilk test to check the probability of a random difference: if this probability is small, the difference is considered statistically significant [12–14].
3. The closeness of a correlation in the Evans sense and its significance by Fisher's criterion are assessed [16, 17]. They are needed to establish whether the variability of one characteristic depends on the variability of another (and the relevance of this dependence) [16, 17].
4. The significance of the difference between the linear and nonlinear correlations by Fisher's criterion is assessed [17].

2.2. Program results

The program searched over 4.145 million variations of the initial approximations for each problem statement within the selected range in order to identify fluctuations between the values of key parameters and the estimated degree of convergence. Thirteen groups of parameters and their correlations were analyzed. The analysis covered only those parameter values that ensured convergence of the numerical method and the spacecraft insertion into the specified final orbit.

Within the range under consideration, the variations of the true anomaly υ_0 (the transfer start point) were revealed to have no effect on the other components of the vectors analyzed. At the same time, for constant values of the other parameters, a larger variation in the true anomaly caused an increase in the final mass. (Within the range of υ_0, this difference between the left and right boundaries was 1 kg on average.)

As it was established, the spacecraft is inserted into the final orbit under the following values of the ratio λ_r / λ_{Vn} (depending on the distance between the initial and final orbits and (or) the distance between the reference orbit and the Earth):

– For problem statement 1 (the initial orbit is the lowest, and the distance corresponds to that of the reference problem), 1.001397624,..., 1.042397661;

– For problem statement 2 (the initial orbit is the lowest, and the distance is increased compared to the reference problem by 100 km), 1.001397624,..., 1.030802292;

– For problem statement 3 (the initial orbit is the lowest, and the range is increased by 200 km compared to the reference problem), 1.007127584,..., 1.025531915;

– For problem statement 4 (this is the reference problem, and the initial orbit is 100 km above the lowest orbit): 0.987421384,..., 1.037090909;

– For problem statement 5 (the highest initial orbit is 200 km higher than the lowest, and the shortest distance is 100 km less than that of the reference problem), 0.983146067,..., 1.038207201.

Beyond these ranges, either convergence is not achieved or the spacecraft does not reach the specified orbit (i.e., it is inserted into a lower or higher orbit). As was discovered, the best solutions by mass are located inside the ranges, far from their left and right bounds.

Also, the transfer time and polar angle have a direct relationship: they should be tuned commensurately to ensure a solution under preliminarily calculated values of the other missing characteristics. An increase in the polar angle should be commensurate with the increase in the transfer to maximize the final mass of the spacecraft in the orbit effectively.

According to the testing results, there is an Evans-significant linear correlation between the values of λ_{V_n} and λ_r (a significance level of 0.95, a linear correlation coefficient of 0.9678). Figure 1 demonstrates no outliers for the dependent parameter, the normality of the data distribution, and the linear dependence.

The analysis revealed a moderately significant linear relationship (in the Evans sense) between the orbit variation index

$$Q = \frac{e_f - e_0}{p_{fb} - p_{0b}},$$

where p_{fb} and p_{0b} are the focal parameters of the final and initial orbits, respectively, reduced to dimensionless form (Fig. 2), and the ratio $\lambda_r / \lambda_{V_n}$.

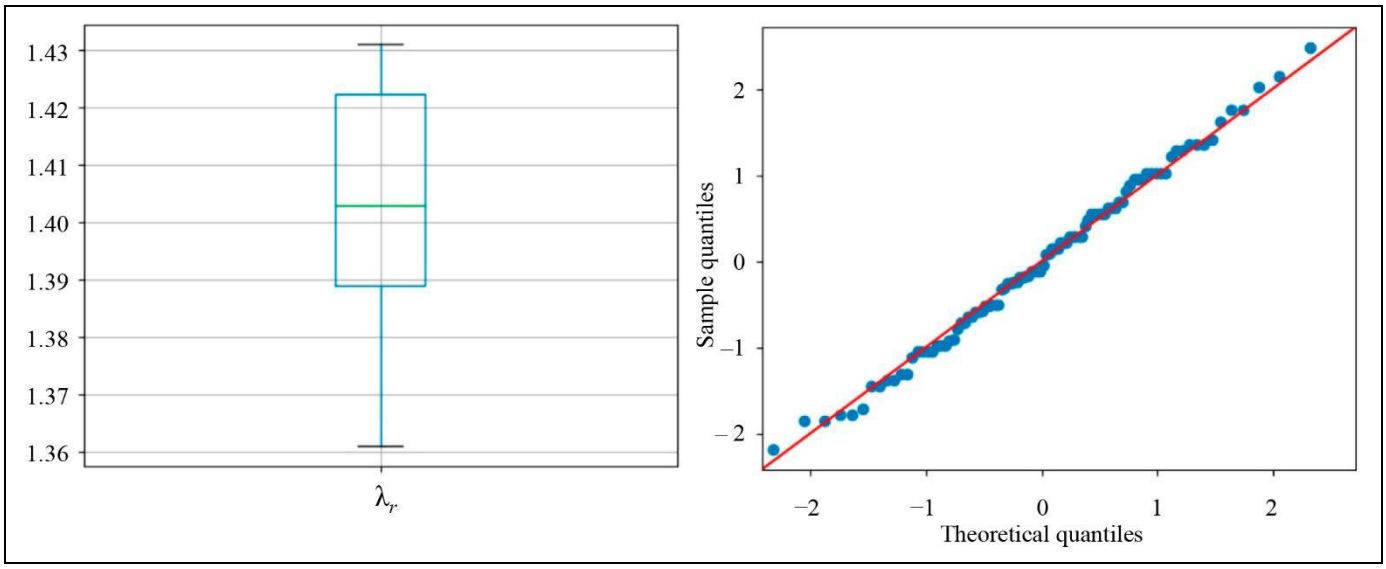

Fig. 1. The results of correlation analysis for λ_{V_n} and λ_r .

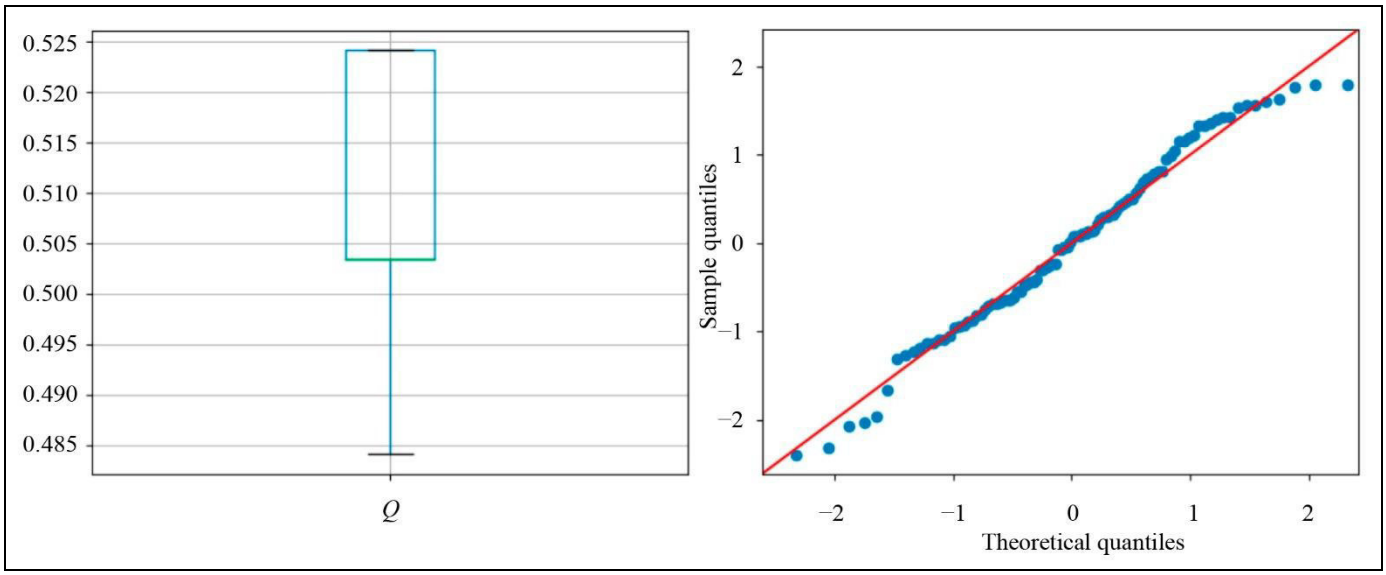

Fig. 2. The results of correlation analysis for Q and $\lambda_r / \lambda_{V_n}$.

A moderately significant linear correlation between the ratio $\lambda_r / \lambda_{V_n}$ and the parameter λ_{V_r} was identified. An Evans-strong nonlinear correlation was established between the polar angle β_f (the transfer end point) and the inter-orbital transfer time T_f. An Evans-strong correlation was found between the ratios T_f/β_f and $\lambda_r / \lambda_{V_n}$. However, it was not possible to clarify the nature of this relationship (probably, due to insufficiently many cases under analysis and the narrow initial range).

The presence of a significant relationship between the true anomaly υ_0 (the start point in the initial orbit) and the ratio T_f/β_f was not confirmed.

2.3. Applying the Results to the Reference Problem to Improve the Solution

The results obtained during this study using a Python program may serve to correct search ranges for initial approximations. Hence, the procedure for finding the optimum can be potentially simplified for typical optimization problems.

The initial values of the parameters are refined to improve the optimization result for the reference problem using the conclusions described in subsection 2.2. More precisely, the values initially found for the conjugate variables λ_{V_r}, λ_{V_n}, and λ_r remain fixed where-

as the true anomaly υ_0 decreases and goes beyond the selected range with the simultaneous increase of the polar angle β_f by 1.7 times commensurately with the transfer time T_k. Next, the residuals are calculated to correct the vector values.

As a result, we obtain a value set of the vector components that solves the problem (Table 2).

Thus, the final result is significantly improved to reach 3206.884 kg. (The final mass at the end point of the transfer is increased by 2.731 kg compared to the result in subsection 2.1.2.)

Figure 3 shows the optimized transfer scheme for the reference problem.

Table 2

The value vector ensuring the optimal transfer within the reference problem

Characteristic	Value
υ_0	–0.5733590707938522
λ_{V_r}	–0.06418827063171273
λ_{V_n}	1.3652318375612795
λ_r	1.4233117301910392
T_f	12.066799357615691
β_f	5.062132315335388

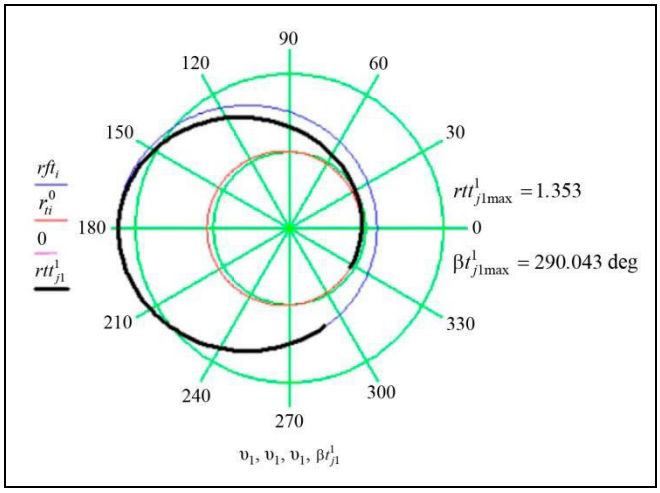

Fig. 3. The optimized transfer scheme for the reference problem (statement 4).

2.4. Discussion and Further Research

This study has been carried out using programs in Mathcad 15 and Python 3.9. The results confirm the effectiveness of the proposed approach to choosing initial approximations based on the correlation analysis of key problem parameters (inter-orbital spacecraft transfer optimization).

In the course of this study, we have revealed several relationships between the vector components ensuring the convergence of the numerical solution for typical optimization problems (inserting a spacecraft into a given orbit). The analysis conclusions have been verified in a computational experiment for the reference problem. According to the experiment's results, the approach is effective: the spacecraft mass in the final orbit has been increased. Also, the search range for the optimum has been refined for typical problems with small deviations in the transfer distance and initial orbit altitude.

Further research will expand these problems in order to refine the current results and formalize them as an algorithm for choosing initial approximations in inter-orbital spacecraft transfer optimization. In particular, the following cases will be investigated:

- many-revolution orbit transfer;
- transition between orbits in different planes;
- transfers with other types of engines (e.g., an electric rocket engine with regulated thrust).

CONCLUSIONS

This paper has extended the applicability of mathematical programming for designing an optimal spacecraft transfer trajectory between near-Earth elliptical orbits. We have described an approach facilitating the choice of effective initial approximations in inter-orbital spacecraft transfer optimization. The results of a computational experiment have confirmed the effectiveness of this approach in the problem statement under consideration.

The results of the study are as follows:

- For the first time, we have revealed the relationship between the parameters of the optimal inter-orbital spacecraft transfer between two elliptical near-Earth orbits. The nature of this relationship has been established using special mathematical and algorithmic support (a Python program) developed for the data analysis and processing system.
- Based on the revealed relationships, we have significantly improved the primary solution (yielded by the Bard method) as well as the solution obtained in the paper [9] (by iterating parameter values within the data grid) for the reference problem (inter-orbital spacecraft transfer optimization).

REFERENCES

1. Bard, Y., *Nonlinear Parameter Estimation*, New York–London: Academic Press, 1979.
2. Kitrell, J.R., Mezaki, R., and Watson, C.C., Estimation of Parameters for Nonlinear Least Squares Analysis, *Industrial & Engineering Chemistry*, 1965, vol. 57, pp. 18–27.

3. Wu, D., Cheng, L., Gong, S., and Baoyin, H., Approximate Time-Optimal Low-Thrust Rendezvous Solutions Between Circular Orbits, *Aerospace Science and Technology*, 2022, vol. 131, part A, art. no. 108011.
4. Petukhov, V.G., Optimization of Interplanetary Trajectories for Spacecraft with Ideally Regulated Engines Using the Continuation Method, *Cosmic Research*, 2008, vol. 46, no. 3, pp. 219–232.
5. Hofmann, C., and Topputo, F., Embedded Homotopy for Convex Low-Thrust Trajectory Optimization with Operational Constraints, *Proceedings of 2022 AAS/AIAA Astrodynamics Specialist Conference*, Charlotte, NC, USA, 2022, pp. 1–16.
6. Jiang, F., Baoyin, F., and Li, J., Practical Techniques for Low-Thrust Trajectory Optimization with Homotopic Approach, *Journal of Guidance, Control and Dynamics*, 2012, vol. 35, no. 1, pp. 245–258.
7. Wu, D., Wu, C., Lin, F., et al., Analytical Costate Estimation by a Reference Trajectory-Based Least-Squares Method, *Journal of Guidance, Control and Dynamics*, 2022, vol. 45, pp. 1–9.
8. Wu, D., Wu, Ch., Lin, F., and Baoyin, H., An Atlas of Optimal Low-Thrust Rephasing Solutions in Circular Orbit, *arXiv:2209.07418v1*, 2022. DOI: 10.48550/arXiv.2209.07418.
9. Savvina, E.V., Inter-orbital Spacecraft Transfer: Trajectory Design by Iterating Parameter Values within a Data Grid, *Control Sciences*, 2023, no. 2, pp. 56–63.
10. URL: https://www.mathcad.com/ (Accessed May 15, 2023.)
11. URL: https://www.python.org/ (Accessed May 15, 2023.)
12. Shapiro, S.S. and Wilk, M.B., An Analysis of Variance Test for Normality (Complete Samples), *Biometrika*, 1965, vol. 52, no. 3/4, pp. 591–611.
13. Mohd Razali, N. and Yap, B.W., Power Comparisons of Shapiro-Wilk, Kolmogorov-Smirnov, Lilliefors and Anderson-Darling Tests, *J. Stat. Stat. Model. Analytics*, 2011, vol. 2, no. 1, pp. 20–33.
14. Rahman, M. and Zakkula, G., A Modification of the Test of Shapiro and Wilk for Normality, *Journal of Applied Statistics*, 1997, vol. 24, pp. 219–236.
15. Simard, R.J. and L'Ecuyer, P., Computing the Two-Sided Kolmogorov-Smirnov Distribution, *Journal of Statistical Software*, 2011, vol. 39, pp. 1–18.
16. Kobzar', A.I., *Prikladnaya matematicheskaya statistika. Dlya inzhenerov i nauchnykh rabotnikov* (Applied Mathematical Statistics. For Engineers and Researchers), Moscow: Fizmatlit, 2006. (In Russian.)
17. Afifi, A.A. and Azen, S.P., *Statistical Analysis: A Computer Oriented Approach*, London–New York: Academic Press, 1979.

This paper was recommended for publication by L.B. Rapoport, a member of the Editorial Board.

Received February 13, 2023, and revised July 4, 2023. Accepted July 18, 2023.

Author information

Savvina, Elena Valer'evna. Applicant for a degree, Moscow, Russia
✉ petrakowae@mail.ru
ORCID iD: https://orcid.org/0009-0007-7083-8617

Cite this paper
Savvina, E.V., Inter-orbital Spacecraft Transfer Optimization: Choosing Initial Approximations Based on Correlation Analysis of Key Parameters. *Control Sciences* **4**, 43–50 (2023). http://doi.org/10.25728/cs.2023.4.5

Original Russian Text © Savvina, E.V., 2023, published in *Problemy Upravleniya*, 2023, no. 4, pp. 48–56.

Translated into English by *Alexander Yu. Mazurov*,
Cand. Sci. (Phys.–Math.),
Trapeznikov Institute of Control Sciences, Russian Academy of Sciences, Moscow, Russia
✉ alexander.mazurov08@gmail.com